Interaction Notes

Note 385

May 1979

On the Physical Realizability of Broad-Band Equivalent Circuits for Wire Loop and Dipole Antennas

Gary W. Streable
L. Wilson Pearson

University of Kentucky
Lexington, KY

Abstract

Results of a study of the feasibility of using Singularity Expansion Method (SEM) data to synthesize broad-band equivalent circuits for loop and wire structures are reported. The positive realness of admittances derived are studied, on the basis of both pole-pair groupings and eigenmode groups within the SEM formalism. Synthesized circuits are given for a center-driven and a quarter-driven straight wire antenna, and for a circular loop. Results are compared with those derived by means of numerical solution of the time-dependent integral equations for each structure. The sensitivities of the response to changes in the values of poles and to circuit element values are considered.

Acknowledgement

This work was sponsored by the Air Force Office of Scientific Research under Grant No. ENG 78-11512.

TABLE OF CONTENTS

Chapter		Page
I.	INTRODUCTION	8
	Description of SEM	8
	Scope of Present Work	9
II.	FORMAL DEVELOPMENT OF EQUIVALENT CIRCUITS	15
	Introduction	15
	Formulation of the Norton Equivalent Problem	15
	Equivalent Admittance Circuits	20
	Sources of SEM Data	24
	Straight Wire Data	24
	Circular Loop Data	28
III.	POSITIVE REAL CONSIDERATIONS	33
	Introduction	33
	Pole-at-a-Time Circuits	33
	Conjugate Pole-Pair Modules	34
	Eigenmode PR Considerations	72
	SEM Pole/Residue Error Effects on PR Considerations	83
IV.	CIRCUIT SYNTHESIS	94
	Introduction	94
	Center-Driven Wire	94
	Terminal Eigenadmittance Results	94
	Pole-Pair Realization Using First Layer Poles	101
	Circuit Performance	106
	Quarter-Driven Wire	109
	Admittance Synthesis for Circular Loop	112
	Type I Poles	121
	Type I and Type III Poles	127
	Sensitivity of Circuits	127
V.	CONCLUSIONS	140
APPENDIX		142
REFERENCES		154

LIST OF FIGURES

Page

Figure 1: The PR condition for an unmodified pole-pair admittance. . . 14

Figure 2: Defining the Norton equivalence admittance and short circuit current. 16

Figure 3: The scatterer/antenna gap geometry 18

Figure 4: The scatterer/antenna admittance and short circuit current formulations 19

Figure 5: Pole-at-a-time equivalent circuit. 23

Figure 6: Pole-pair equivalent circuit 25

Figure 7: Eigenadmittance equivalent circuit 26

Figure 8: SEM poles for the straight wire. 29

Figure 9: The circular loop geometry 31

Figure 10: Classification of SEM poles for the circular loop into type I, type II, and type III. 32

Figure 11: Parameter tests for straight wire pole-pair admittances of pole 1, first layer 38

Figure 12: Parameter tests for straight wire pole-pair admittances of pole 2, first layer 39

Figure 13: Parameter tests for straight wire pole-pair admittances of pole 3, first layer 40

Figure 14: Parameter tests for straight wire pole-pair admittances of pole 4, first layer 41

Figure 15: Parameter tests for straight wire pole-pair admittances of pole 5, first layer 42

Figure 16: Parameter tests for straight wire pole-pair admittances of pole 2, second layer. 44

Figure 17: Parameter tests for straight wire pole-pair admittances of pole 3, second layer. 45

Figure 18: Parameter tests for straight wire pole-pair admittances of pole 4, second layer. 46

Page

Figure 19: Parameter tests for straight wire pole-pair admittances of pole 2, third layer 47

Figure 20: Real part of straight wire pole-pair admittance at z/L = .5 for pole 1, first layer 48

Figure 21: Real part of straight wire pole-pair admittance at z/L = .5 for pole 3, first layer 49

Figure 22: Real part of straight wire pole-pair admittance at z/L = .5 for pole 5, first layer 50

Figure 23: Real part of straight wire pole-pair admittance at z/L = .25 for pole 1, first layer. 51

Figure 24: Real part of straight wire pole-pair admittance at z/L = .25 for pole 2, first layer. 52

Figure 25: Real part of straight wire pole-pair admittance at z/L = .25 for pole 3, first layer. 53

Figure 26: Real part of straight wire pole-pair admittance at z/L = .25 for pole 4, first layer. 54

Figure 27: Real part of straight wire pole-pair admittance at z/L = .25 for pole 5, first layer. 55

Figure 28: Real part of straight wire pole-pair admittance at z/L = .5 for pole 2, second layer. 56

Figure 29: Real part of straight wire pole-pair admittance at z/L = .5 for pole 4, second layer. 57

Figure 30: Real part of straight wire pole-pair admittance at z/L = .25 for pole 2, second layer 58

Figure 31: Real part of straight wire pole-pair admittance at z/L = .25 for pole 3, second layer 59

Figure 32: Real part of straight wire pole-pair admittance at z/L = .25 for pole 4, second layer 60

Figure 33: Real part of circular loop pole-pair admittance for type I pole of mode 1. 62

Figure 34: Real part of circular loop pole-pair admittance for type I pole of mode 2. 63

Figure 35: Real part of circular loop pole-pair admittance for type I pole of mode 3. 64

Page

Figure 36: Real part of circular loop pole-pair admittance for type I pole of mode 4. 65

Figure 37: Real part of circular loop pole-pair admittance for type I pole of mode 5. 66

Figure 38: Real part of circular loop pole-pair admittance for type III pole, mode 2. 68

Figure 39: Real part of circular loop pole-pair admittance for the first type II pole of mode 2 69

Figure 40: Real part of circular loop pole admittance for the second type II pole of mode 2. 70

Figure 41: Real part of circular loop pole-pair admittances of the first type II poles of modes 1-6, showing the consistent negative behavior of these admittances. 71

Figure 42: The postulated eigenmodes for the straight wire. 74

Figure 43: Real part of straight wire terminal eigenadmittances for mode 3 at z/L = .5 76

Figure 44: Real part of straight wire terminal eigenadmittance for mode 5 at z/L = .5 77

Figure 45: Real part of straight wire terminal eigenadmittance for mode 2 at z/L = .25. 78

Figure 46: Real part of straight wire terminal eigenadmittance for mode 3 at z/L = .25. 79

Figure 47: Real part of straight wire terminal eigenadmittance for mode 4 at z/L = .25. 80

Figure 48: Real part of straight wire terminal eigenadmittance for mode 5 at z/L = .25. 81

Figure 49: Real part of straight wire terminal eigenadmittance for mode 6 at z/L = .25. 82

Figure 50: Effect of ±5% change on parameter test IIB for pole-pair admittance of pole 1, first layer of the straight wire 85

Figure 51: Effect of ±5% change on parameter test IIA for pole-pair admittance of pole 1, first layer of the straight wire 86

Page

Figure 52: Effect of ±10% change on parameter test IIB for pole-pair admittance of pole 2, first layer of the straight wire 88

Figure 53: Effect of ±10% change on parameter test IIA for pole-pair admittance of pole 2, first layer of the straight wire 89

Figure 54: Effect of ±10% change on parameter test IIB for pole-pair admittance of pole 3, first layer of the straight wire 90

Figure 55: Effect of ±10% change of parameter test IIA for pole-pair admittance of pole 3, first layer of the straight wire 91

Figure 56: Effect of ±10% change on parameter test IIB for pole-pair admittance of pole 2, second layer of the straight wire 92

Figure 57: Effect of ±10% change on parameter test IIA for pole-pair admittance of pole 2, second layer of the straight wire 93

Figure 58: Equivalent circuit using terminal eigenadmittance modules for center-driven wire, modes 1, 3, 5, and 7 97

Figure 59: Modified Bott-Duffin synthesis module. 102

Figure 60: Equivalent circuit using nine first layer pole-pair admittances of the center-driven wire. 104

Figure 61: Comparison of the response of the eigenadmittance circuit to TWTD. 107

Figure 62: Comparison of the response of the first layer pole-pair circuit to TWTD. 108

Figure 63: Equivalent circuit for quarter-driven antenna. 113

Figure 64: Comparison of the response of the quarter-driven wire circuit to TWTD. 120

Figure 65: Equivalent circuit for the circular loop using type I pole-pair admittances. 122

Figure 66: Comparison of the response of the type I pole-pair circuit to TWTD. 126

Page

Figure 67a: Equivalent circuit for the circular loop using type I and type III poles, modes 0 and 1. 128

Figure 67b: Equivalent circuit for the circular loop using type I and type III poles, modes 2-10 129

Figure 68: Comparison of the response of the type I and type III pole circuit to TWTD. 137

Figure 69: Effect of element errors on circuit performance 139

CHAPTER I

INTRODUCTION

1.1 Description of SEM

Much attention has been focused on the use of the singularity expansion method (SEM) to solve broad-band transient electromagnetic field problems involving scatterers since its formalism was developed by Baum [1,2] in 1971. SEM formalism grew from the experimental observation that the transient response of scatterers is dominantly composed of one or more damped sinusoids. Since such damped sinusoids correspond to conjugate pole-pairs in the complex frequency plane (or s-plane), Baum postulated that a complete representation of the transient response could be obtained by knowledge of all s-plane singularities of the object's response. Such s-plane singularities potentially include poles, essential singularities, branch cuts, and entire functions. A complete SEM representation of a scatterer consists of a set of singularities, the modal current distribution associated with a singularity, and a normalizing coefficient. Marin [3] showed that perfectly conducting objects in free space, such as are dealt with in the present work, have only pole singularities. Hence only pole singularities are considered in this work.

Because the SEM approach reduces the problem of finding a transient response for a given object to that of finding the object's singularities, the associated modal distributions, and the coupling factors which weight a given singularity's contribution to the response for a given exciting waveform, we see that SEM offers a more compact and efficient way of representing transient responses than previous methods. These methods include numerical solutions of differential/integral equations in the time or frequency domain, and integral

operator modal approaches. The connection of the latter approach, sometimes referred to as the eigenmode expansion method (EEM), to SEM has been demonstrated by Baum [4]. In the present work extensive use of EEM in conjunction with SEM is made. The utility of SEM lies in the low and intermediate frequency ranges, and is particularly useful for studying the response of scatterers to the nuclear electromagnetic pulse (EMP) because of the presence of frequencies whose wavelengths range from long to short compared to scatterer dimensions in such pulses. In addition to compactness and efficiency, SEM offers greater physical insight into a problem than other methods.

1.2 Scope of Present Work

The motivation for the present work derives from the insight that it may be possible to construct passive RLC (resistor, inductor, capacitor) circuits from the pole and residue data of SEM. Such circuits might then be used to predict the transient current response of an object to various waveforms. This idea has been formalized by Baum [5,6] and the present work centers on the feasibility of this approach for the construction of some realizable equivalent circuits for radiation-gathering structures - in particular on the positive real considerations of realizability for convenient formalisms.

In a previous work Hess [17] has performed an EMP coupling analysis using transfer impedances derived from SEM. Schaubert [16] has recently constructed lumped-element equivalent circuits for a center-driven dipole and a Yagi antenna, using experimentally derived SEM data. Schaubert extracted SEM data by means of Prony's algorithm from the antenna terminal voltage waveform due to a step-like excitation, and used this data to construct the total impedance of the antennas. Schaubert then used Brune's synthesis method to

derive equivalent circuits. The present work uses theoretically derived SEM data and addresses the problem of realizing the antenna impedance by individual, transformerless, circuit modules which can be related to the SEM data.

Baum [5,6] suggested the construction of equivalent circuits on a pole at a time basis, a conjugate pole-pair basis, and an eigenmode basis, and gave generalized formal circuits for each type of synthesis. The realizability of the formal circuits was not treated in detail. The formal development of SEM leading to equivalent circuits is left to Chapter II. The case of conjugate pole-pair synthesis is examined briefly and related to earlier work by Guillemin [7], in order to illustrate some of the salient aspects of the current work. A more detailed consideration of this and related problems is given in Chapter III.

The physical realizability of a given impedance or admittance quality hinges on whether or not that quantity is a positive real (PR) function of the complex frequency s. A positive real function is defined as a function that is real for s real, is analytic in the right half-plane, and whose real part is positive along the $j\omega$ axis. Additionally, any poles on the $j\omega$ axis are simple with real and positive residues. It is instructive to study the conditions under which a conjugate pole-pair exhibits positive realness ("PRness").

The admittance associated with the n^{th} SEM pole is written as

$$Y_n(s) = \frac{a_n}{s - s_n} , \qquad (1.1)$$

where $s_n = \sigma_n + j\omega_n$ is the complex pole and $a_n = \alpha_n + j\beta_n$ is the complex residue. A modified form of this admittance, which has the property of being zero at zero frequency, is written as

$$Y_n'(s) = \frac{a_n}{s - s_n} + \frac{a_n}{s_n} \tag{1.2}$$

so that $Y_n'(o) = 0$ is physically consistent with the terminal admittance of a simply-connected scatterer.

SEM poles are either purely real or occur in conjugate pairs. The conjugate pair case is the more general one. The admittance of the n^{th} conjugate pole-pair is then, in unmodified form,

$$Y_n^{cp}(s) = \frac{a_n}{s - s_n} + \frac{a_n^*}{s - s_n^*} \tag{1.3}$$

or

$$Y_n^{cp}(s) = \frac{2\ \text{Real}(a_n)s - 2\ \text{Real}(a_n^* s_n)}{s^2 - 2\ \text{Real}(s_n)s + |s_n|^2} \ . \tag{1.4}$$

In this form we see that the coefficients of $Y_n^{cp}(s)$ are real valued, as they must be for circuit realizability. The other criterion necessary to ensure realizability of $Y_n^{cp}(s)$ is the non-negativeness of its real part along the $j\omega$ axis.

Guillemin [7] showed that for an unmodified admittance function formed by conjugate pole-pairs to be PR, certain conditions must be met. If we let

$$Y_n^{cp}(s) = \frac{d_1 s + d_0}{s^2 + b_1 s + b_0} \ , \tag{1.5}$$

with

$$d_1 = 2\alpha_n \qquad b_1 = -2\sigma_n$$

$$d_0 = -2\ \mathrm{Real}(a_n^* s_n) \qquad b_0 = |s_n|^2 = \sigma_n^2 + \omega_n^2 .$$

$$= -2(\alpha_n\sigma_n + \beta_n\omega_n) \tag{1.6}$$

We see that b_1 and b_0 are positive for a pole in the left half-plane, while d_1 and d_0 may be of either sign. In order to find what conditions need to apply to d_1 and d_0 for $Y_n^{cp}(s)$ to be realizable, we need to find its real part, and check for non-negativeness at $s = j\omega$. This leads to the condition

$$d_0 b_0 + (d_1 b_1 - d_0)\omega^2 \geq 0 . \tag{1.7}$$

This requires

$$d_1 b_1 \geq d_0 \geq 0 , \tag{1.8}$$

which leads to the PR conditions

$$-\alpha_n\sigma_n + \beta_n\omega_n \geq 0 \tag{1.9}$$

and

$$-\alpha_n\sigma_n - \beta_n\omega_n \geq 0 . \tag{1.10}$$

We can combine these conditions into a single expression which reflects the necessary restriction on the residue for a PR function to result. This expression is

$$\frac{\alpha_n}{|\beta_n|} \geq \frac{\omega_n}{-\sigma_n} . \tag{1.11}$$

This condition is illustrated graphically in Figure 1. These and similar PR conditions are used extensively in Chapter III. For $Y_n^{cp}(s)$ to be PR, the residue must lie within the shaded portion of the a-plane. Unfortunately, it is seen that most SEM poles and residues fail to meet this criterion, and ways of circumventing this difficulty are devised. The parameter tests which are required for modified conjugate pole-pairs have been derived, and are presented in Chapter III.

In Chapter II, the formal development of SEM in conjunction with EEM as applied to equivalent circuits is given, and the sources of SEM data used in this study explained. Chapter III deals with PR considerations of functions derived from SEM data on conjugate pole-pair and eigenmode bases, and examines pole/residue error considerations. Chapter IV encompasses some synthesized circuits for wire and loop objects, and compares the results obtained from these circuits and analyzed by a SCEPTRE circuit analysis program to results obtained from a thin wire-time domain (TWTD) program. Also in Chapter IV the sensitivity of these circuits is considered. Chapter V gives the conclusions reached by this study, and points out areas which need further consideration.

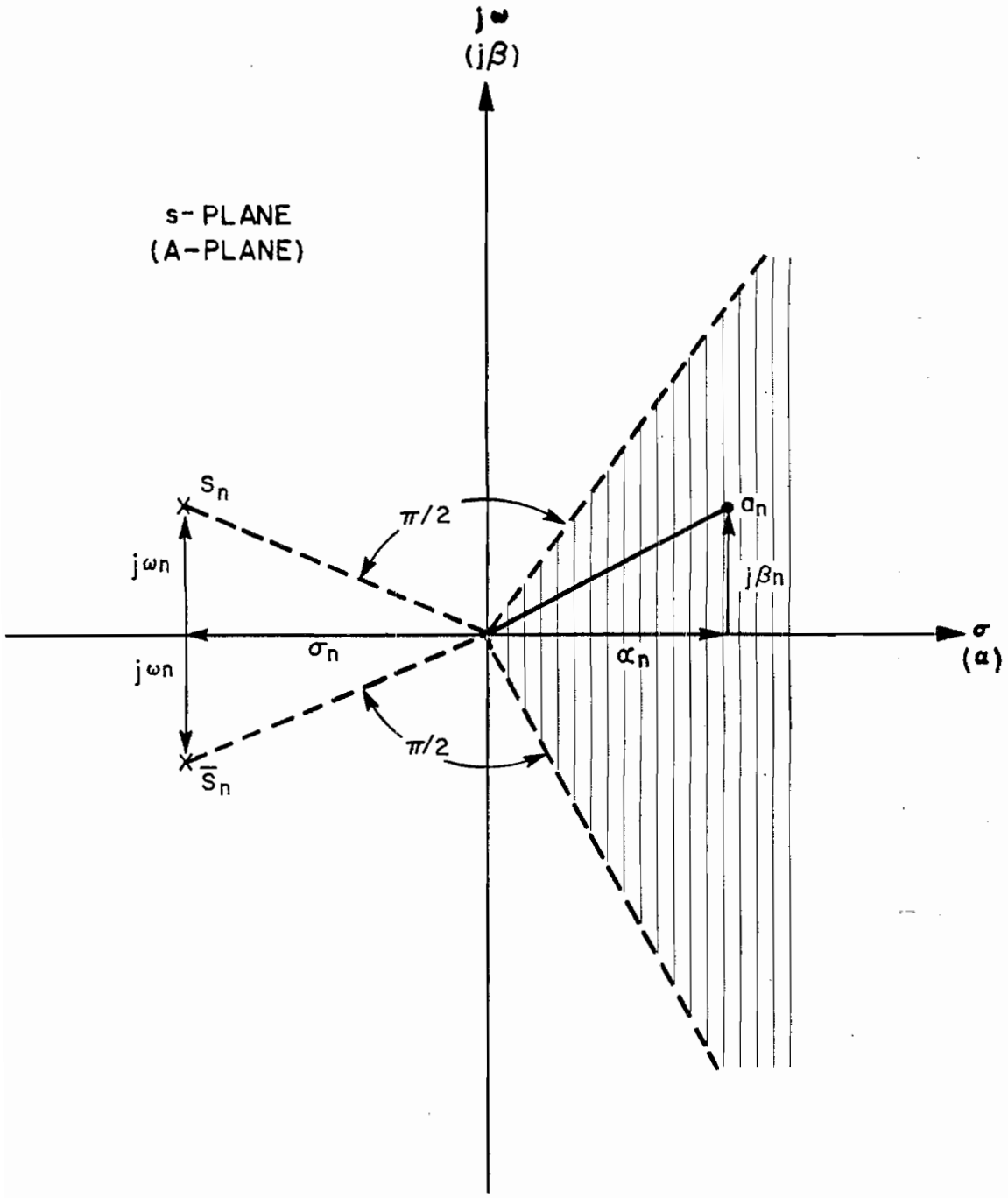

Figure 1: The PR condition for an unmodified pole-pair admittance. The a-plane is superimposed on the s-plane.

CHAPTER II

FORMAL DEVELOPMENT OF EQUIVALENT CIRCUITS

2.1 Introduction

In this section we consider the problem of the broadband admittance of an arbitrary scatterer or antenna at a gap region in the object. The approach is to cast the object's terminal pair formed by the gap into the form of a Norton equivalent circuit. Then, using SEM, the equivalent admittance is found in the form of a residue series in the complex frequency variable. Subsequently, network synthesis techniques are applied and equivalent circuits constructed. Three different generic circuit configurations are considered, corresponding to three different levels of grouping the SEM poles. In the first circuit, the admittance formed from the individual poles is the basic module. In the second the pole-pair admittance formed by grouping a conjugate pole-pair together is the basic module. Finally, the admittance formed by grouping the poles according to eigenmodes with which they are associated, as directed by EEM results, provides the basic module. The admittance formed by eigenmode grouping we term a "terminal eigenadmittance".

In the last part of the chapter the sources of the SEM data used in this study are discussed.

2.2 Formulation of the Norton Equivalent Problem

Figure 2 gives the steps required in defining the Norton equivalent for an active circuit with a single port. The active circuit can be replaced by a single equivalent admittance and a current generator in parallel, as in Figure 2a. In Figure 2b the methods for finding the current generator and

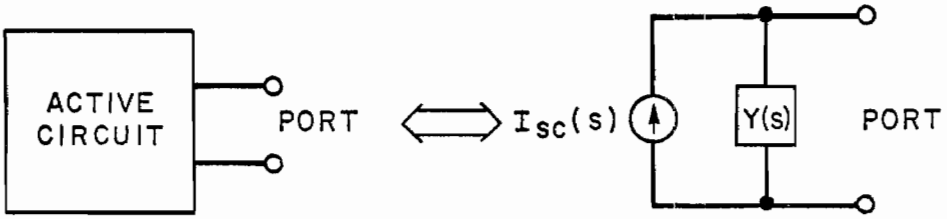

Figure 2a

Figure 2b

Figure 2: Defining the Norton equivalence admittance and short circuit current.

equivalent admittance, both necessary for the replication of the active circuit as seen by the port, are illustrated. The short-circuit current is found by shorting the port of the active circuit, and the equivalent admittance is found by setting the sources of the active circuit to zero and measuring the admittance seen by the port. The following development is essentially that of Baum [5]. It is reproduced here for the sake of completeness.

The single port scatterer problem is defined in Figure 3. In this figure, S_a is the surface of the scatterer, all of which is not shown. The gap which is formed by parting the scatterer with a plane is denoted by S_g. $\hat{a}_g$ is a unit vector defining gap orientation and Δ is the gap width.

Using this geometry, we desire to find the Norton equivalent representation of the antenna as seen by the gap (feed-point). The method is illustrated in Figure 4. The equivalent admittance is found with the aid of Figure 4a. The first step is to specify an electric field at the feed point. The ratio of gap current response to the voltage associated with the specified field yields the terminal admittance. We choose a field that is divergenceless in the gap volume, i.e., a quasi-static electric field. The field is represented then by

$$\vec{E}_g(\vec{r},t) = +V(t)\vec{e}_g(\vec{r}) \ , \qquad (2.1)$$

where $\vec{e}_g(\vec{r}) = \frac{\hat{a}_g}{\Delta}$. $V(t)$ is the gap voltage.

Having defined the electric field across the gap, we need a suitable definition of the current $I(t)$ through the gap. For this we integrate the current density over the surface S_g of the gap and average over the longitudinal direction of the gap.

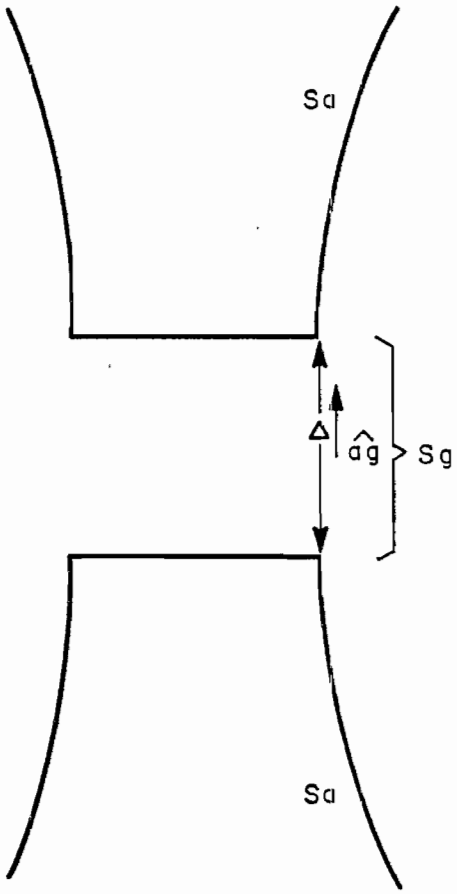

Figure 3: The scatterer/antenna gap geometry.

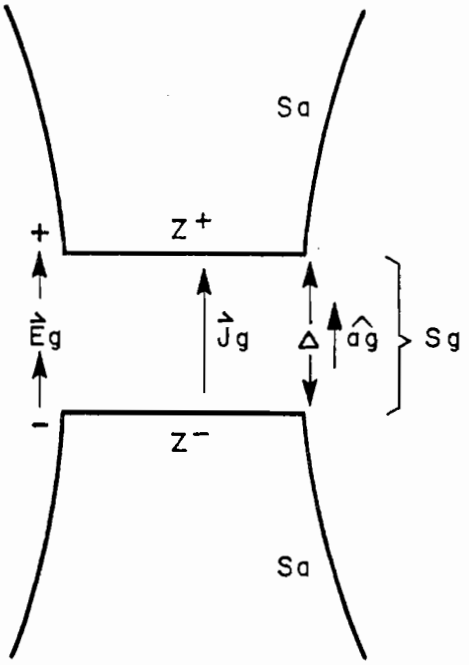

Figure 4a

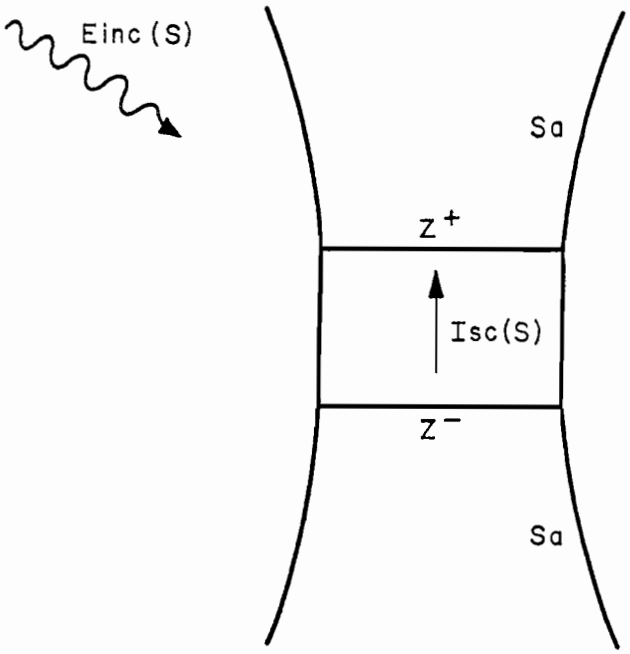

Figure 4b

Figure 4: The scatterer/antenna admittance and short circuit current formulations.

$$I(t) = \int_{S_g} \vec{J}(\vec{r},t) \cdot \vec{e}_g(\vec{r})\, ds\, dz$$

$$= \langle \vec{J}(\vec{r},t) \; ; \; \vec{e}_g(\vec{r}) \rangle_g \qquad (2.2)$$

where $\vec{J}(\vec{r},t)$ is the surface current density, $z^{+,-}$ denote the edges of the gap, and the notation $\langle\rangle_g$ denotes spatial integration over the cylindrical surface forming the gap.

The equivalent admittance of the gap is then

$$\tilde{Y}_g(s) = \frac{\tilde{I}(s)}{\tilde{V}(s)} = \frac{1}{\tilde{V}(s)} \langle \tilde{\vec{J}}(\vec{r},s) \; ; \; \vec{e}_g(\vec{r}) \rangle_g \qquad (2.3)$$

where ~ represents the two-sided Laplace transform.

The procedure for finding the short-circuit current is detailed in Figure 4b. Here the sources are represented by an electric field incident on the antenna. The short-circuit current through the shorted gap is then calculated from Equation (2.2), with $\tilde{\vec{E}}_{inc}(\vec{r},s) = \vec{e}_g(\vec{r})\tilde{V}_{inc}(s)$.

The present work is concerned entirely with the equivalent admittance depicted in Figure 4a and the positive real considerations of that solution. Therefore the derivation of the short-circuit current generator is not given here. Readers interested in this subject are referred to Baum [5].

2.3 Equivalent Admittance Circuits

We construct formal equivalent admittance circuits using the singularity expansion of the current $\tilde{\vec{J}}(\vec{r},s)$ as a tool. Three such circuits are constructed. These circuits, in order of the complexity of the modules from which they are constructed, are composed of

- pole at a time admittances
- pole-pair admittances
- terminal eigenadmittances

The singularity expansion of the current in the frequency domain is [5]

$$\tilde{\vec{J}}(\vec{r},s) = \tilde{V}(s)\left[\sum_n \sum_i \tilde{\eta}'_{ni} \bar{J}_{ni}(\vec{r})(s - s_{ni})^{-1} + \tilde{\vec{J}}^e(\vec{r},s)\right] , \qquad (2.4)$$

where $\tilde{V}(s)$ is the voltage across the gap, $\tilde{\eta}'_{ni}$ is the class I coupling coefficient, and $\bar{J}_{ni}(\vec{r})$ is the natural current mode. The index n indexes over the eigenmode sets of poles, and the index i indexes the individual poles in an eigenmode set. $\tilde{\vec{J}}^e(\vec{r},s)$ is a possible entire function contribution. Several researchers [8] have conjectured this contribution to be zero when the summations are ordered over eigenmodes as indicated in (2.4). The entire function contribution is not considered in this work.

Inserting this form of $\tilde{\vec{J}}(\vec{r},s)$ in Equation (2.3), we obtain

$$\tilde{Y}_g(s) = \left\langle \left[\sum_n \sum_i \tilde{\eta}'_{ni} \bar{J}_{ni}(\vec{r})(s - s_{ni})^{-1} + \tilde{\vec{J}}^e(\vec{r},s)\right] ; \vec{e}_g(\vec{r}) \right\rangle_g \qquad (2.5)$$

or

$$\tilde{Y}_g(s) = \sum_n \sum_i a_{ni}(s - s_{ni})^{-1} + \tilde{Y}^e(s) \qquad (2.6)$$

$$= \sum_n \sum_i \tilde{Y}_{ni}(s) + \tilde{Y}^e(s) , \qquad (2.7)$$

where

$$a_{ni} = \langle \tilde{\eta}'_{ni} \bar{J}_{ni}(\vec{r}) ; \vec{e}_g(\vec{r}) \rangle_g \qquad (2.8)$$

and $\tilde{Y}^e(s)$ is the entire function contribution, if present. The term a_{ni} is termed the residue associated with a pole s_{ni}.

Equation (2.7) is now used to construct formal circuit diagrams. The first of these is given in Figure 5, in which the modules are formed from one pole at a time. In this figure the port representing the antenna gap is on the right, with voltage $\tilde{V}(s)$ across it and current $\tilde{I}(s)$ into it. The modules are placed in parallel as dictated by Equation (2.7), and the entire function modules are also shown.

Many objects, such as dipole antennas, exhibit a zero admittance at zero frequency. It is desirable to modify the above admittance forms to exhibit this property. We do this by subtracting off the value of the admittance at zero. Writing the admittance in this form gives

$$\tilde{Y}_g(s) = \sum_n \sum_i a_{ni} \left[(s - s_{ni})^{-1} + s_{ni}^{-1}\right] + \tilde{Y}^{e'}(s) \qquad (2.9)$$

$$= \sum_n \sum_i \tilde{Y}'_{ni}(s) + \tilde{Y}^{e'}(s) \,, \qquad (2.10)$$

where $Y'_{ni}(s)$ is termed the modified admittance module by Baum. This form differs from the unmodified form by only the addition of a constant term. The equivalent circuit construction with modified admittances would take the same form as Figure 5. We note that the modified form is inappropriate to the pole at zero for multiply connected objects because the subtractive factor is undefined.

Since in general both the residues and poles in Equation (2.6) are complex, pole-at-a-time modules may contain unrealizable elements. This is demonstrated in the next chapter. As a step toward the development of realizable circuits, modules formed by grouping conjugate pole-pairs together are

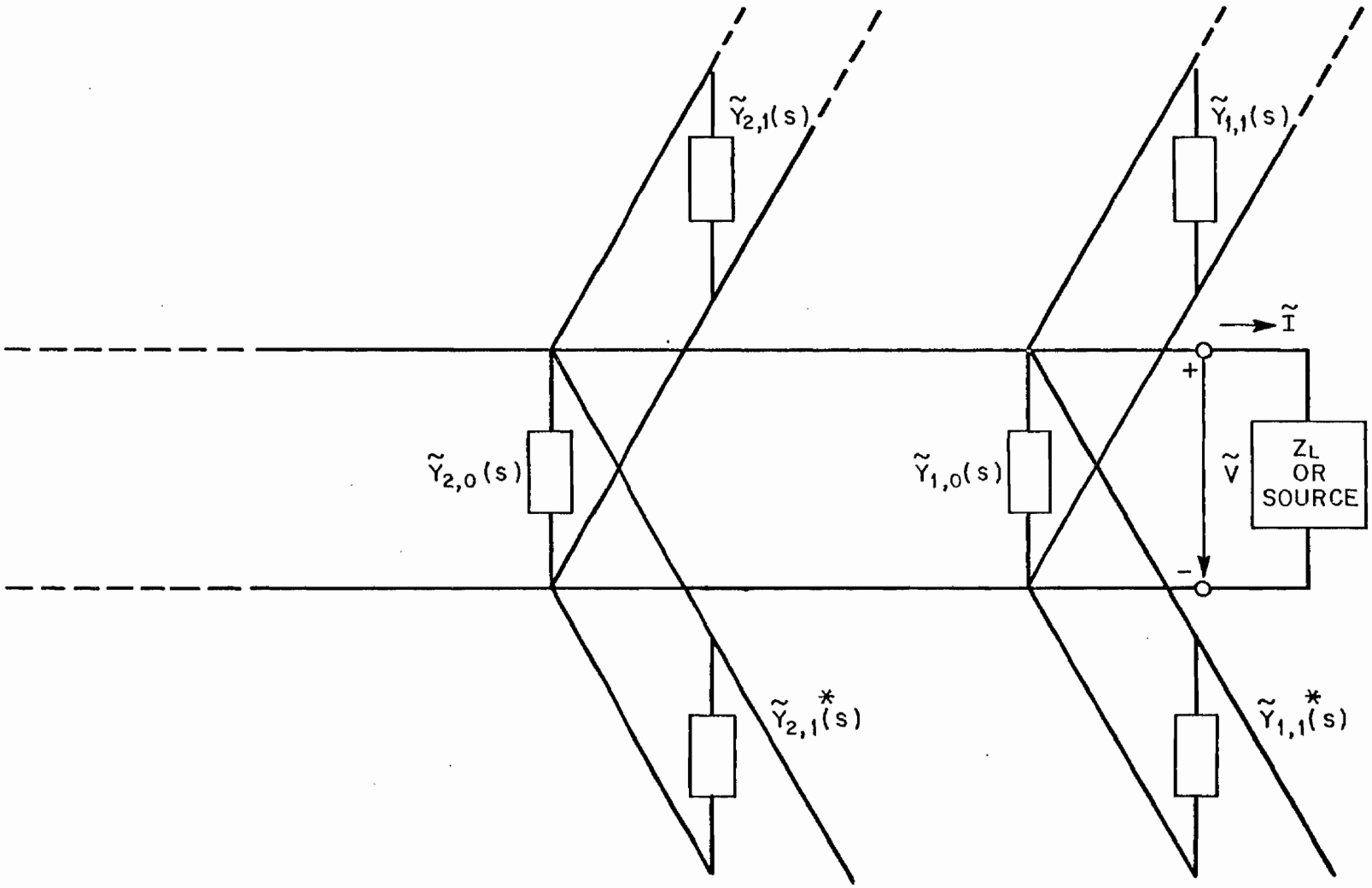

Figure 5: Pole at a time equivalent circuit.

studied. This can be done for both modified and unmodified admittances. In the unmodified case we have, for the pole-pair module,

$$\tilde{Y}_{ni}^{cp}(s) = \tilde{Y}_{ni}^{+}(s) + \tilde{Y}_{ni}^{-}(s) \ , \tag{2.11}$$

where

$$\tilde{Y}_{ni}^{+}(s) = \frac{a_{ni}}{s - s_{ni}} \tag{2.12}$$

and $\tilde{Y}_{ni}^{-}(s)$ is the conjugate. Figure 6 illustrates this circuit arrangement. In this figure admittances whose poles have no imaginary part are designated by $\tilde{Y}_{n0}(s)$.

The final circuit considered consists of terminal eigenadmittance modules, and is represented in Figure 7. Here all poles belonging to an eigenmode are gathered into one module, and the complete circuit is the parallel sum of these modules. Again, either modified or unmodified forms may be used. The module for the n^{th} unmodified eigenadmittance is

$$\tilde{Y}_{n}^{eig}(s) = \sum_{i} \tilde{Y}_{ni}^{cp}(s) + \tilde{Y}_{n0}(s) \ . \tag{2.13}$$

In Chapter III the PRness of these different circuit constructions is discussed, and in Chapter IV passive, realizable circuits are built to give the admittance of straight wire and circular loop antennas.

2.4 Sources of SEM Data

2.4.1 Straight Wire Data

In a previous work Tesche [9] has derived the SEM data for the straight wire, using a method of moments (MoM) solution to Pocklington's

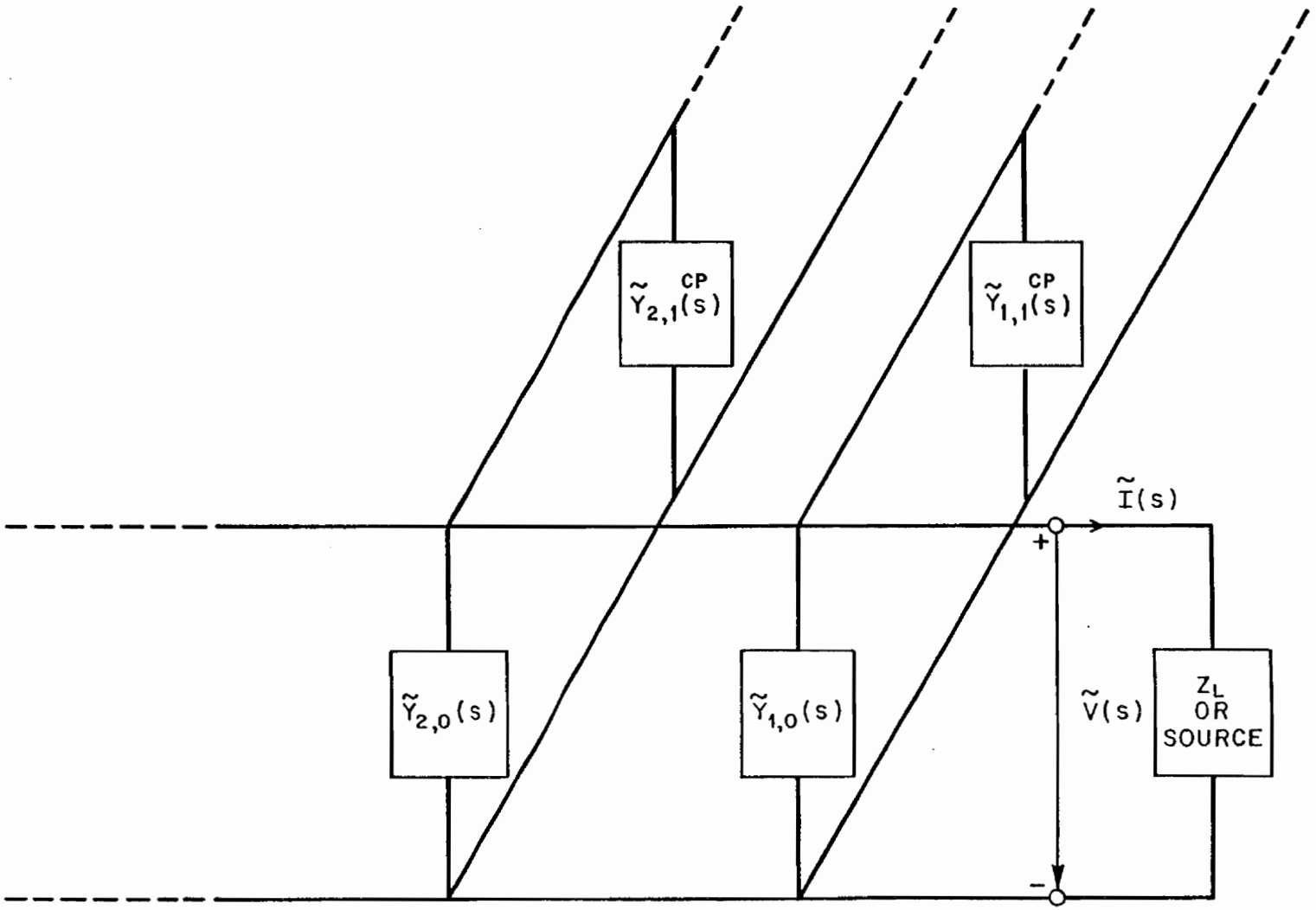

Figure 6: Pole-pair equivalent circuit.

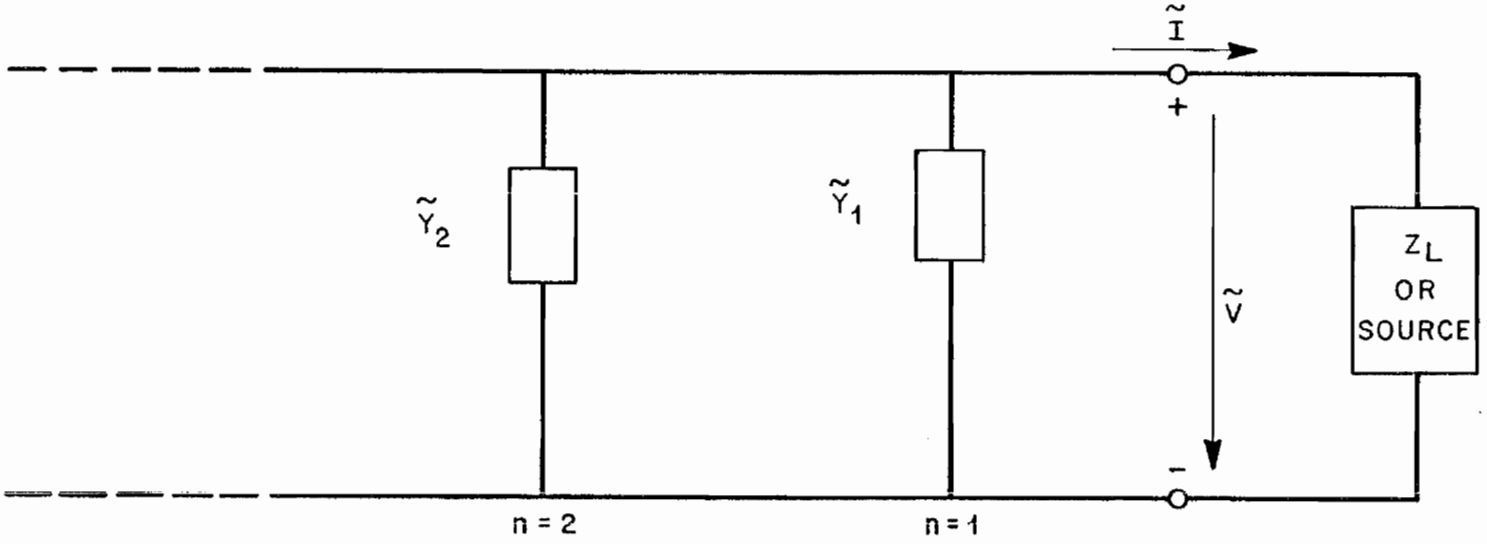

Figure 7: Eigenadmittance equivalent circuit.

integro-differential equation for the axial current flowing on the wire $I(z,s)$. This equation has the form

$$-s\,\varepsilon_0 E^{inc}(z,s) = \left[\frac{\partial^2}{\partial z^2} - \frac{s^2}{c^2}\right]\int_0^L I(z',s)K(z,z',s)\,dz' , \qquad (2.14)$$

where

$$K(z,z',s) = \frac{1}{\pi d}\int_0^{2\pi} \frac{e^{-\frac{s}{c}R}}{4\pi R}\,ad\phi \qquad (2.15)$$

and

$$R = \left[(z - z')^2 + d^2 \sin^2\left(\frac{\phi}{2}\right)\right]^{1/2} \qquad (2.16)$$

and L is the length of the antenna and d is the wire diameter.

When Equation (2.13) is cast into MoM form, the result is

$$\overline{\overline{z(s)}}\;\overline{I(s)} = \overline{V(s)} \ . \qquad (2.17)$$

Here $\overline{\overline{z(s)}}$ is the system nxn matrix, where n is the number of zones on the antenna, and $\overline{I}$ and $\overline{V}$ are, respectively, the response and source vectors, each of dimension n. Using this formulation, then the SEM poles are found by solving

$$\det\,\overline{\overline{z(s_{ni})}} = 0 \qquad (2.18)$$

for the nontrivial solutions. The natural current modes are found from the set of equations

$$\overline{\overline{z(s_{ni})}}\;\overline{I(s_{ni})} = 0 \ . \qquad (2.19)$$

The normalization coefficient β_{ni} is found by computing

$$\beta_{ni} = \frac{1}{\underline{I}_{ni} \frac{\partial}{\partial s} \underline{\underline{z(s)}}\Big|_{s_{ni}} \underline{I}_{ni}} \tag{2.20}$$

Using these equations, an SEM data base was constructed for a straight wire with an aspect ratio (diameter/length) of .01. It was found convenient to use 64 zones for the MoM equations. The resulting data agrees with the results reported by Tesche [9].

The SEM poles for the wire fall in layers in the left-hand s-plane, indicated in Figure 8. Poles are indexed by (m,n), where m is the layer and n is the pole, numbered sequentially by distance from the $\frac{\sigma L}{\pi c}$ axis, where C is the speed of light. Layer one consists of those poles closest to the $j\omega$ axis, layer two of the next closest, etc. Reference to this layer scheme of ordering poles will be made frequently.

2.4.2 Circular Loop Data

The SEM loop data is an important complement to the numerical data derived for the wire, in so much as the electric field integral equation for the loop can be approximately solved analytically due to symmetry by expanding the current into a Fourier series, as done by Wu [10]. Also the loop represents a doubly-connected object, as opposed to the singly-connected wire, and the difference in the SEM representation of the admittance for these two objects can be investigated. Namely the wire evidences zero admittance as $s \to 0$ while the loop admittance does not. Due to the analytical tractability of the loop integral equation it is possible to identify and group the poles by eigenmodes, which will be useful when the investigation of eigenadmittances is made in Chapter III.

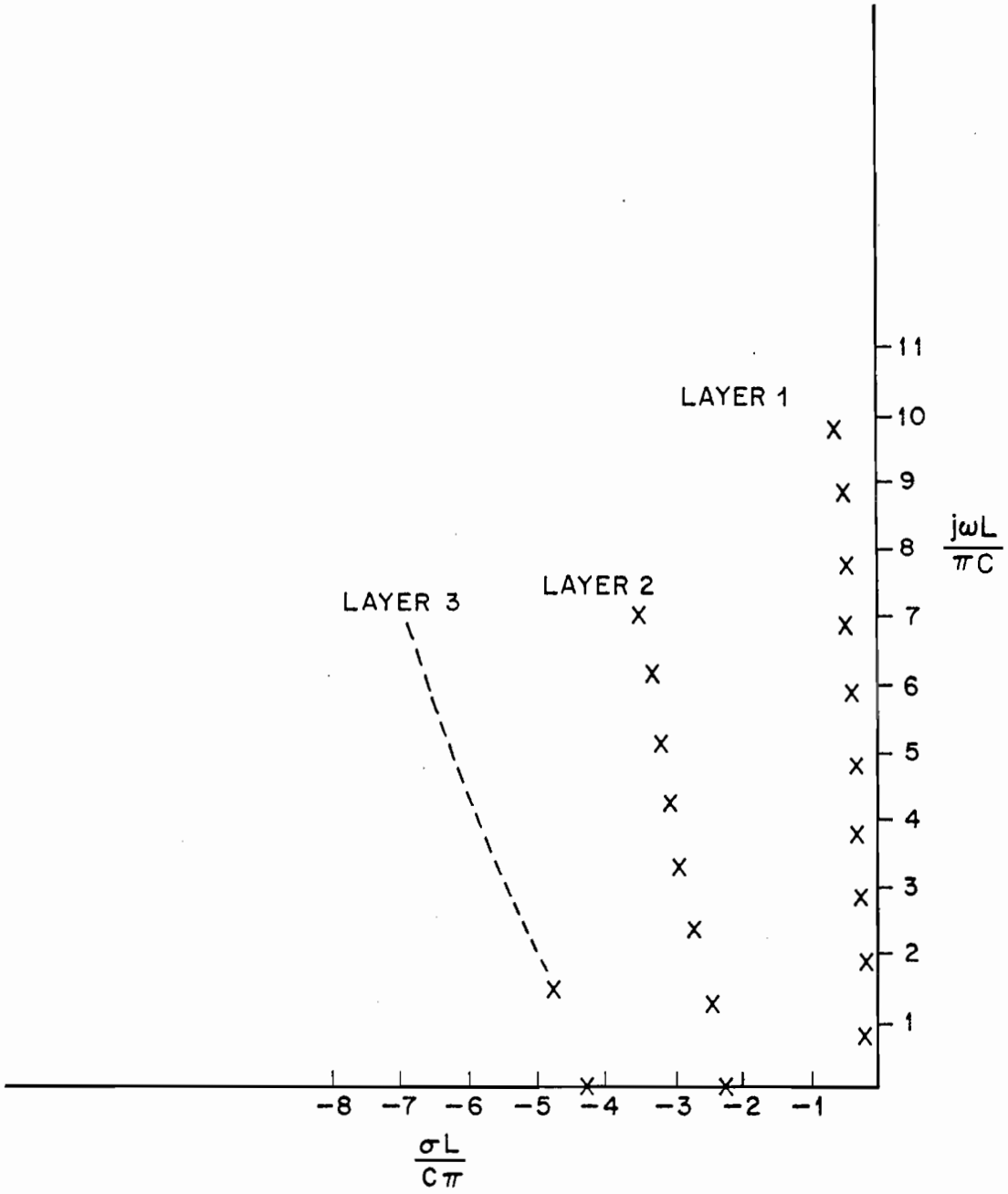

Figure 8: SEM poles for the straight wire.

The SEM current expansion given by Umashankar [11], based on Wu's results, is

$$I(\phi,s) = \frac{\tilde{V}_0(s)}{\eta\pi} \sum_n \sum_i \frac{a_{ni}}{s - s_{ni}} e^{-jn\phi} , \qquad (2.21)$$

where n is the index over modes and i the index over poles in a mode and η is the free space impedance. $\tilde{V}(s)$ is the transform of the input waveform. The modal currents are of the form $e^{-jn\phi}$. Equation (2.21) is the representation from which the gap admittance for the loop is derived. Figure 9 gives the loop geometry.

When discussing the poles of an eigenmode for the loop, Wilton and his co-workers break the poles into three groups [11,12], and this practice will be followed here. Figure 10 shows this classification. The type I pole for a mode is that pole which lies closest to the $j\omega$ axis. Type II poles, of which there are a finite number, lie in a semicircular arc veering towards the negative real axis. Type III poles, which are infinite in number for a mode, lie along the $j\omega$ axis. The SEM data for the loop used in this study was computed by Blackburn [12], and has been fully corroborated by Umashankar [11].

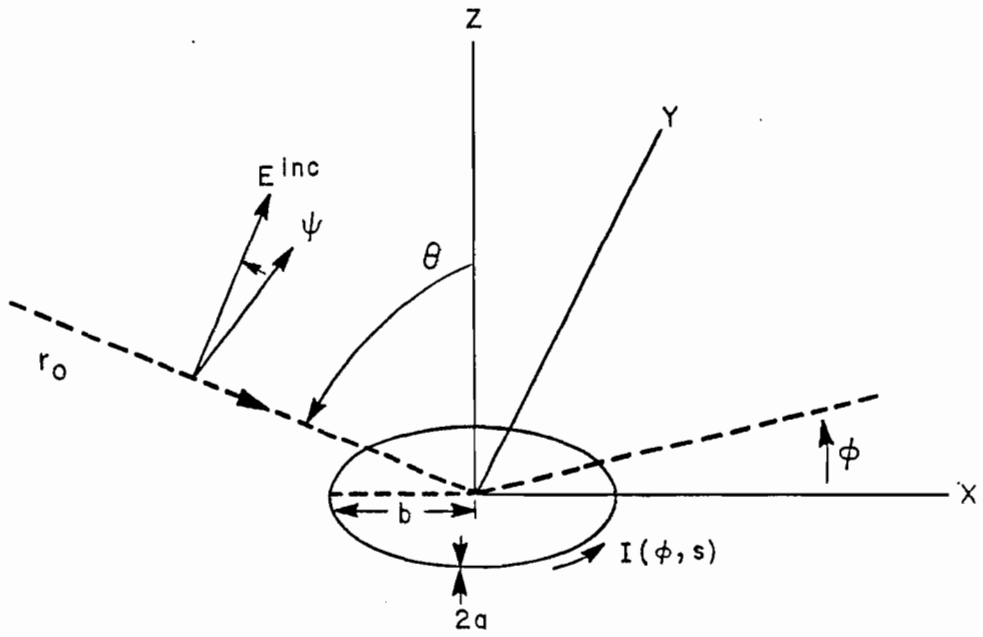

Figure 9: The circular loop geometry.

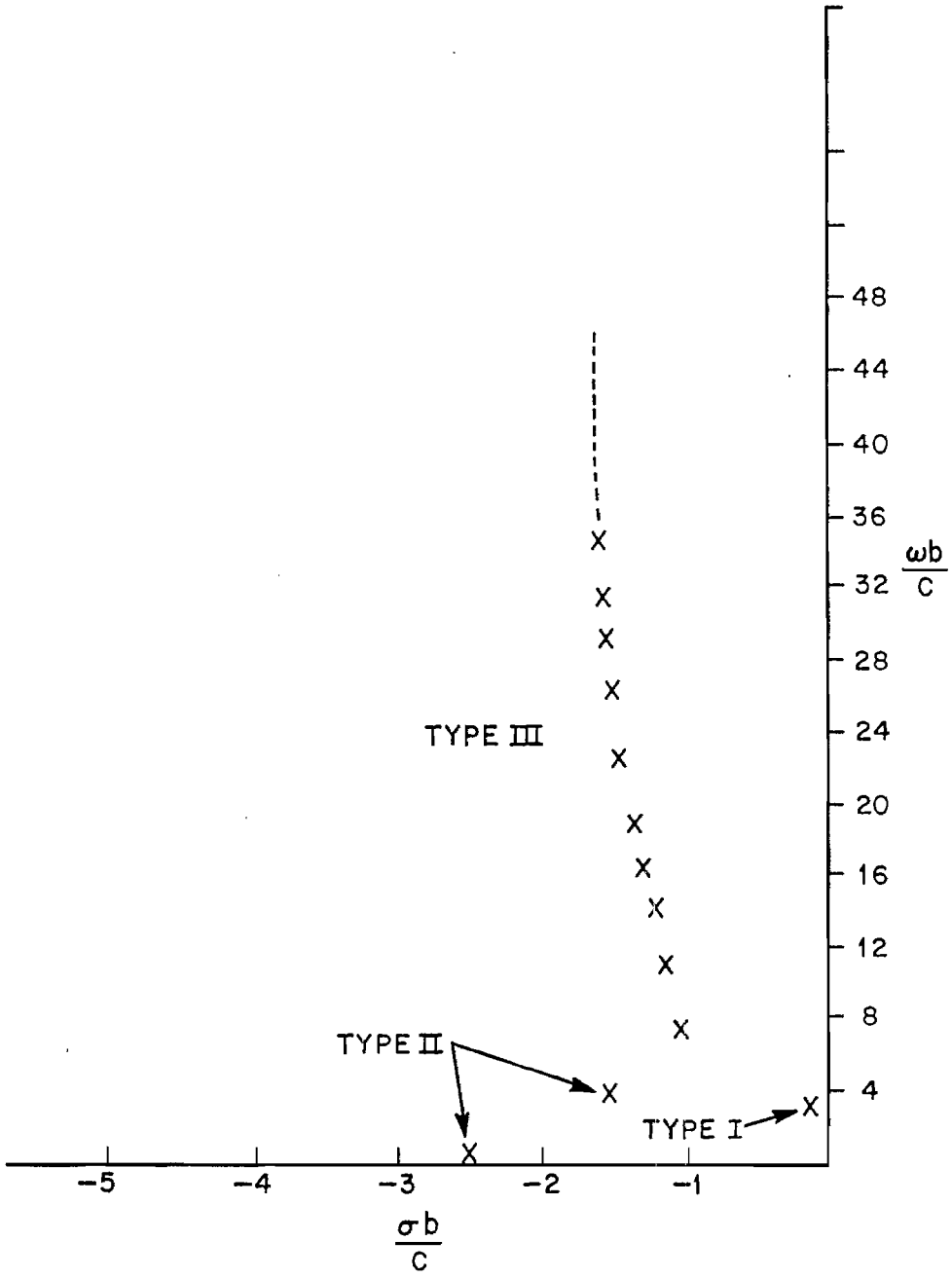

Figure 10: Classification of SEM poles for the circular loop into type I, type II, and type III.

CHAPTER III

POSITIVE REAL CONSIDERATIONS

3.1 Introduction

In this chapter the three different modules (pole-at-a-time, pole-pair, and terminal eigenadmittance) used to construct the equivalent admittance circuits are examined to determine their PRness and hence their realizability. Admittance modules from both the straight wire and circular loop are examined. Parameter tests for PRness, as defined in Chapter I, are constructed and used extensively. Also, the admittances of some modules are studied by graphs depicting the real part along the $j\omega$ axis. The question of the effect of numerical errors on the PRness of modules is addressed.

3.2 Pole-at-a-Time Circuits

Ideally, it would be desirable if the admittance at the feed point could be realized by constructing individual circuit modules on a pole at a time basis, as illustrated in Figure 5. A consideration of the individual modules in detail shows that such a realization is untenable. The admittance of an unmodified module in SEM terms is given by

$$\tilde{Y}_{ni}(s) = \frac{a_{ni}}{(s - s_{ni})} \quad . \tag{3.1}$$

This is recognizable as an RL series circuit, with the values of the inductor and resistor given by

$$L = \frac{1}{a_{ni}} \tag{3.2}$$

and

$$R = -\frac{s_{ni}}{a_{ni}} . \tag{3.3}$$

However, since the SEM data consists generally of complex poles and residues, then the L and R elements take on complex values, and are hence unrealizable. Only in the case where a SEM pole lies on the negative real axis is the circuit realizable.

A consideration of the modified pole at a time circuit module reveals the same situation. Here we have

$$Y'_{ni}(s) = \frac{a_{ni}}{s - s_{ni}} + \frac{a_{ni}}{s_{ni}} = \frac{a_{ni}s}{s_{ni}(s - s_{ni})} . \tag{3.4}$$

The general complex form of the residue guarantees unrealizability.

Given that some SEM poles lie near the jω axis, the question might be asked: Will the imaginary parts of the circuit elements, in either modified or unmodified form, be negligible? Taking the pole which is closest to the jω axis for the wire, for the center-driven case we obtain the following values:

Unmodified	Modified
$L = 833.61 - j233.97$	$C = -1.36 \times 10^{-3} - j1.32 \times 10^{-4}$
$R = 146.39 + j782.47$	$R = 146.39 + j782.47$

We can see from this example that the imaginary parts are not negligible.

3.3 Conjugate Pole-Pair Modules

From the results in Section 3.2, we see that for realization of a circuit, it is necessary to have real coefficients for the powers of s in $\tilde{Y}_{ni}$.

This can be done by combining conjugate pole-pairs into one module. For SEM data, this is done as follows for the unmodified case

$$\tilde{Y}_{ni}^{cp}(s) = \frac{a_{ni}}{s - s_{ni}} + \frac{a_{ni}^*}{s - s_{ni}^*} , \tag{3.5}$$

where * indicates conjugation. Simplifying, we have

$$\tilde{Y}_{ni}^{cp}(s) = \frac{2\ \text{Real}(a_{ni})s - 2\ \text{Real}(a_{ni}^* s_{ni})}{s^2 - 2\ \text{Real}(s_{ni})s + |s_{ni}|^2} . \tag{3.6}$$

Similarly for the modified case we have

$$\tilde{Y}_{ni}^{cp'}(s) = \frac{2\ \text{Real}(a_{ni} s_{ni}^*)s^2 - 2\ \text{Real}(a_{ni}^* (s_{ni})^2)s}{|s_{ni}|^2 (s^2 - 2\ \text{Real}(s_{ni})s + |s_{ni}|^2)} . \tag{3.7}$$

We see that in both cases the coefficients of s are real. In addition, all coefficients in the denominators are positive, since all poles lie in the left-hand part of the complex plane.

In the Introduction, the conditions placed on the residues for the unmodified admittance of Equation (3.6) to be a PR function are given. The conditions for the modified admittance to be PR are derived in the following paragraphs.

Rewrite Equation (3.7) as

$$\tilde{Y}(s) = \frac{d_1 s^2 + d_2 s}{b_1 s^2 + b_2 s + b_3} , \tag{3.8}$$

where

$$d_1 = 2\,\text{Real}(a_{ni}s_{ni}^*) \qquad b_1 = |s_{ni}|^2$$

$$d_2 = -2\,\text{Real}(a_{ni}^*(s_{ni})^2) \qquad b_2 = -2|s_{ni}|^2\,\text{Real}(s_{ni})$$

$$b_3 = |s_{ni}|^4 .$$

Then the real part of $\tilde{Y}(s)$ at $s = j\omega$ is

$$\text{Real}\,\tilde{Y}(s) = \frac{d_1b_1\omega^4 + (d_2b_2 - d_1b_3)\omega^2}{b_1^2\omega^4 + (b_2^2 - 2b_1b_3)\omega^2 + b_3^2} . \tag{3.9}$$

Because the denominator formed in this way is the square of an absolute value, it is always positive. Thus the question of $\tilde{Y}(s)$ being positive real devolves to

$$d_1b_1\omega^4 + (d_2b_2 - d_1b_3)\omega^2 \geq 0 \qquad \text{for } \omega \geq 0 . \tag{3.10}$$

Setting the first derivative of this function to zero to find the extrema yields such a point at $\omega = 0$. Since this point must be a minimum for a PR function, evaluating the second derivative at $\omega = 0$ yields the first, low frequency, PR condition

$$2(d_2b_2 - d_1b_3) \geq 0 . \tag{3.11}$$

The other PR condition is obtained from observing that Equation (3.10), to be PR at high frequency, must have a nonnegative coefficient for the ω^4 term. This yields the condition

$$d_1b_1 \geq 0 . \tag{3.12}$$

These conditions are seen to be necessary and sufficient for Equation (3.7) to be PR. Translating the coefficients of these two conditions into the pole and residue terms, where $a_{ni} = \alpha_{ni} + j\beta_{ni}$ and $s = \sigma_{ni} + j\omega_{ni}$, we get

$$2|s_{ni}|^2(\alpha_{ni}\sigma_{ni} + \beta_{ni}\omega_{ni}) \geq 0 \tag{3.13}$$

and

$$4|s_{ni}|^2\left[\alpha_{ni}\sigma_{ni}\left(\sigma_{ni}^2 - 3\omega_{ni}^2\right) + \beta_{ni}\omega_{ni}\left(3\sigma_{ni}^2 - \omega_{ni}^2\right)\right] \geq 0 . \tag{3.14}$$

Equation (3.13) is called the high frequency parameter test for modified pole-pair admittances and (3.14) is the low frequency parameter test, also for modified pole-pair admittances. Both of these tests must be met (i.e., ≥ 0) for the modified pole-pair admittance to be PR. The parameter test for unmodified pole-pair admittances is derived in Chapter I and repeated here as

$$-\alpha_{ni}\sigma_{ni} - |\beta_{ni}|\omega_{ni} \geq 0 . \tag{3.15}$$

For convenience we name Equation (3.15) parameter test I, the low frequency condition of Equation (3.14) parameter test IIA, and the high frequency condition of Equation (3.13) parameter test IIB.

The usefulness of these tests is illustrated in Figures 11 through 15. These figures display the parameter tests for both modified and unmodified pole-pair admittances for the first five poles of the first layer of the straight wire, and illustrate how the values of the tests vary as a function of the gap location on the wire. The solid line is the parameter test for unmodified pole-pair admittances and the dashed lines are for the modified admittances. PR regions for both admittance forms are marked by shading.

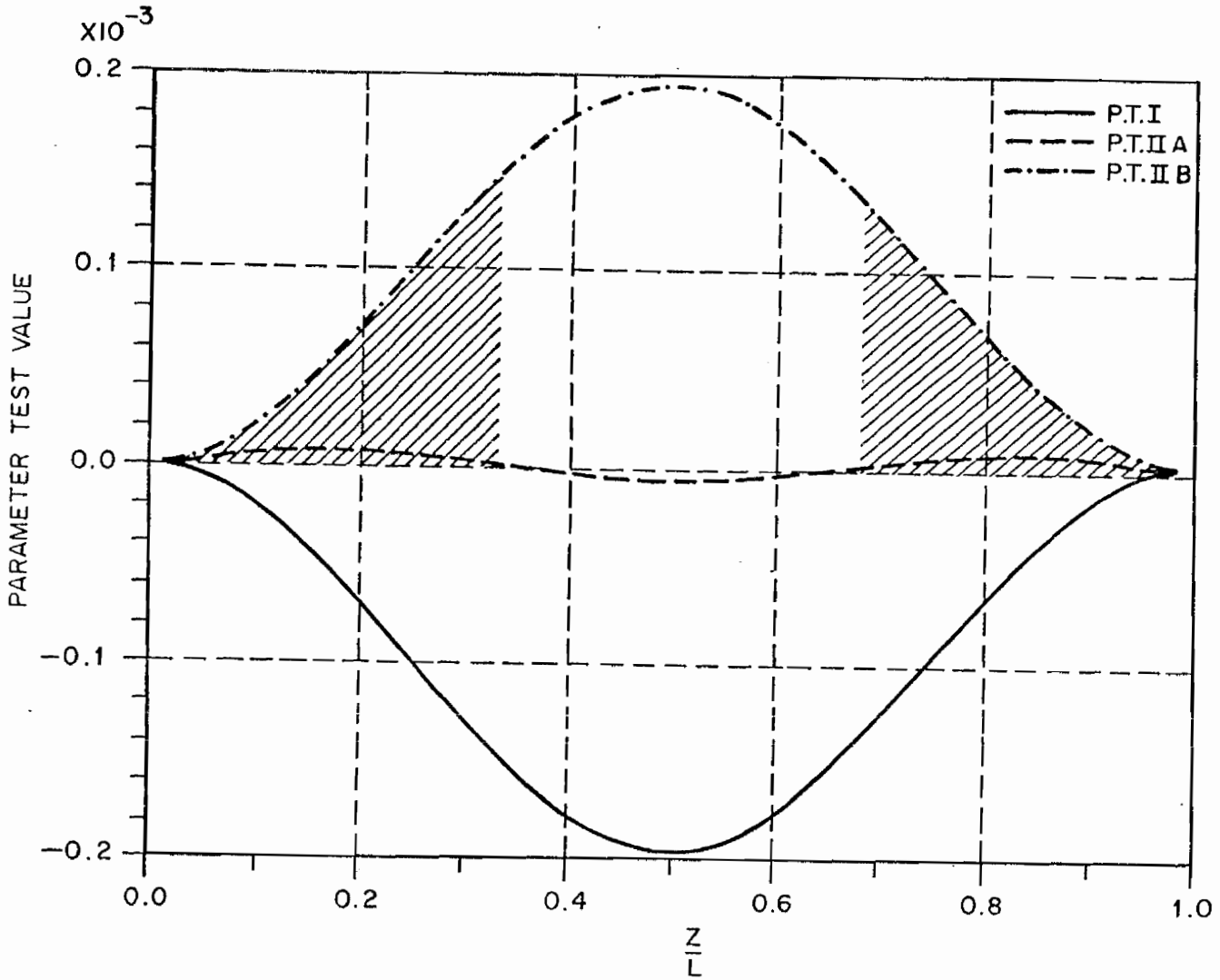

Figure 11: Parameter tests for straight wire pole-pair admittances of pole 1, first layer. The shading indicates where the PR conditions are met, in either modified (dashed lines) or unmodified (solid line) admittances.

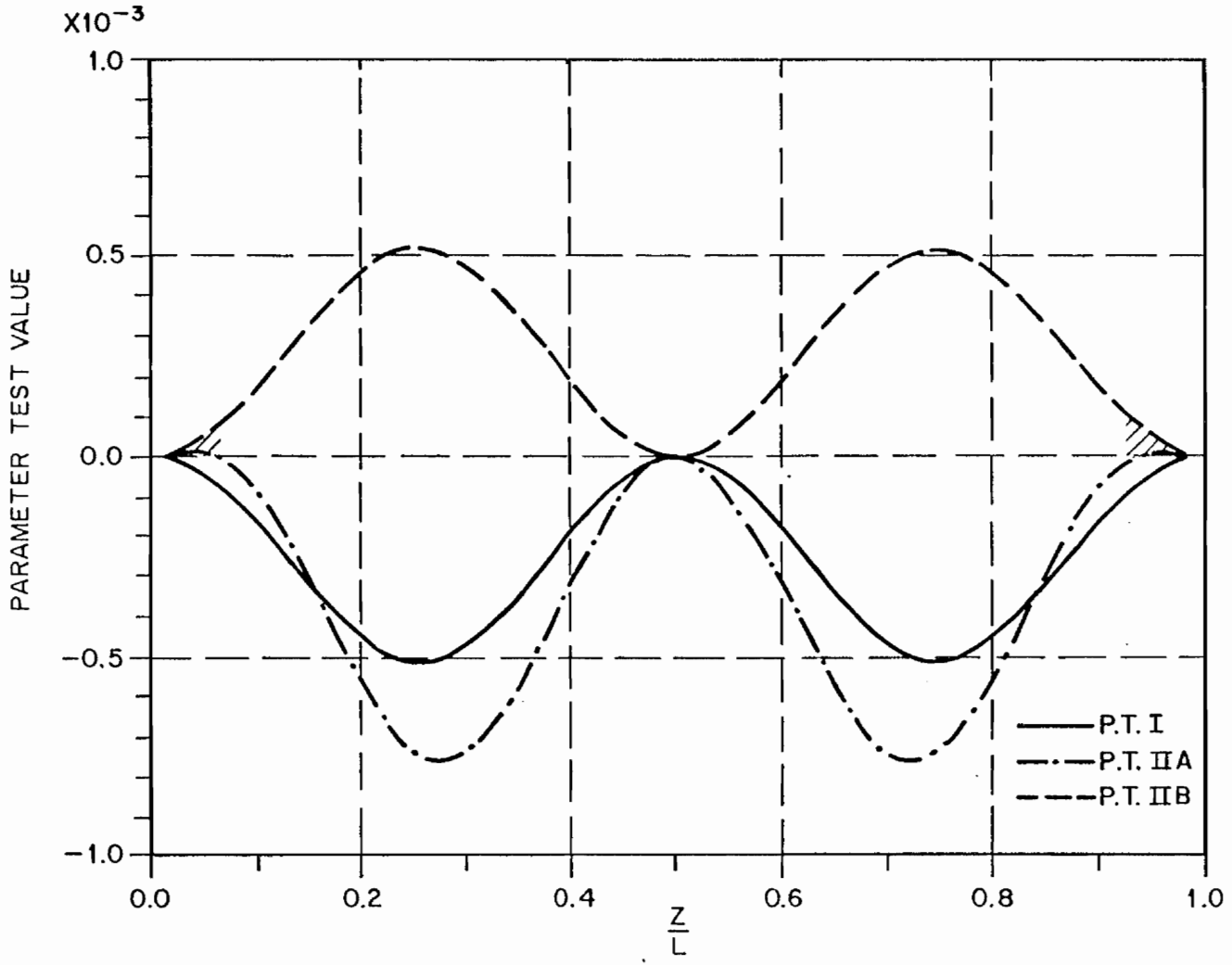

Figure 12: Parameter tests for straight wire pole-pair admittances of pole 2, first layer.

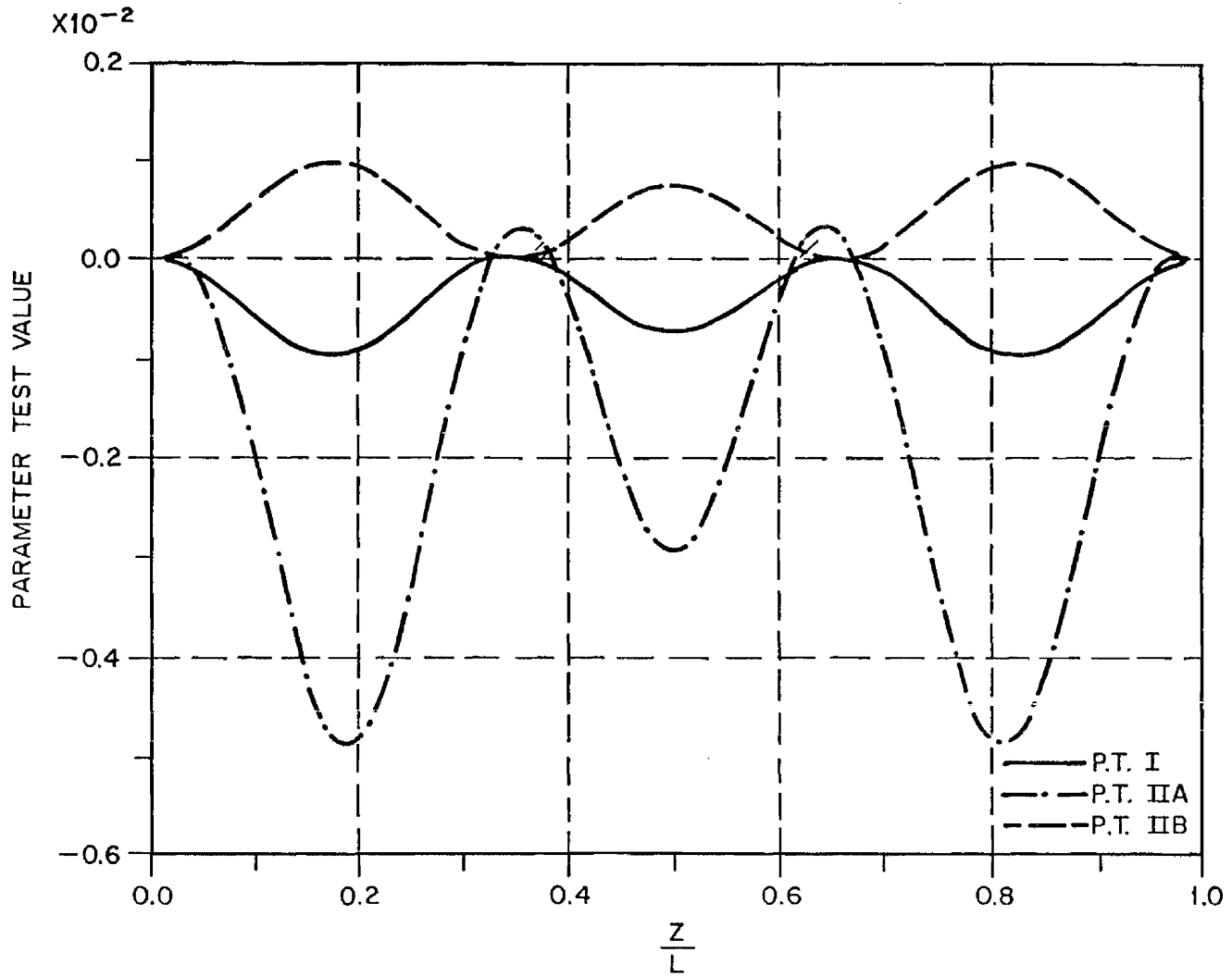

Figure 13: Parameter tests for straight wire pole-pair admittances of pole 3, first layer.

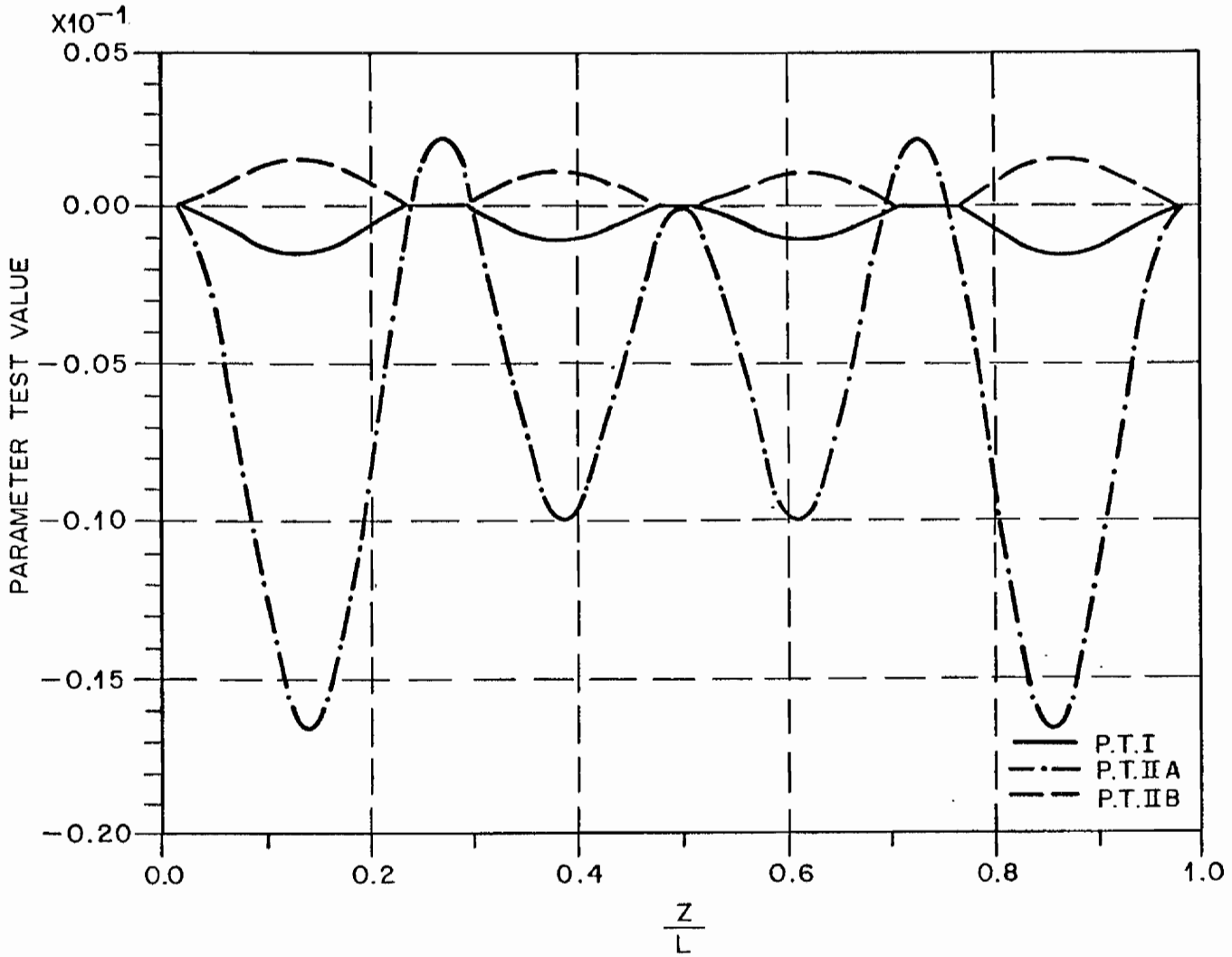

Figure 14: Parameter tests for straight wire pole-pair admittances of pole 4, first layer.

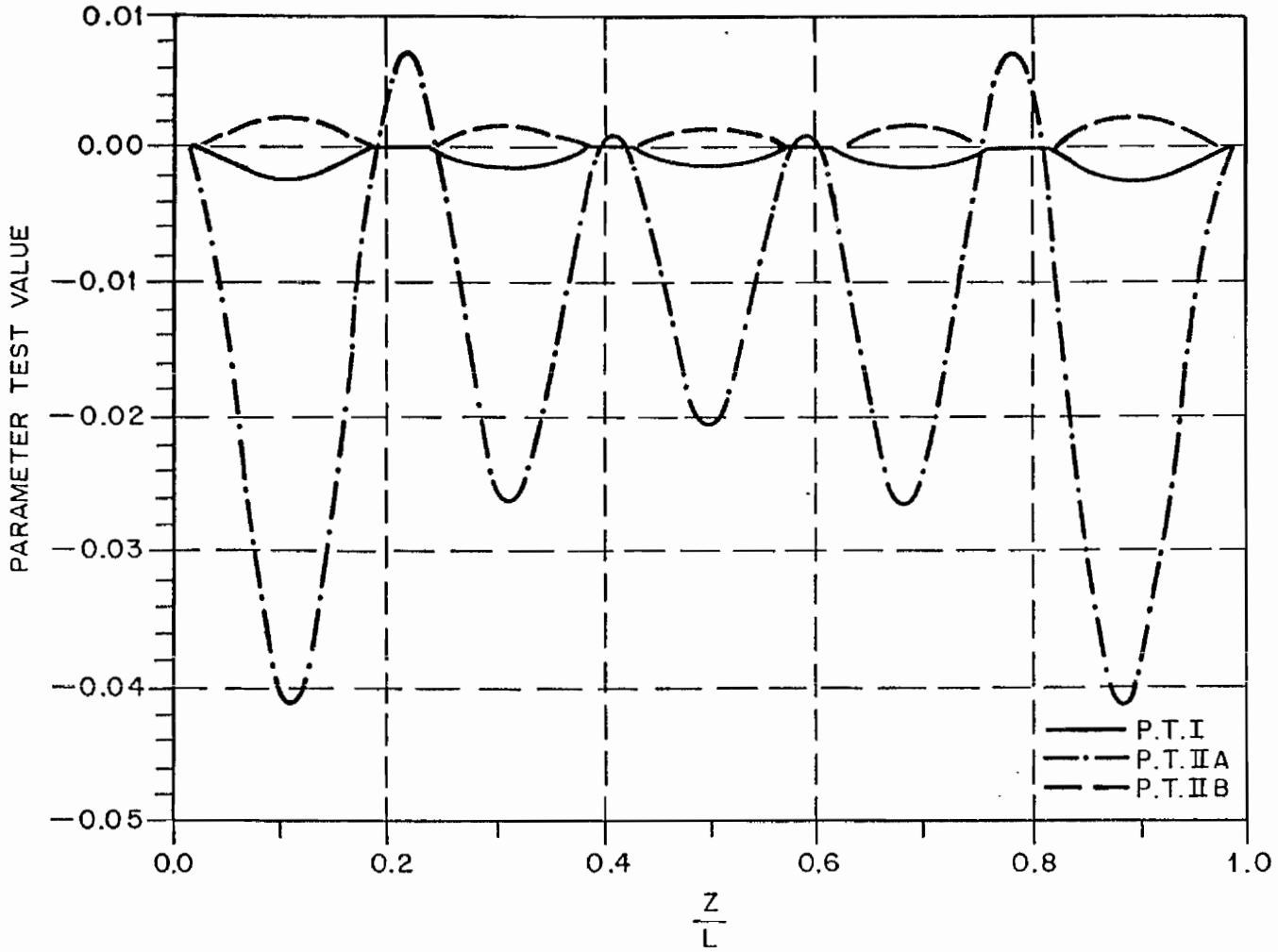

Figure 15: Parameter tests for straight wire pole-pair admittances of pole 5, first layer.

The x-axis is the normalized distance from one end of the antenna, and the y-axis is the value of the parameter tests. For the equivalent circuit corresponding to a particular feed location to be realizable on a pole-by-pole basis, the pole-pair admittance for each pole-pair must be PR.

Note that for these first layer poles, which are the primary contributors to the circuit admittance due to their proximity to the $j\omega$ axis, only the important case of pole 1 seems to be PR (in modified form) over a wide region of the wire. Also note that in no case for the first layer poles is the unmodified form of the admittance realizable, and for the modified form, apart from pole 1, only isolated spots on the antenna appear PR. Figures 16 through 19 indicate the parameter tests for the first three pole-pair admittances of the second layer which lie off the real axis, and the second pole-pair admittance of the third layer.

These graphs indicate only a qualitative measure of positive realness, however. If we look at the real part of the modified conjugate pole-pairs directly, greater insight into the realizability is available. Figures 20 through 27 display the real part of the modified admittance along the $j\omega$ axis for the first five poles of the first layer for the center and quarter locations of the wire. Figures 28 through 32 show the real part of the pole-pair admittances of the second layer poles.

In these graphs the solid line indicates the modified pole-pair admittance real part. The dashed line indicates the amount of shift between the modified and unmodified admittance. In other words, the dashed lines indicate the zero axis for the modified form. Several facts can be observed from these graphs. The first layer poles are the primary contributors to the admittance, as their peaks are 25 to 100 times greater than the peaks of the

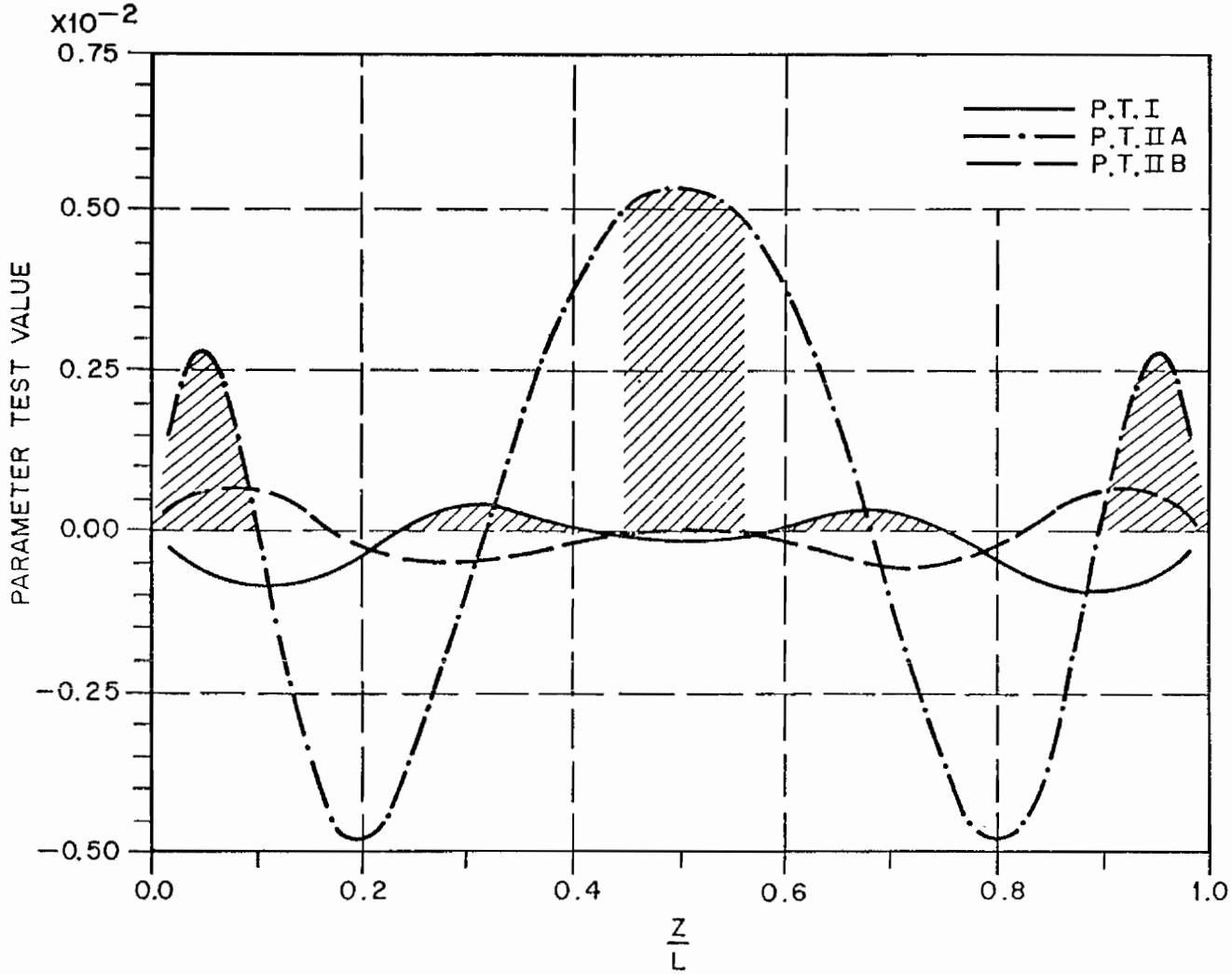

Figure 16: Parameter tests for straight wire pole-pair admittances of pole 2, second layer.

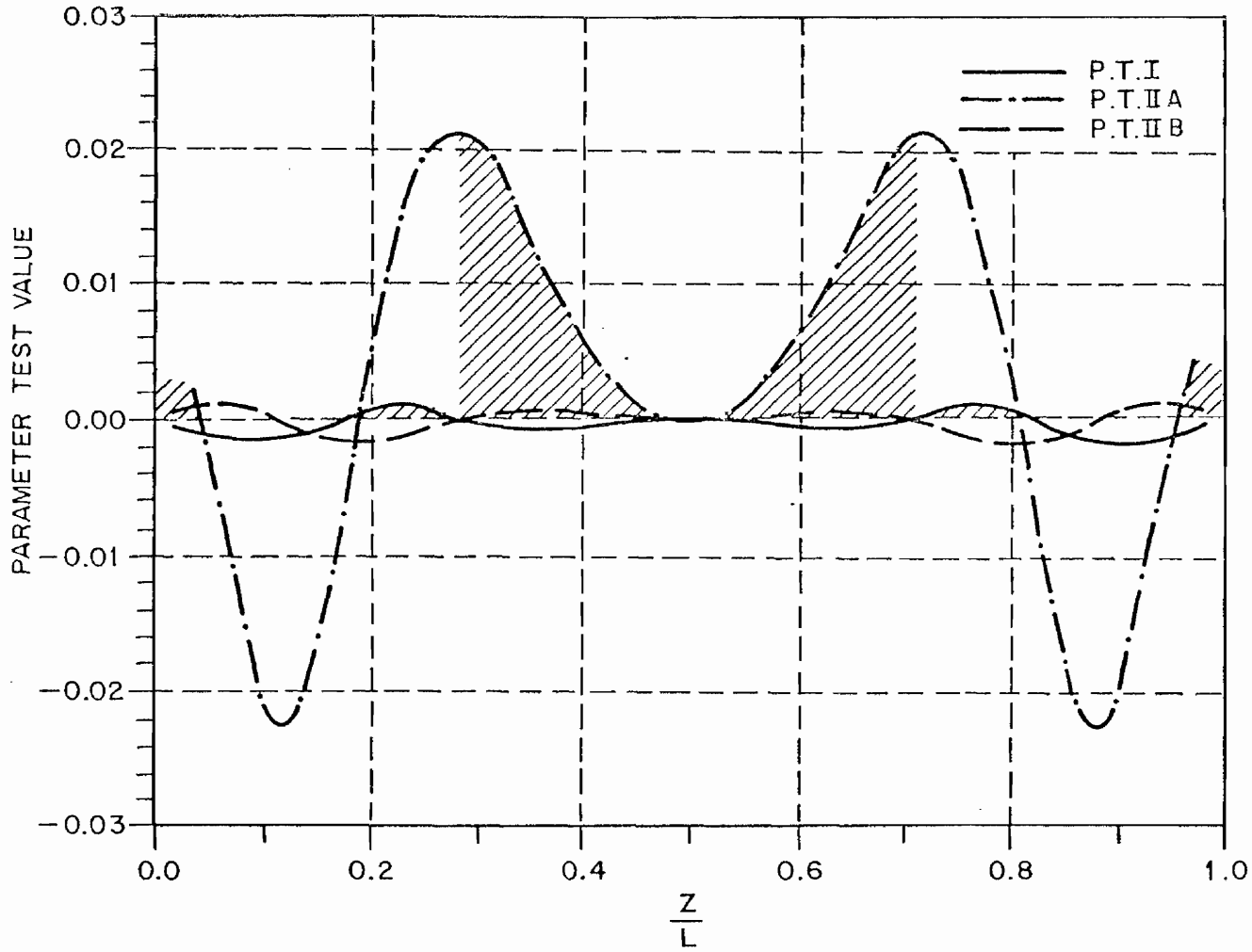

Figure 17: Parameter tests for straight wire pole-pair admittances of pole 3, second layer.

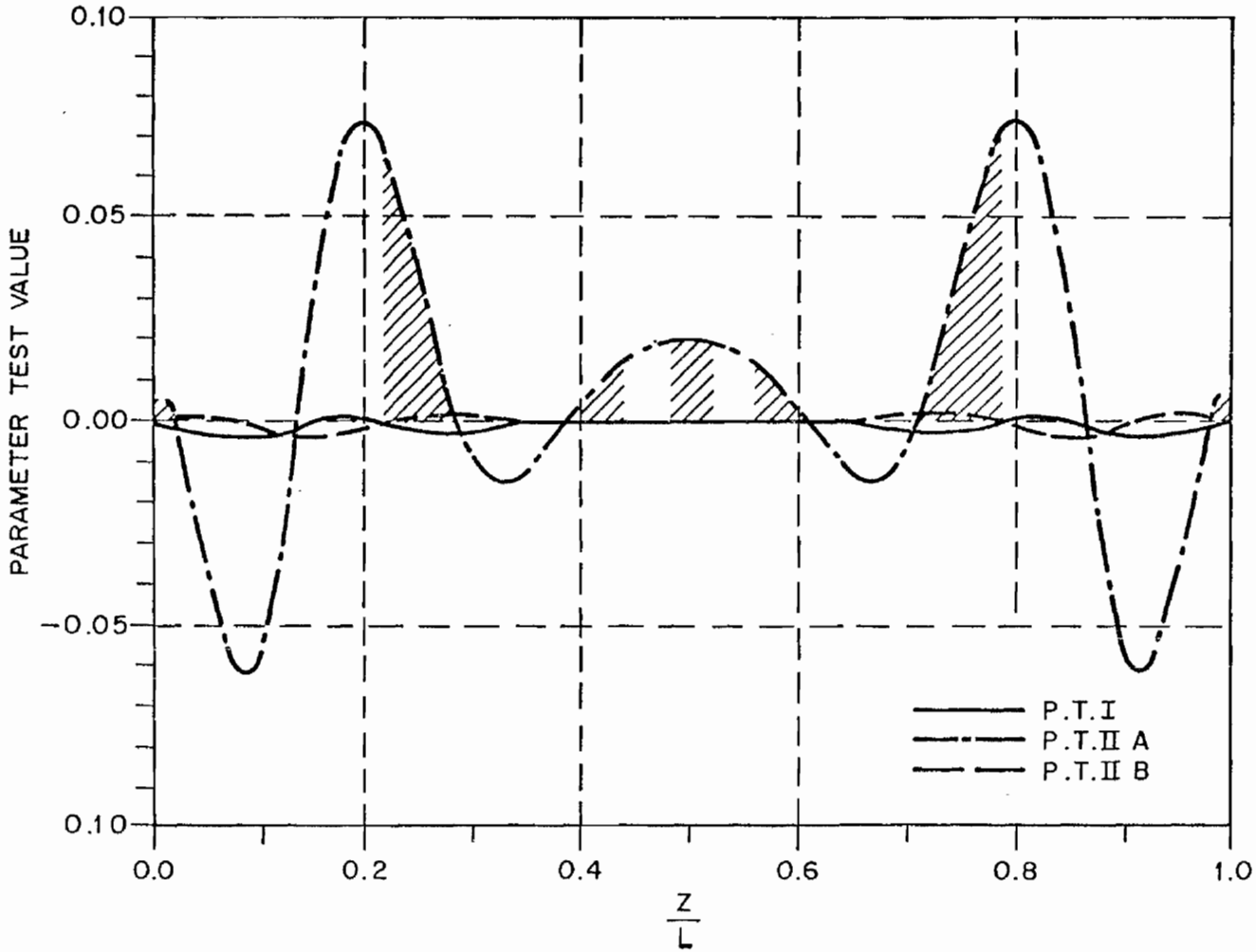

Figure 18: Parameter tests for straight wire pole-pair admittances of pole 4, second layer.

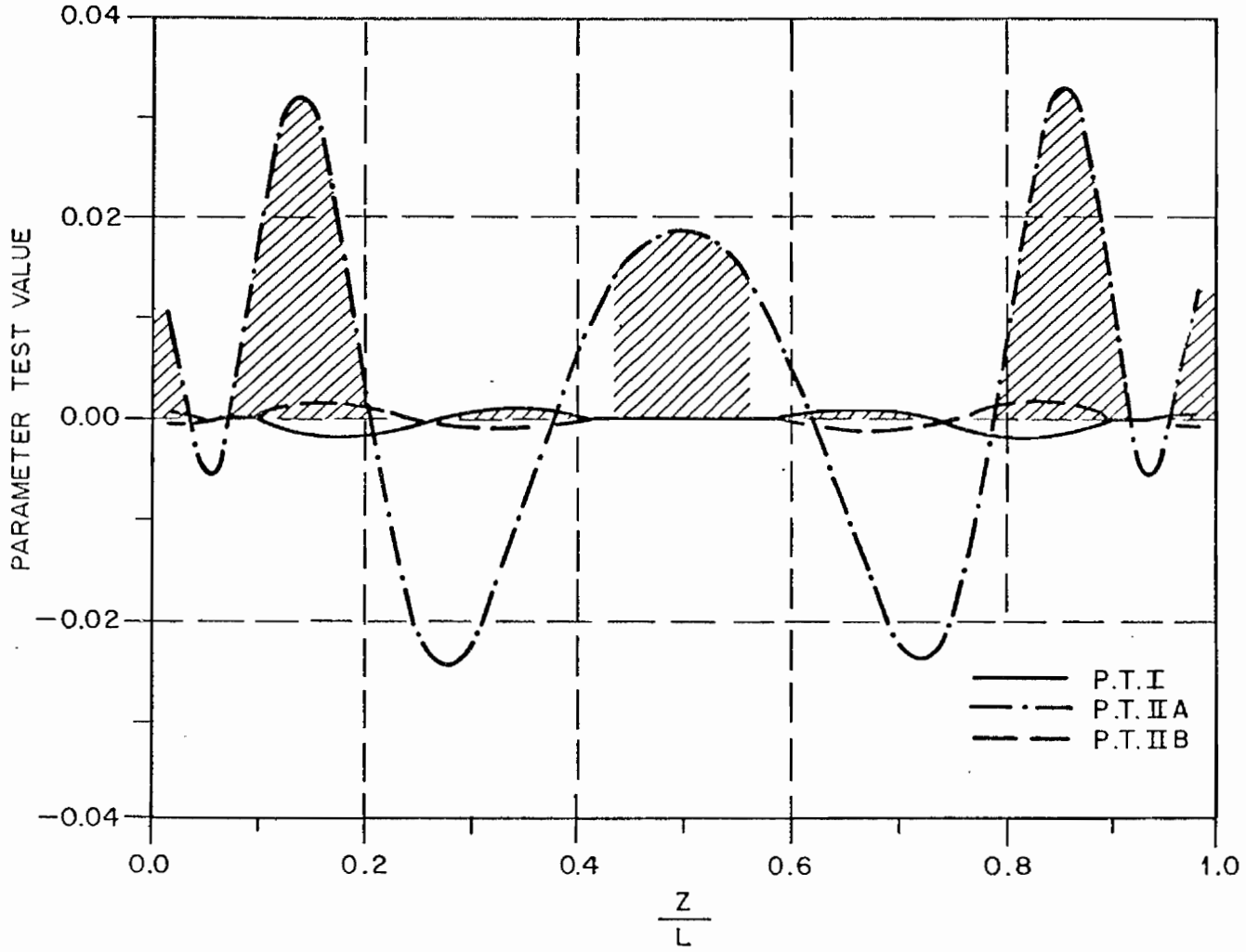

Figure 19: Parameter tests for straight wire pole-pair admittances of pole 2, third layer.

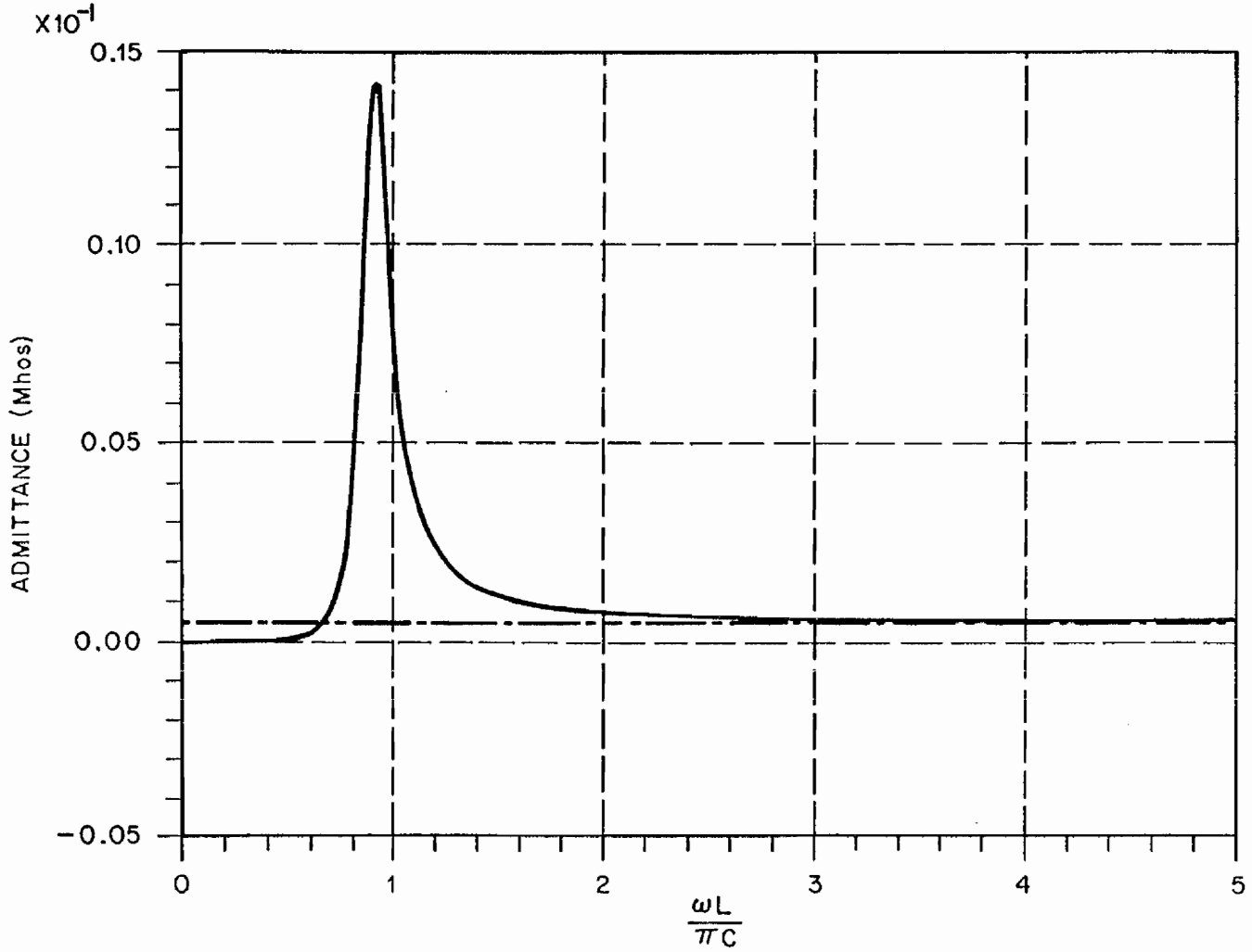

Figure 20: Real part of straight wire pole-pair admittance at z/L = .5 for pole 1, first layer. There is a slight negative area in the low frequency region.

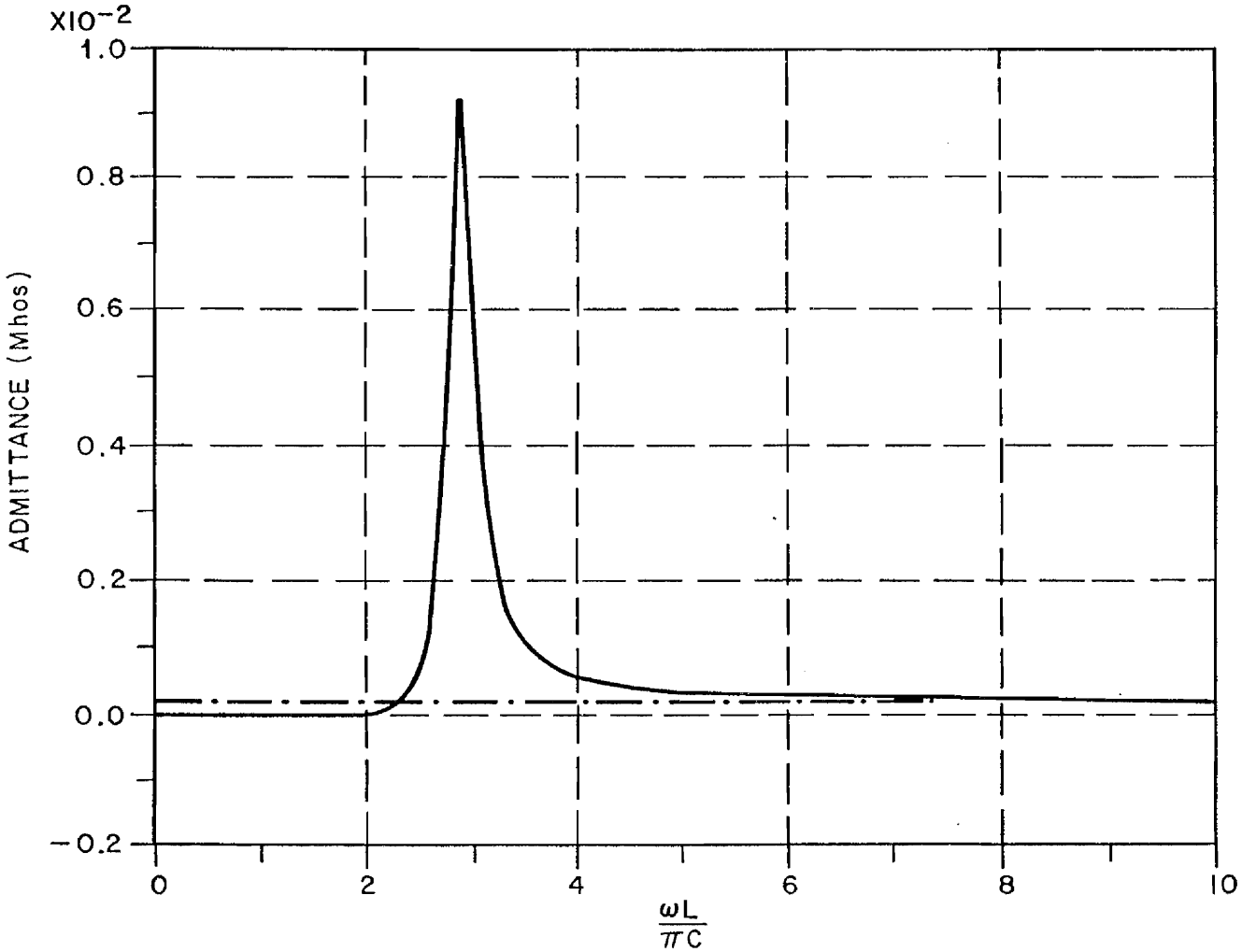

Figure 21: Real part of straight wire pole-pair admittance at z/L = .5 for pole 3, first layer. There is a slight negative area in the low frequency region.

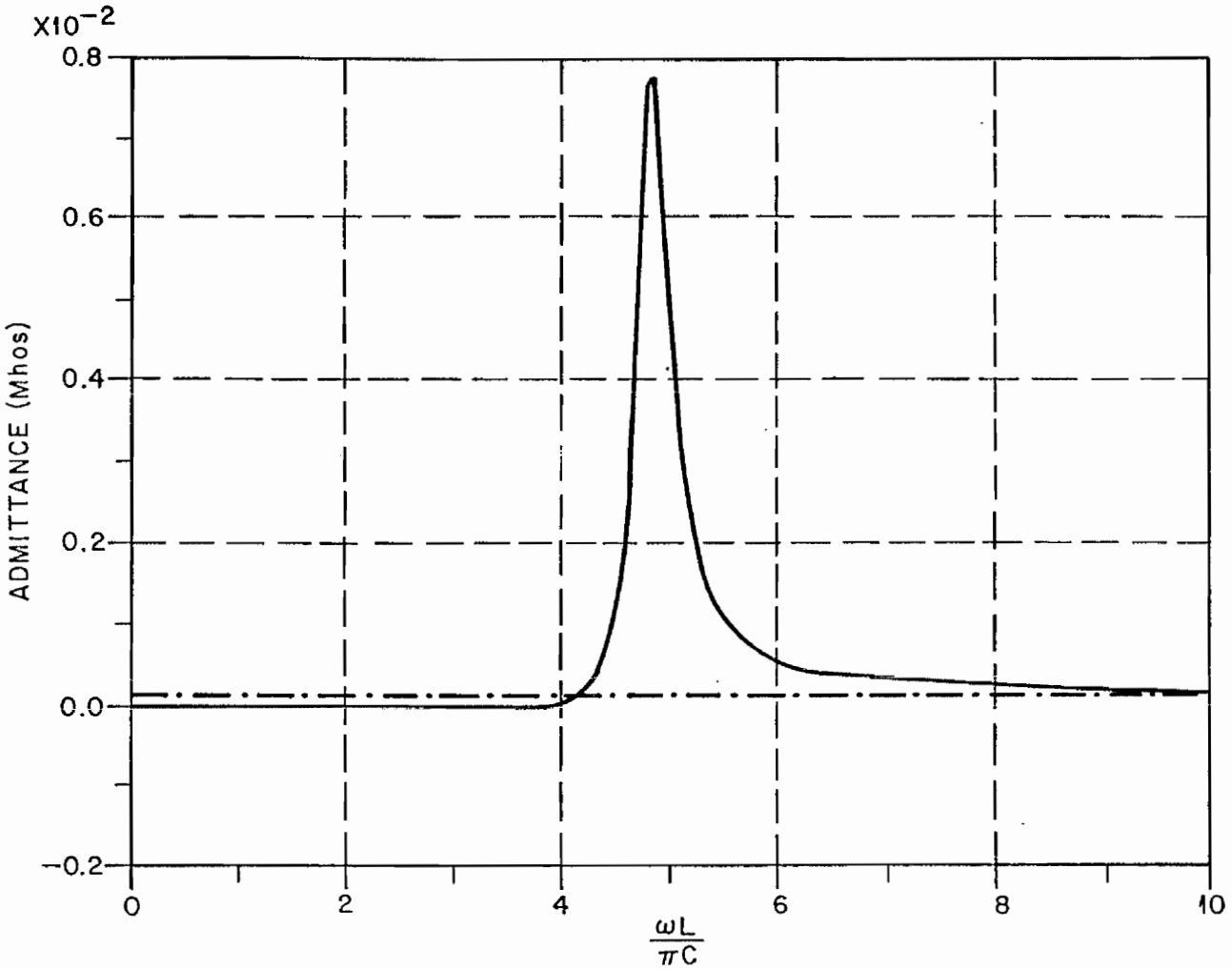

Figure 22: Real part of straight wire pole-pair admittance at z/L = .5 for pole 5, first layer. There is a small negative area in the low frequency region.

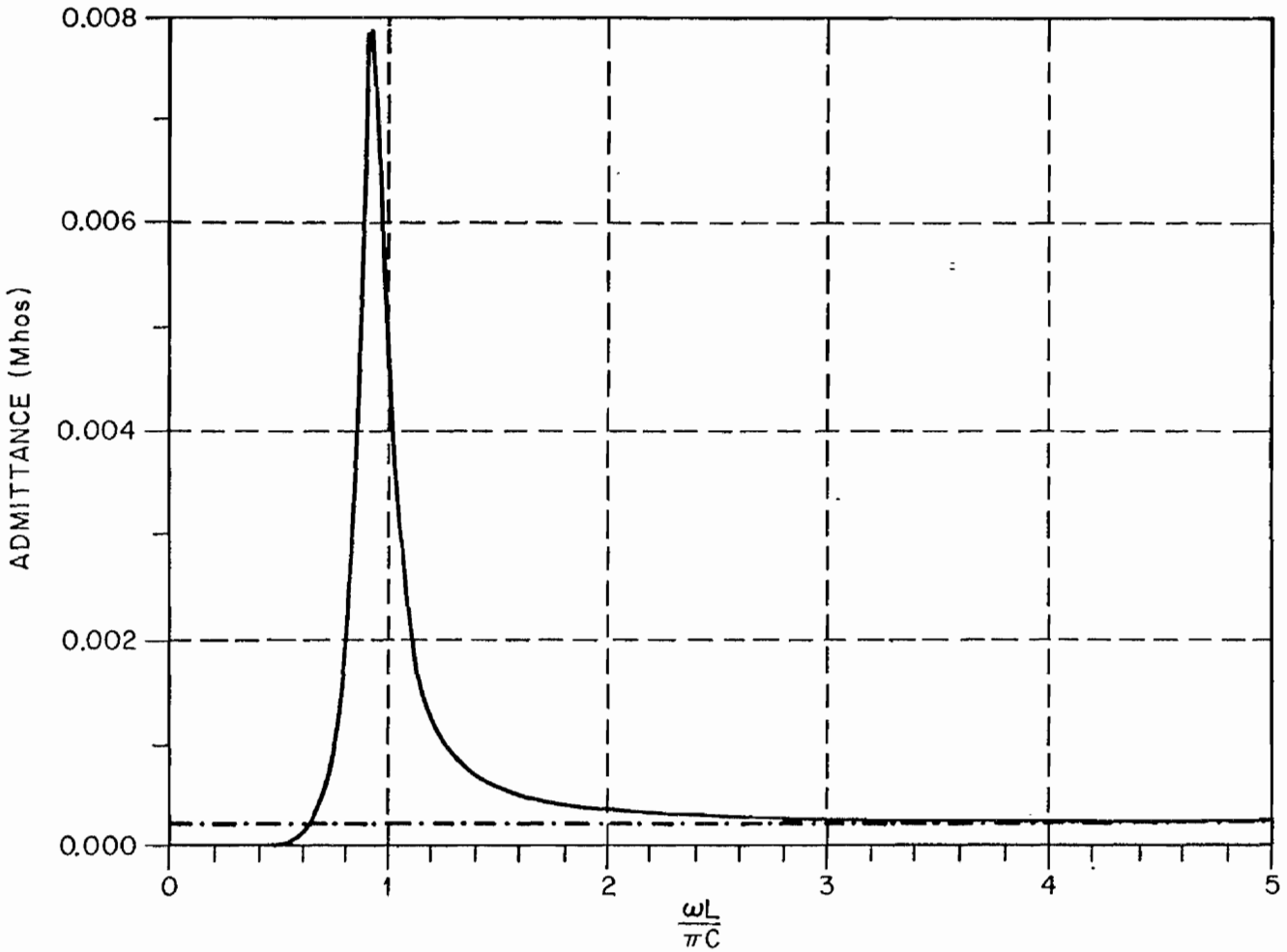

Figure 23: Real part of straight wire pole-pair admittance at z/L = .25 for pole 1, first layer. It is entirely positive.

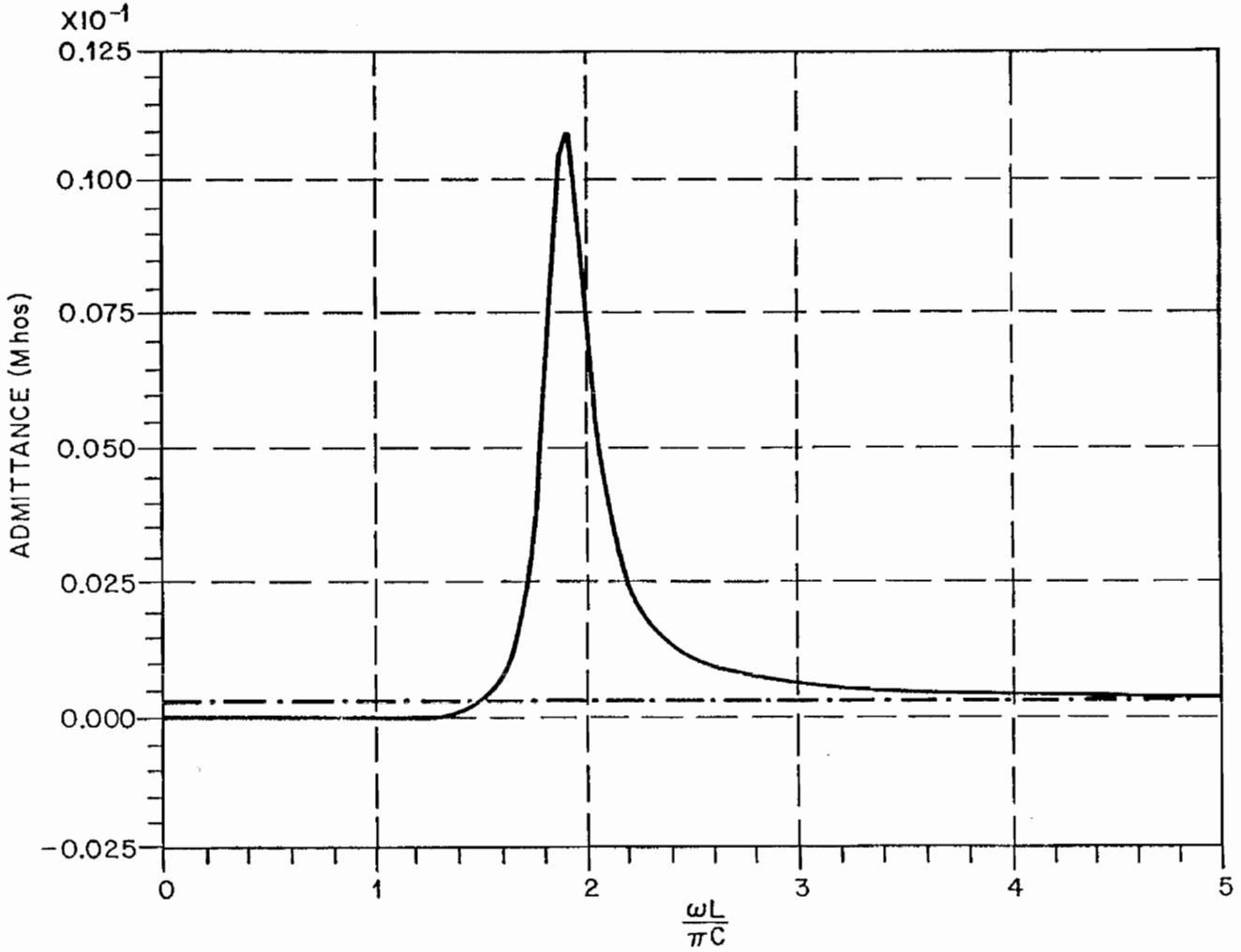

Figure 24: Real part of straight wire pole-pair admittance at z/L = .25 for pole 2, first layer. Ther is a slight negative area in the low frequency region.

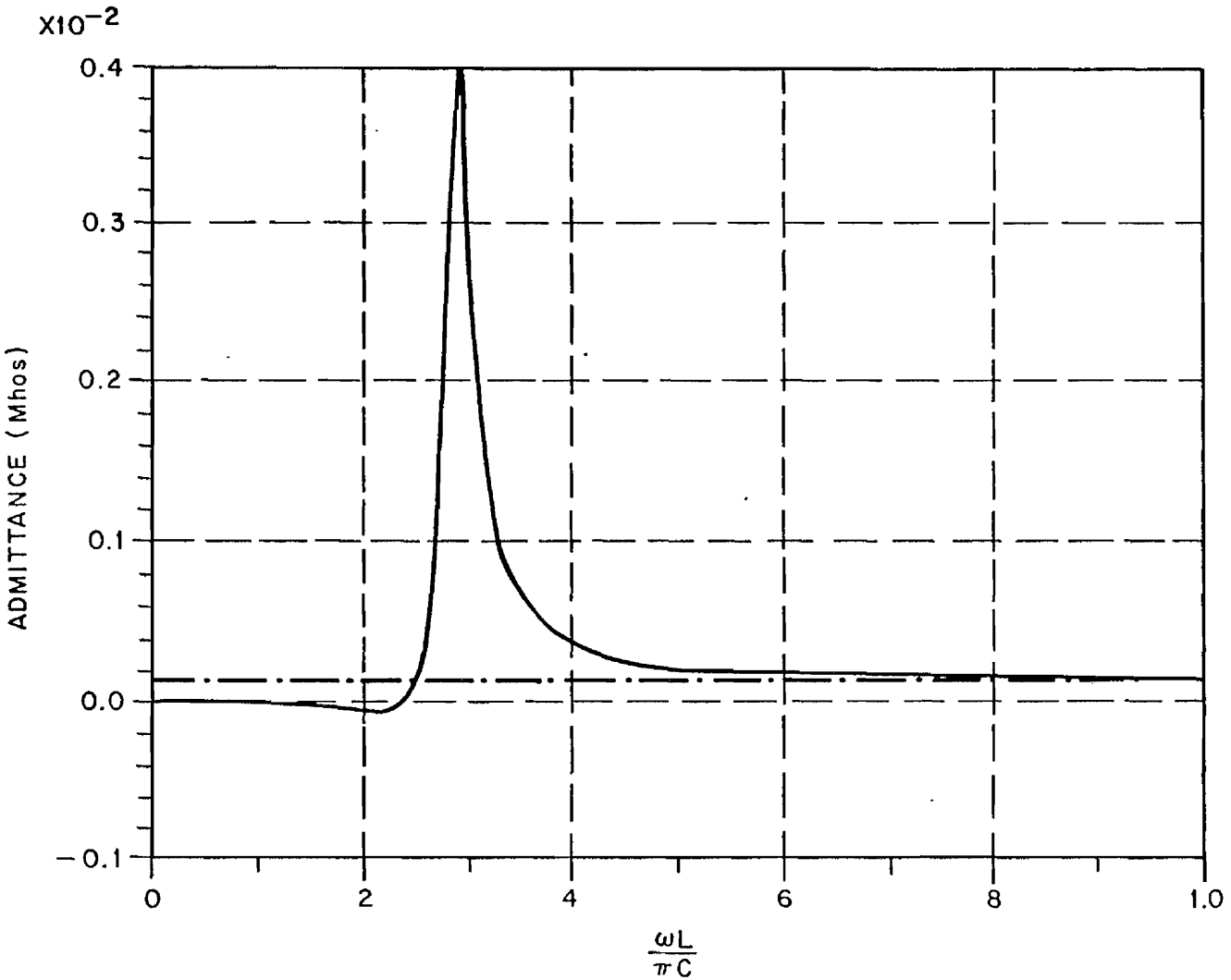

Figure 25: Real part of straight wire pole-pair admittance at z/L = .25 for pole 3, first layer. The negative area is apparent.

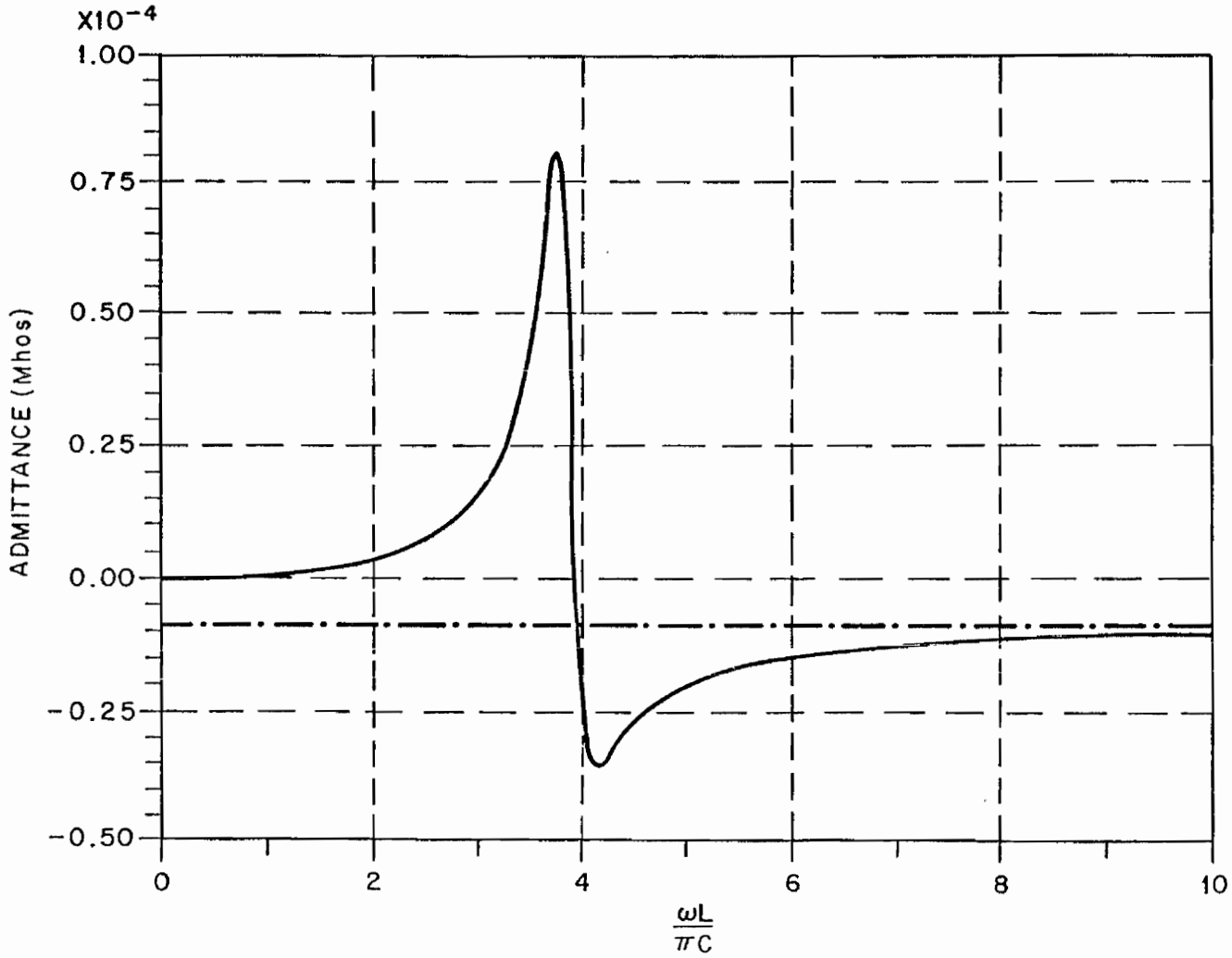

Figure 26: Real part of straight wire pole-pair admittance at z/L = .25 for pole 4, first layer.

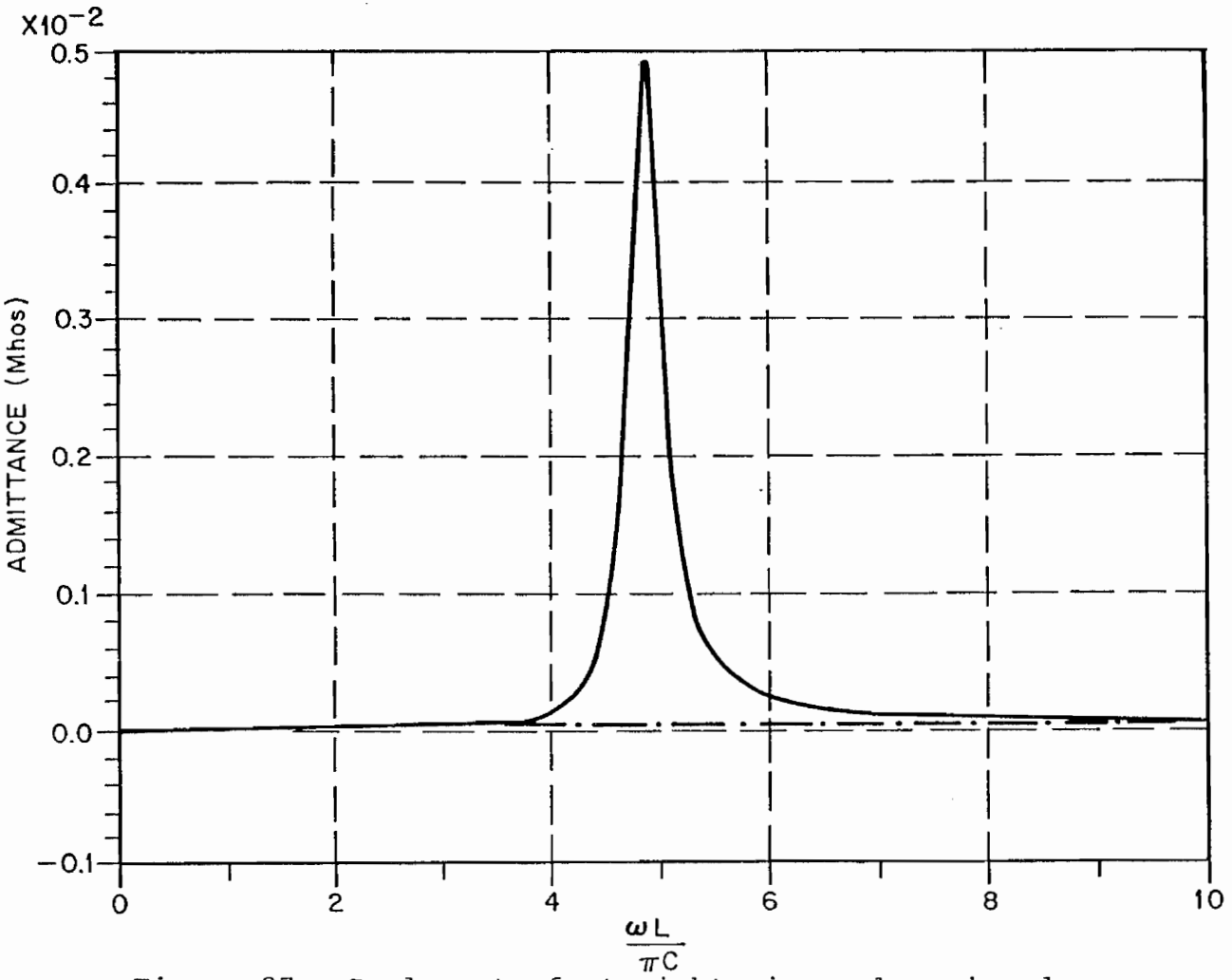

Figure 27: Real part of straight wire pole-pair admittance at z/L = .25 for pole 5, first layer. There is a slight negative area in the low frequency region.

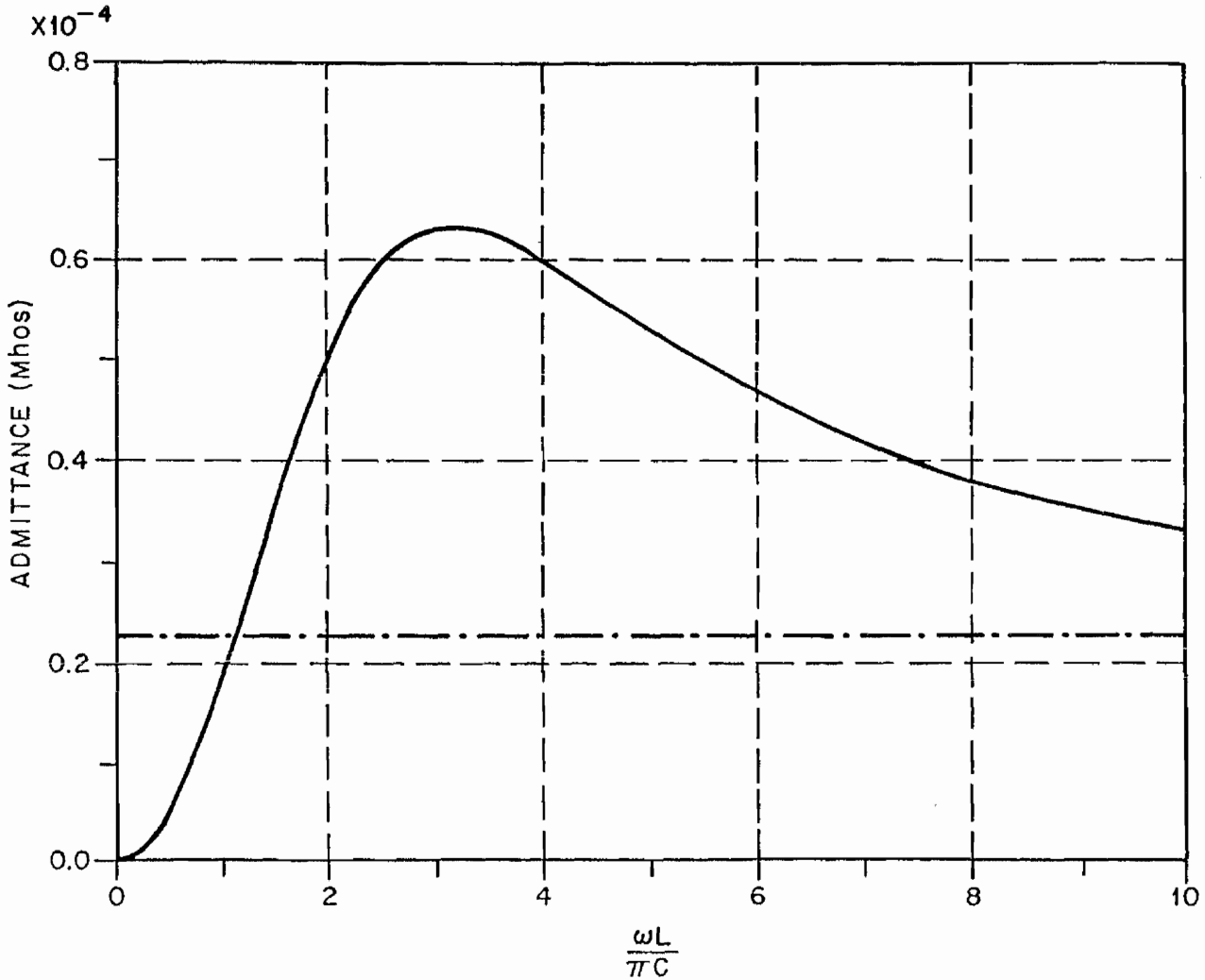

Figure 28: Real part of straight wire pole-pair admittance at z/L = .5 for pole 2, second layer. It is entirely positive.

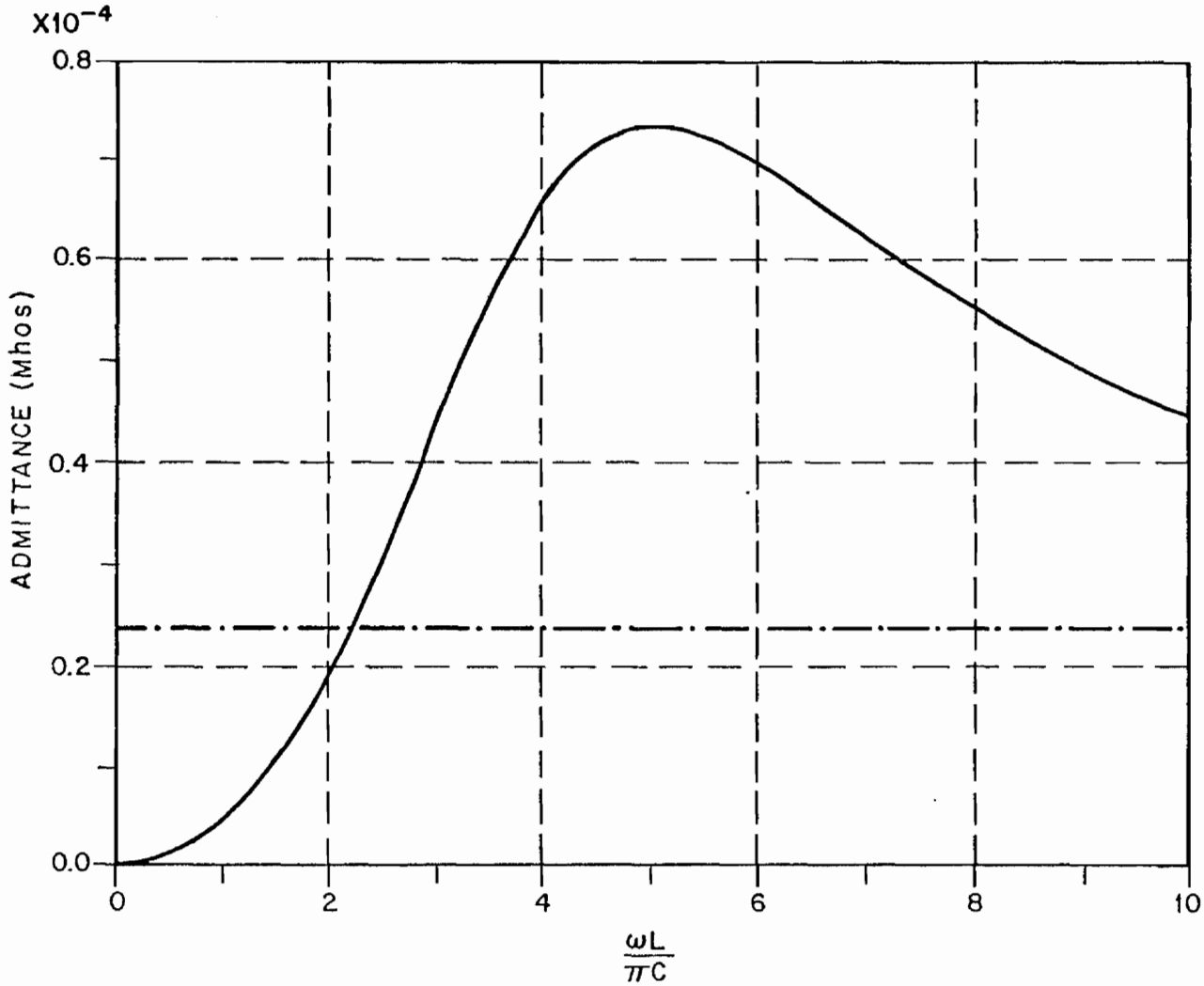

Figure 29: Real part of straight wire pole-pair admittance at z/L = .5 for pole 4, second layer. It is entirely positive.

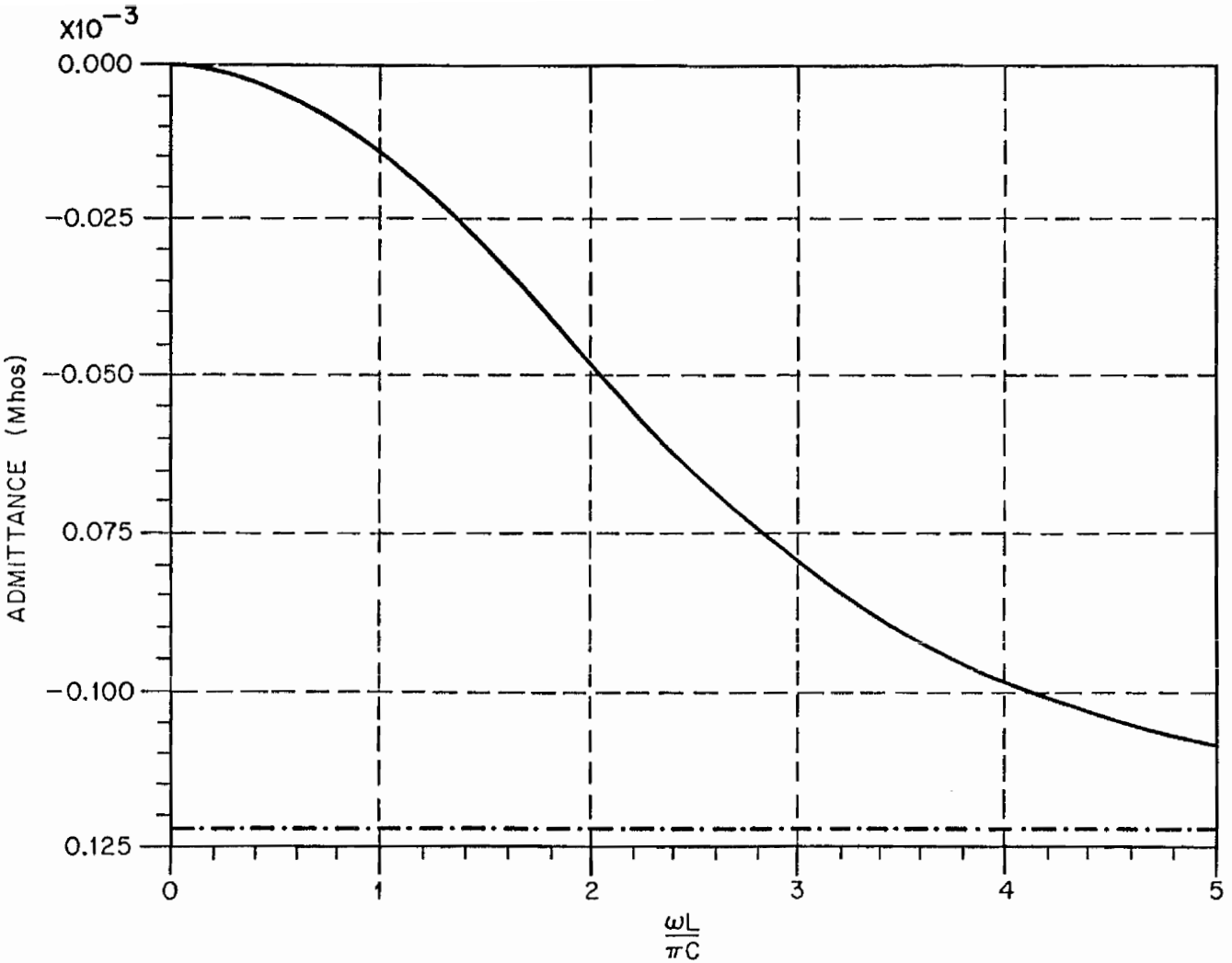

Figure 30: Real part of straight wire pole-pair admittance at z/L = .25 for pole 2, second layer.

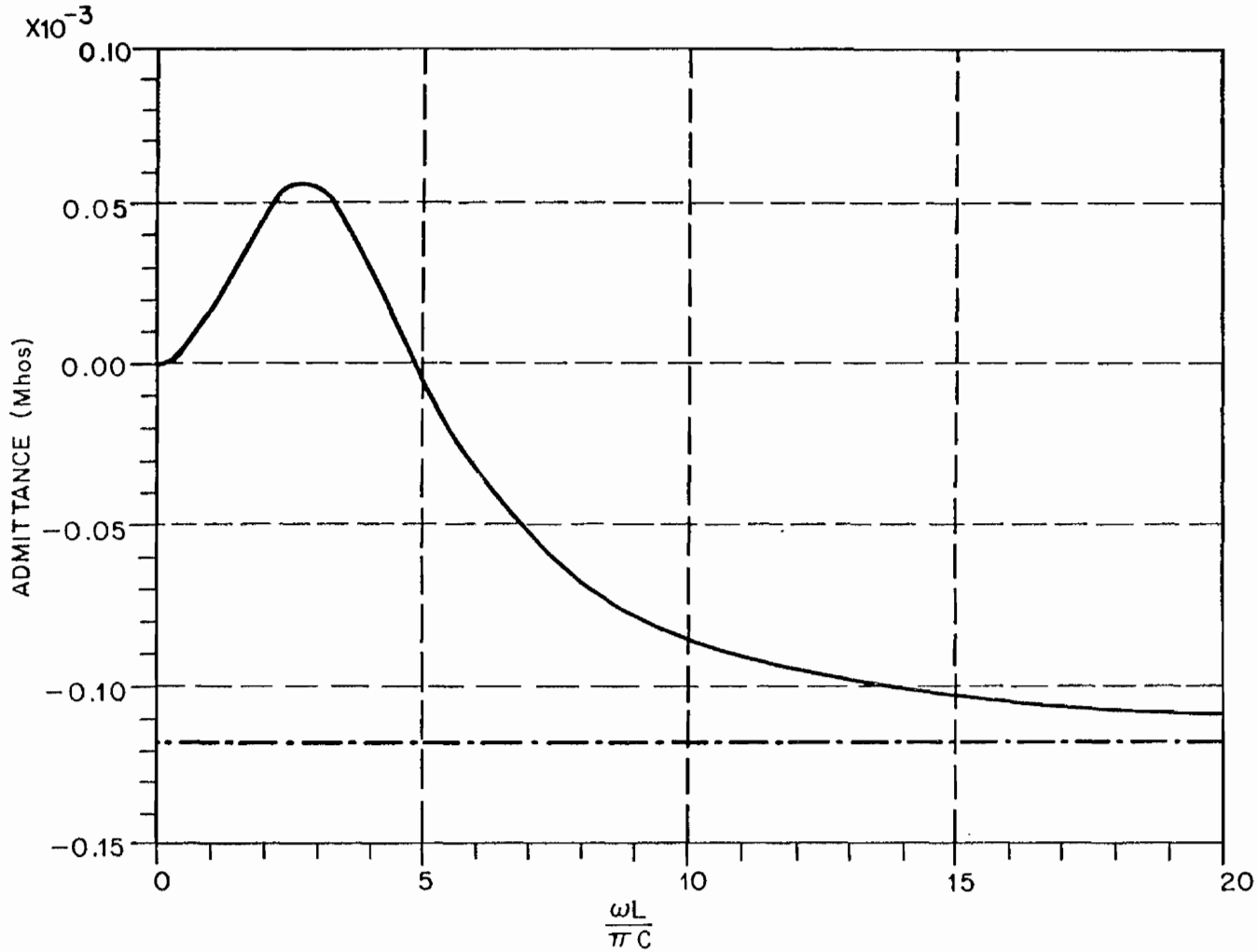

Figure 31: Real part of straight wire pole-pair admittance at z/L = .25 for pole 3, second layer.

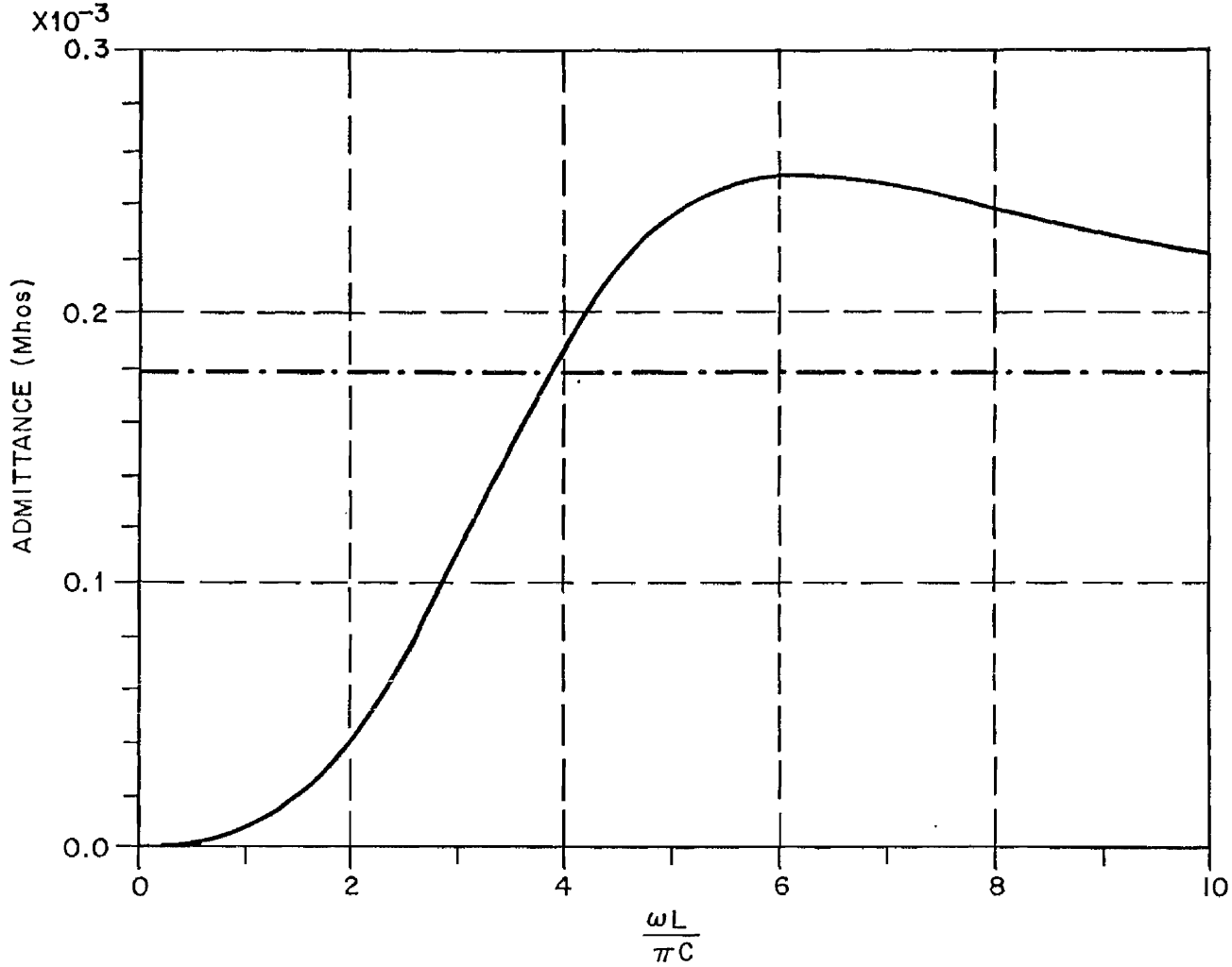

Figure 32: Real part of straight wire pole-pair admittance at z/L = .25 for pole 4, second layer.

more deeply embedded poles. The level shift due to the use of modified admittances for first layer poles is positive, indicating that without modification these poles would all have substantial negative regions for frequencies below the admittance peaks. All of the first layer poles except for pole 1 at the 1/4 point are non-PR. This result, as well as the PR quality of pole 1 at the 1/4 point, is predicted by the PR condition curves of the last section. However, now we can see that the violation of PRness is small in some cases, and consistently has the same character for first layer poles; i.e., the negative portion occurs as a result of the low frequency violation of the PR conditions and results in a small negative dip before the main peak of each admittance. This behavior suggests two questions: 1) Is the small negativeness attributable to numerical error?; and 2) If there are no numerical errors, can the admittance still be realized with perhaps some negligible negative components? It is shown subsequently that the answer to question 1 is "yes" only for a few isolated and predictable cases. The second of these questions is addressed in Chapter IV.

It is worthwhile at this point to examine the PR character of the conjugate pole-pair admittances formed for the circular loop. The type I modified pole-pairs for modes one through five are shown in Figures 33 through 37. These poles are the major contributors to the overall admittance of the loop. These admittances are quite similar in character to the first layer pole-pair admittances for the wire. Except for mode 1, these admittances are slightly non-PR, exhibiting a negative low frequency behavior. The loop, unlike the straight wire, has a nonzero admittance at $\omega = 0$. This gives rise to an SEM pole for the loop at $s = 0$.

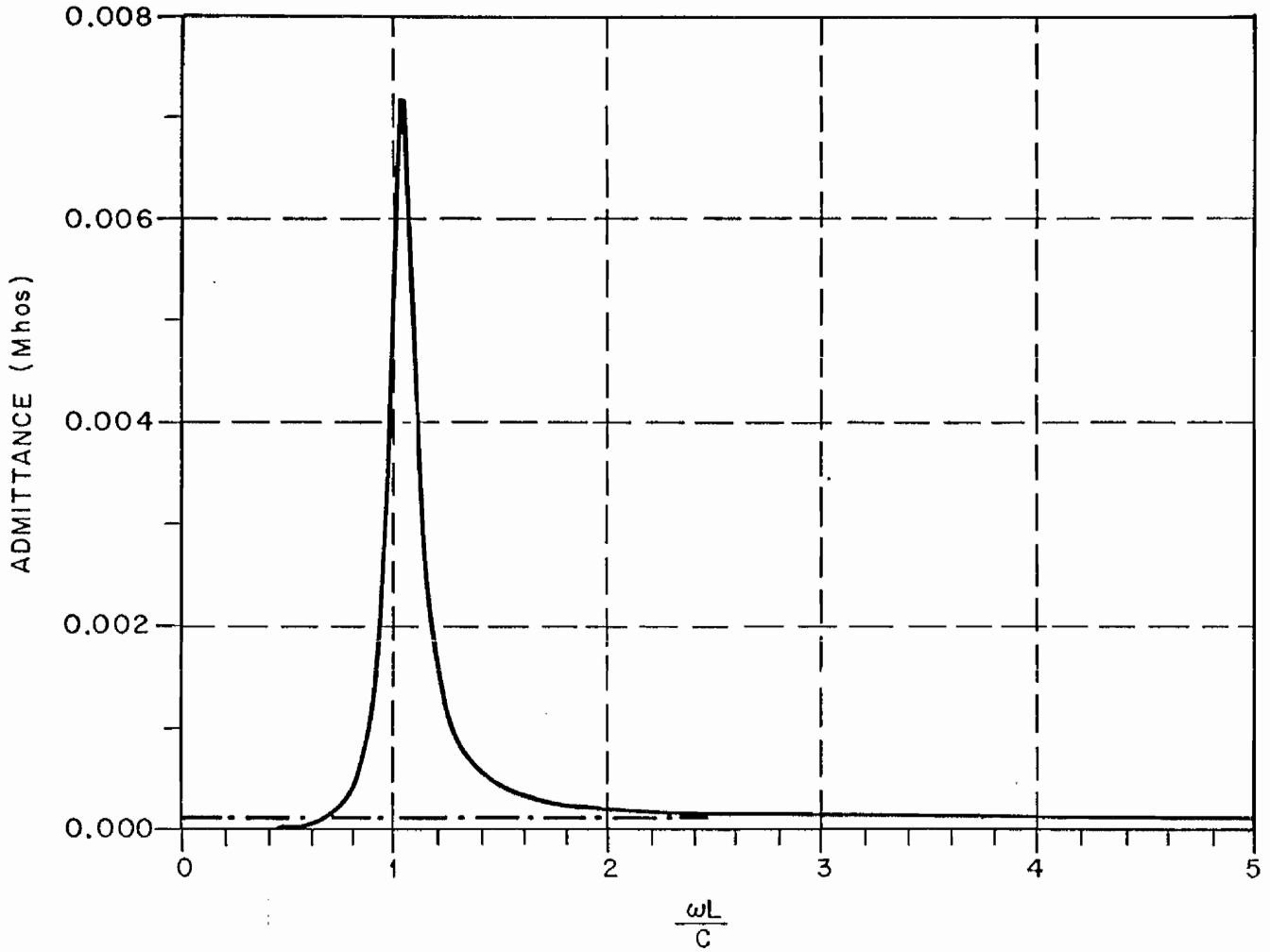

Figure 33: Real part of circular loop pole-pair admittance for type I pole of mode 1. It is entirely positive.

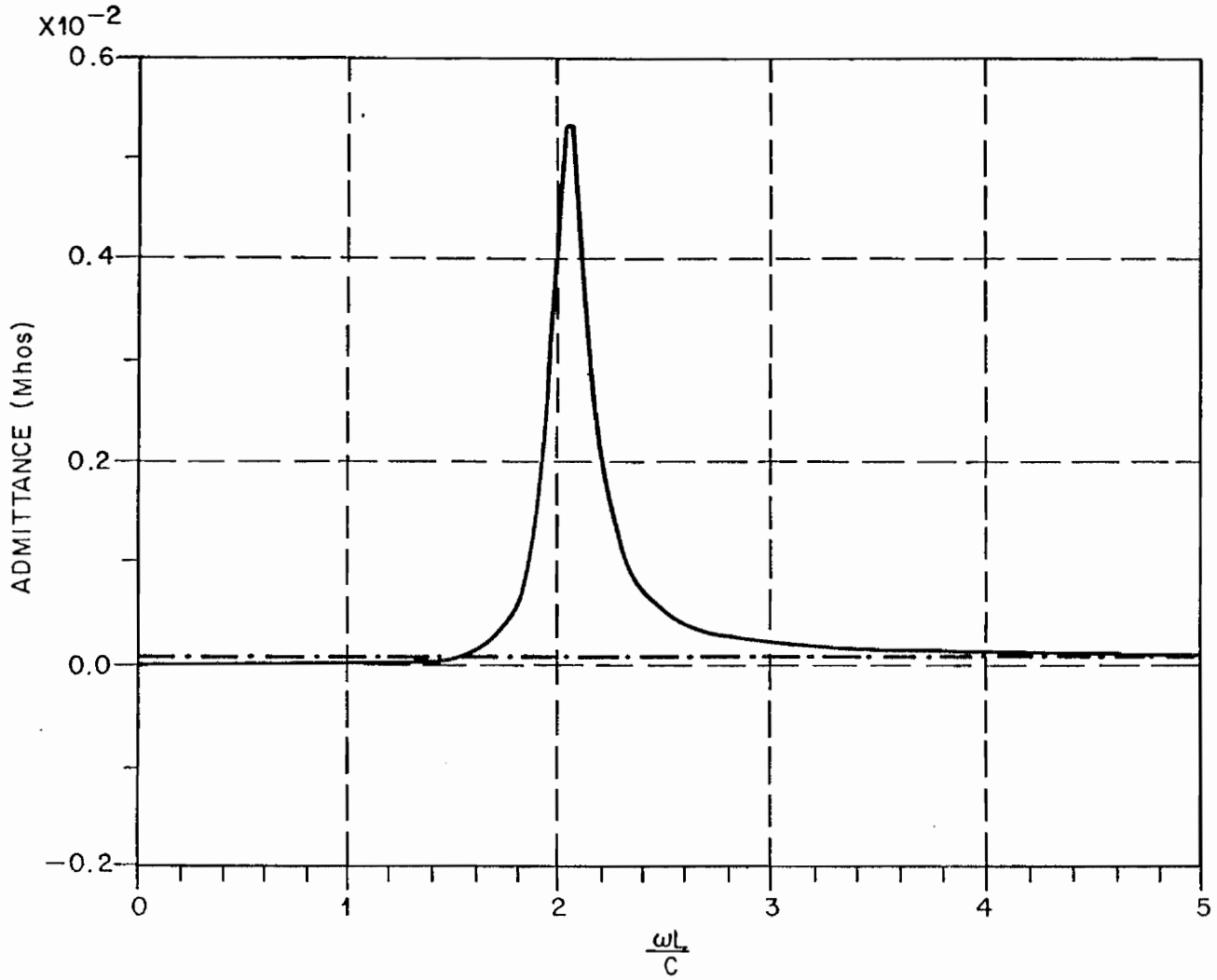

Figure 34: Real part of circular loop pole-pair admittance for type I pole of mode 2. There is a slight negative area in the low frequency region.

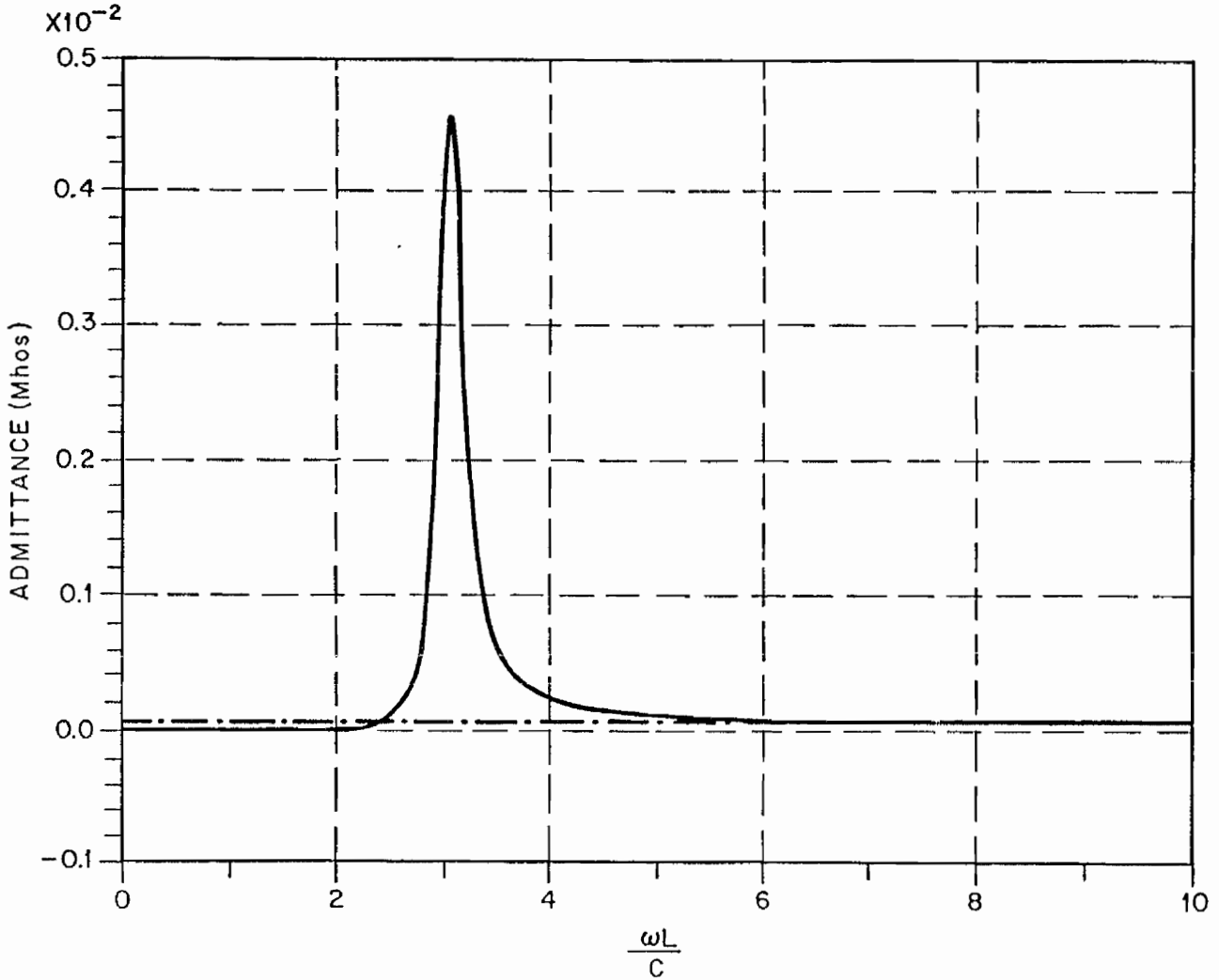

Figure 35: Real part of circular loop pole-pair admittance for type I pole of mode 3. There is a slight negative area in the low frequency region.

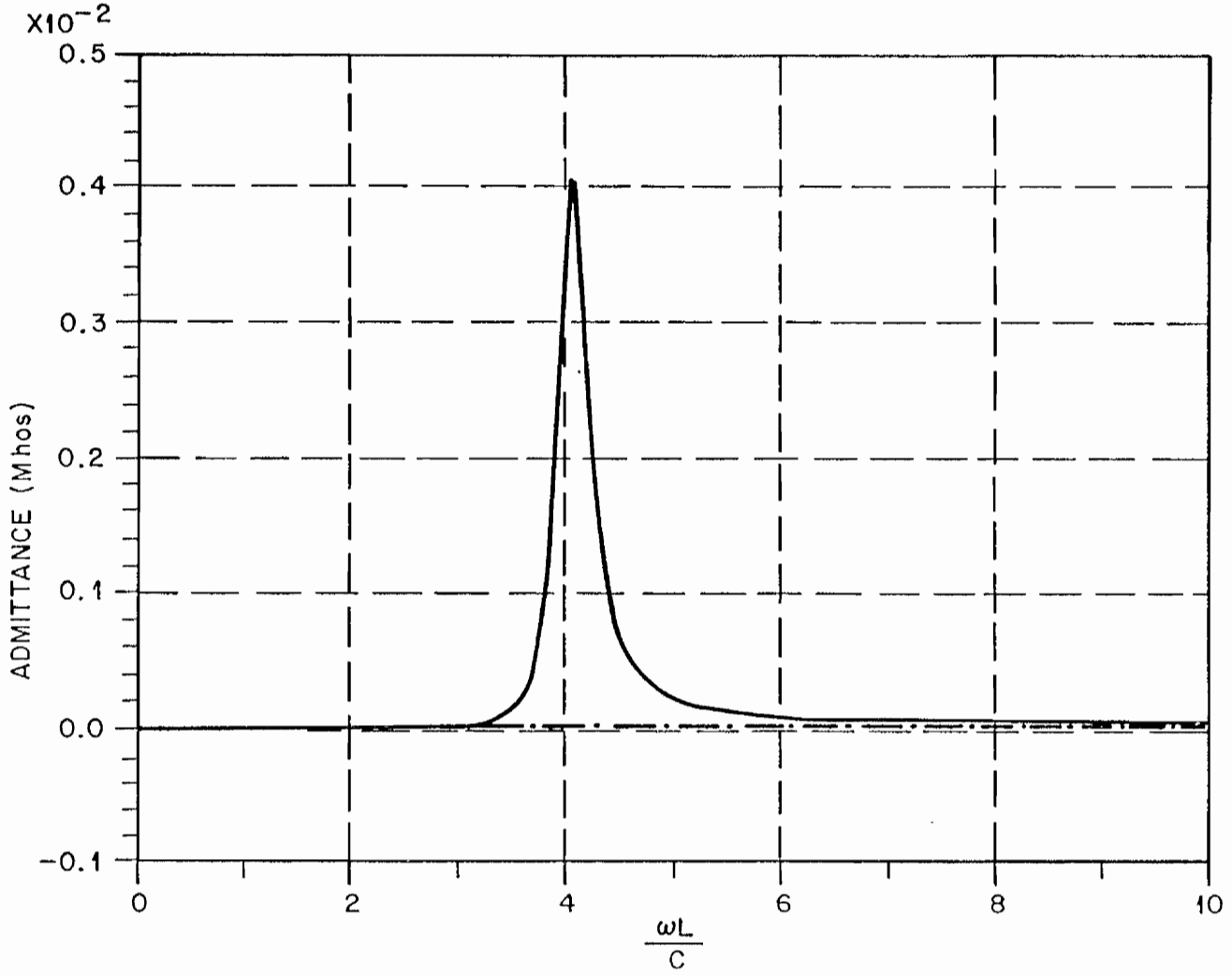

Figure 36: Real part of circular loop pole-pair admittance for type I pole of mode 4. There is a slight negative area in the low frequency region.

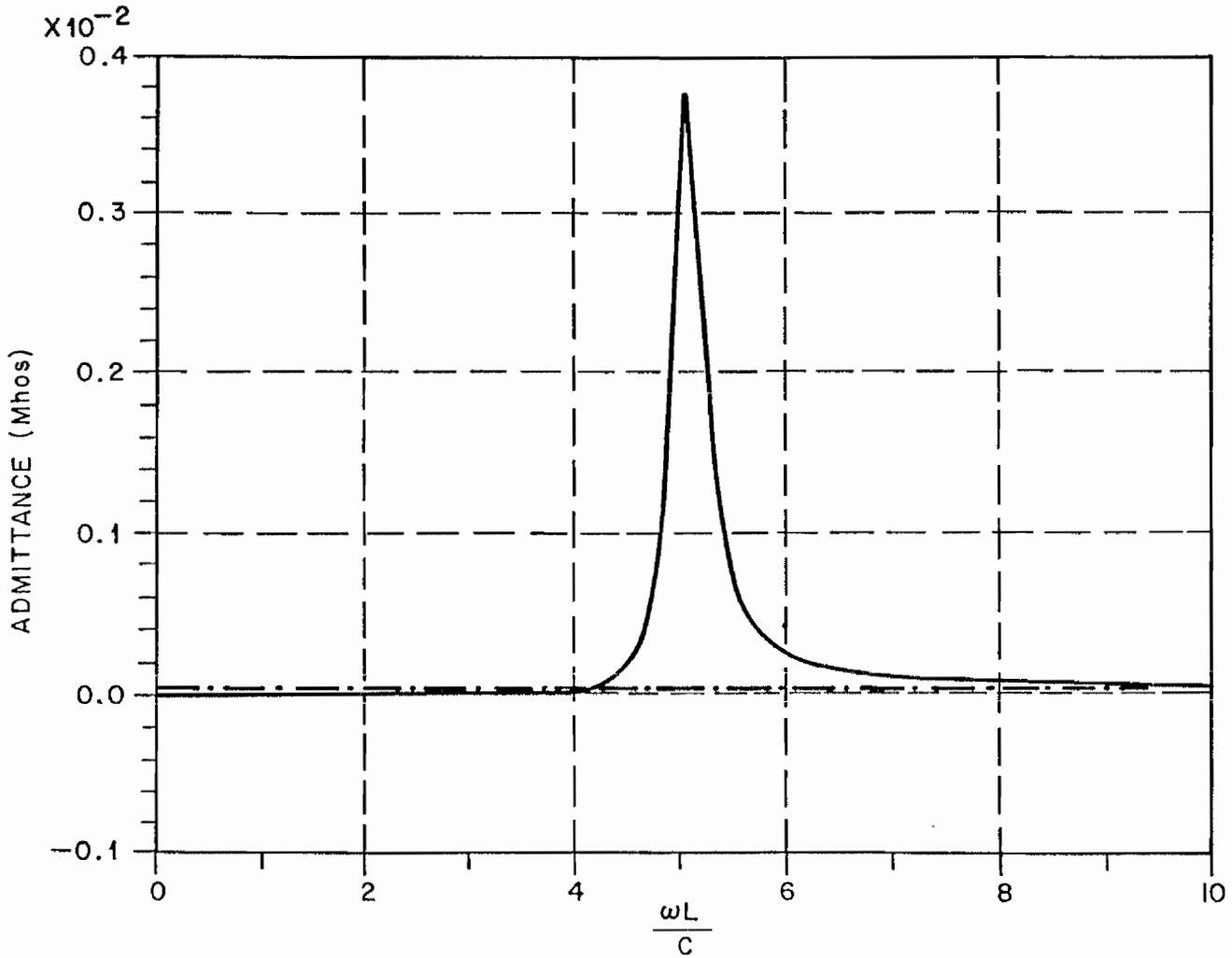

Figure 37: Real part of circular loop pole-pair admittance for type I pole of mode 5. There is a slight negative area in the low frequency region.

The character of the modified pole-pair admittances formed using the type III poles of mode 2 are shown in Figure 38. Similar admittance curves characterize all type III pole-pair admittances. The characteristics are an initial positive value rising to a peak, which then falls to a negative peak and a negative final value as frequency goes to infinity. The peak value for the first type III, mode 2 pole is 240 times lower than the peak of the type I, mode 2 pole.

The modified pole-pair admittances for the type II poles of mode 2 are shown in Figures 39 and 40. The figure for the pole lying on the negative real axis is not a pole-pair, of course, but only a modified pole construction. The peak admittance from this pole is some 130 times lower than the type I pole of mode 2. The character of the type II pole lying closest to the $j\omega$ axis is entirely negative, with a peak value some 50 times lower than the type I pole peak. This negative behavior is a characteristic of the type II pole closest to the $j\omega$ axis, as Figure 41 indicates.

In summary, the following conclusions regarding pole-pair PRness are established:

- For the straight wire
  - Dominant layer 1 pole-pair admittances are non-PR in unmodified form, exhibiting a negative value at zero frequency.
  - Modified layer 1 pole-pair admittances are in general non-PR, exhibiting only a very slight negative value in the low frequency region. Exceptions occur at isolated locations on the wire for all pole-pairs, and pole-pair 1 is PR over most of the antenna.
  - Deeper embedded pole-pairs, which contribute much less to the total admittance, are PR on various intervals, sometimes in modified form and other times unmodified.
- For the circular loop
  - The dominant type I pole-pairs are non-PR in unmodified form, exhibiting a negative value at zero frequency.

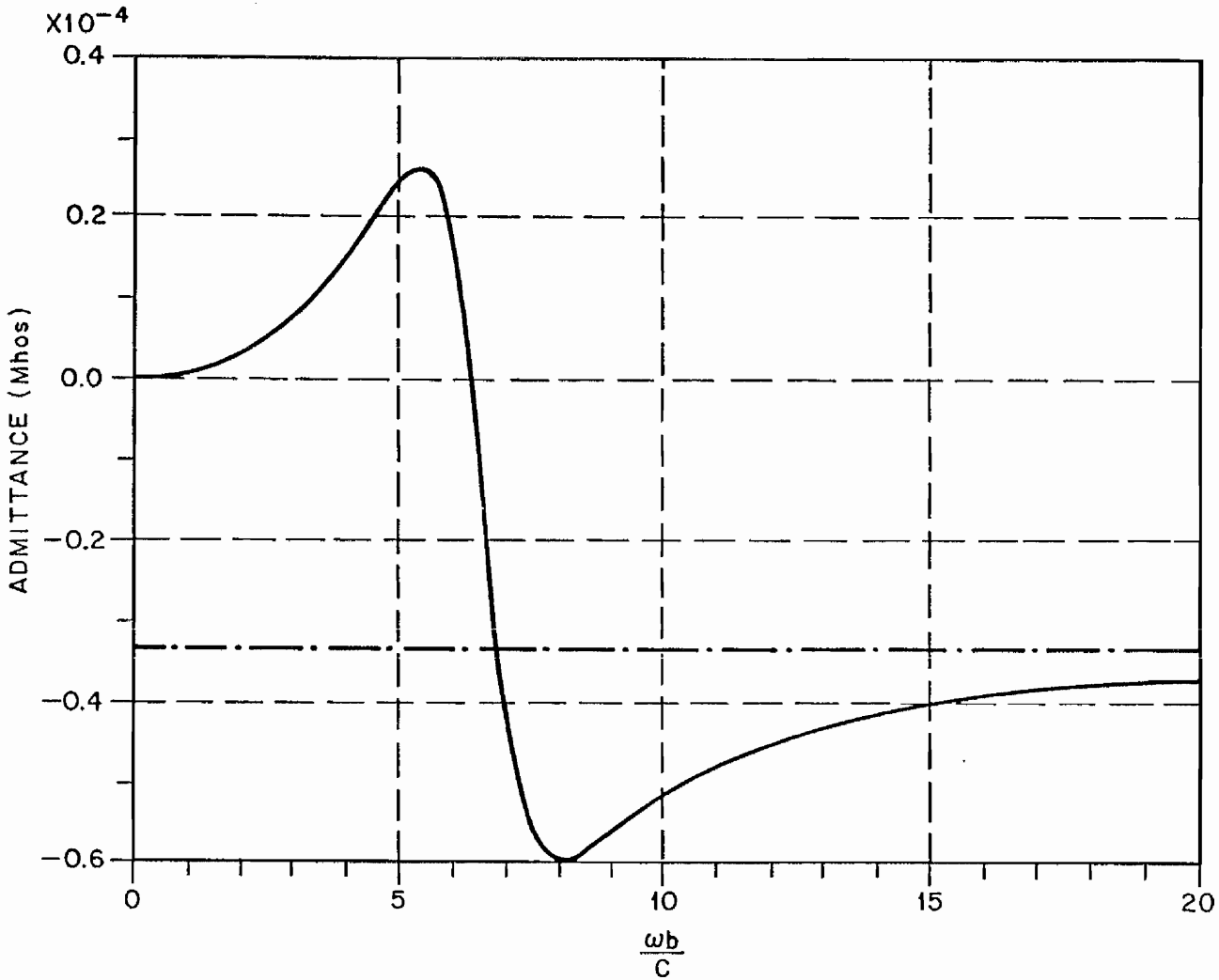

Figure 38: Real part of circular loop pole-pair admittance for type III pole, mode 2.

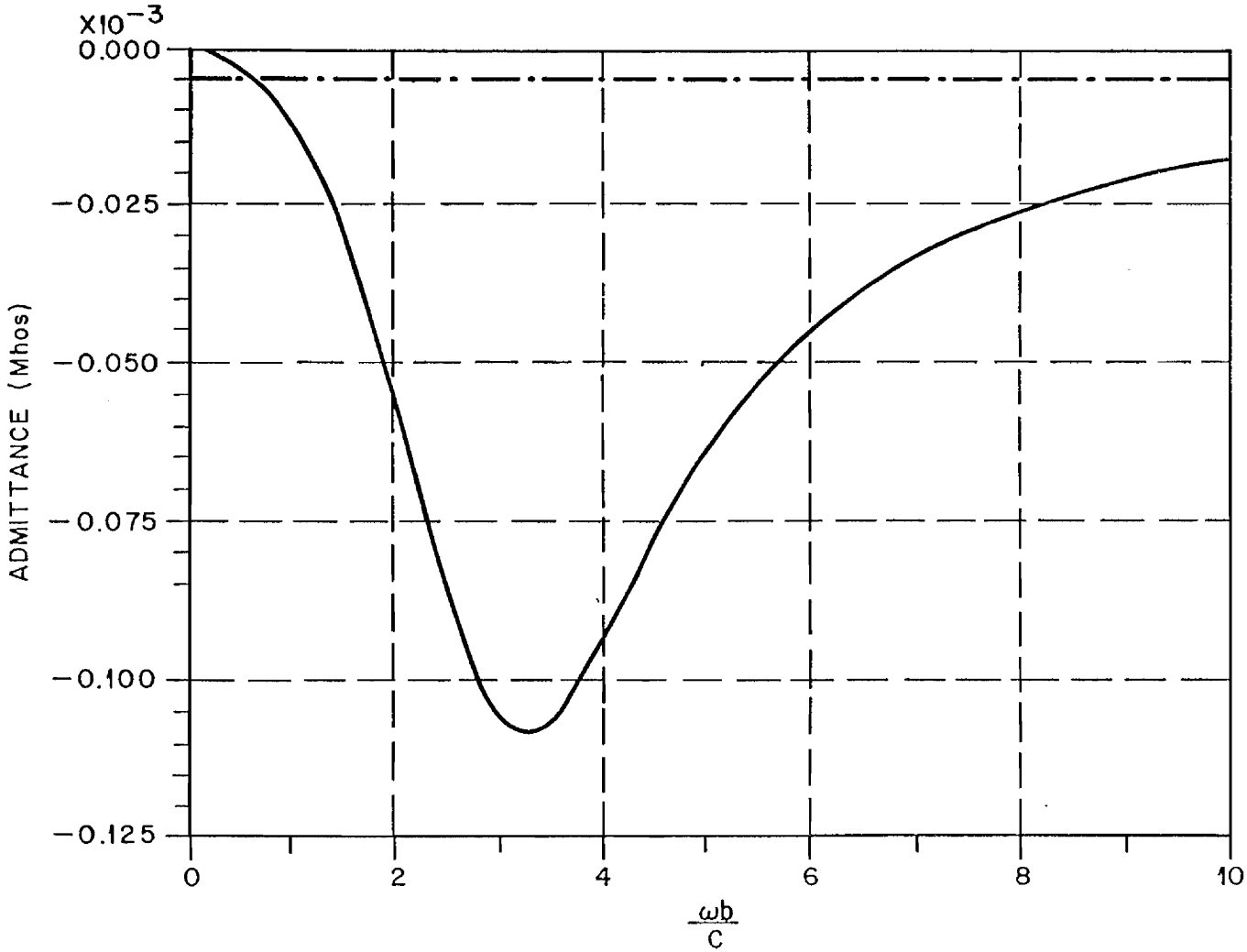

Figure 39: Real part of circular loop pole-pair admittance for the first type II pole of mode 2. It is entirely negative.

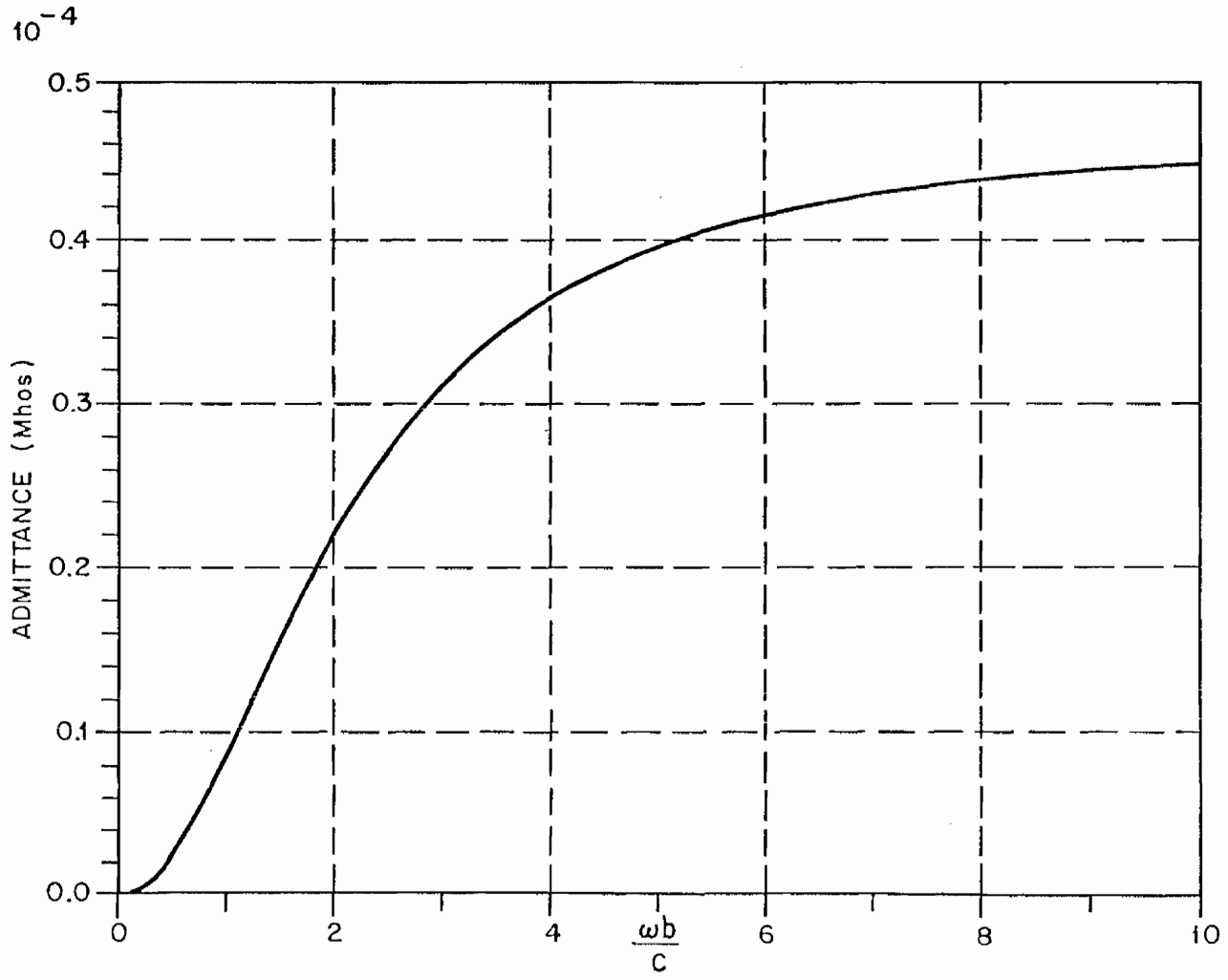

Figure 40: Real part of circular loop pole admittance for the second type II pole of mode 2.

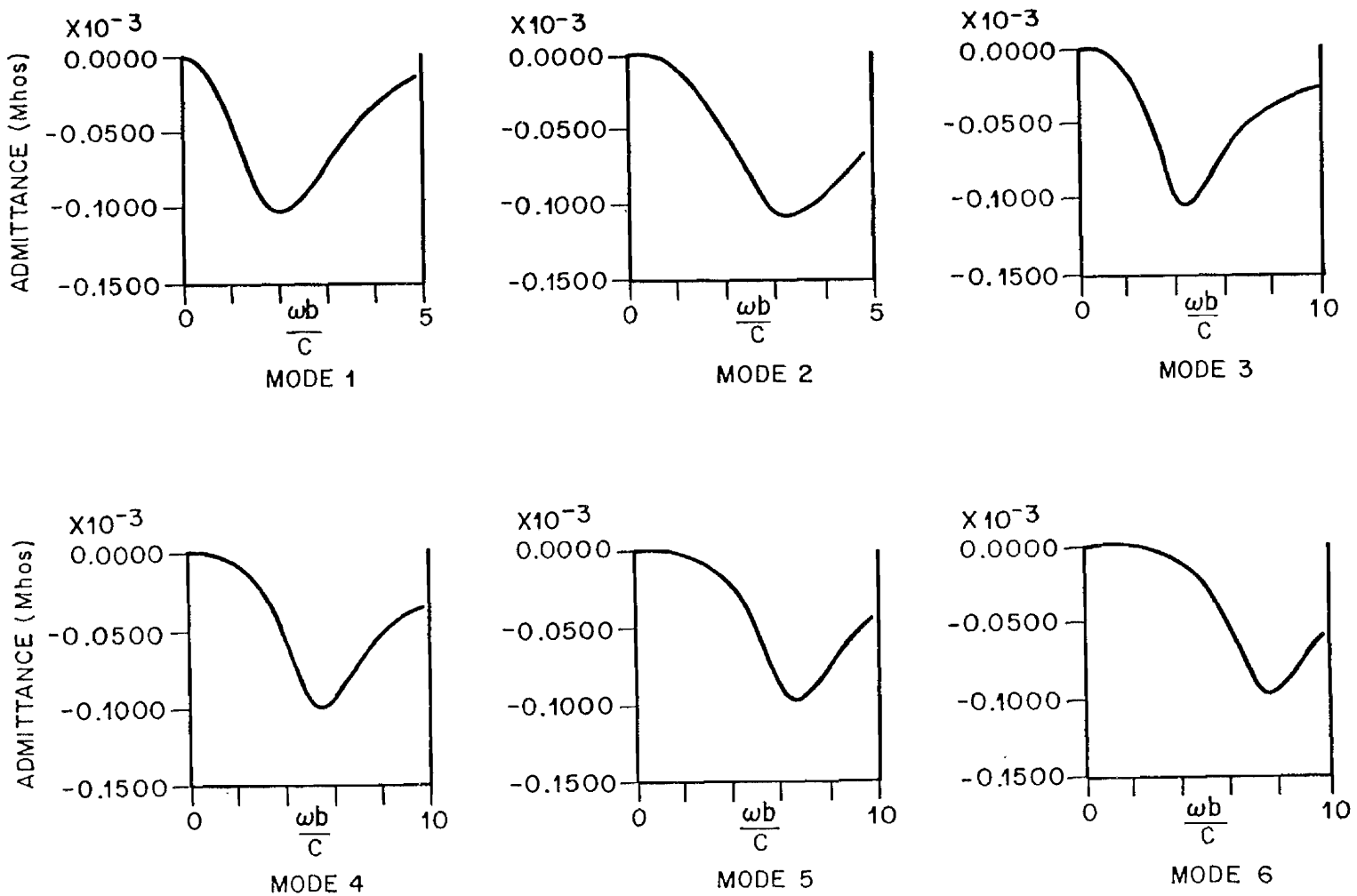

Figure 41: Real part of circular loop pole-pair admittances of the first type II poles of modes 1-6, showing the consistent negative behavior of these admittances.

- Modified type I pole-pairs are in general non-PR, exhibiting a slight negative value in the low frequency region. An exception is the pole-pair of mode 1, which is PR.

- Type II pole-pairs, which contribute much less to the total admittance than do type I, exhibit a range of PRness. The type II pole-pair closest to the $j\omega$ area is non-PR in unmodified or modified form, and the pole admittance (not a pole-pair) which lies on the $-\sigma$ axis is PR. Other type II pole-pairs are not PR in either form.

- Type III pole-pairs, which also have small contributions to the total admittance, are non-PR in modified or unmodified form.

3.4 Eigenmode PR Considerations

When the synthesis of equivalent circuits is carried out on a terminal eigenadmittance basis, the theory of the eigenmode expansion provides some very useful insights into the problem of finding PR functions. First we note that the inverse eigenvalues $\lambda_n^{-1}(s)$ are positive real functions, as they derive from an impedance integral equation for a passive object [6]. The PRness of the inverse eigenvalues $\lambda_n^{-1}(s)$, which are termed eigenadmittances by Baum [4], has been demonstrated by Wilton [13]. This proof is reproduced in the Appendix for the sake of completeness. However, the PRness of these eigenvalues does not insure the PRness of the associated terminal eigenadmittances of Equation (2.13), as we demonstrate in the Appendix. Additionally, the construction of terminal eigenadmittances depends on the availability of the eigenmode groupings of poles. For analytically tractable objects, such as the loop or sphere, such groupings are available; however, for objects such as the wire, where the poles are found numerically, the task of grouping the poles by eigenmodes is much more difficult. For a complex object where the poles are experimentally derived, if at all, complete grouping information is not likely to be available.

Wilton and his colleagues [13] have derived eigenmode groups of poles for the wire on a numerical basis. They have used these groupings as

the basis of conjecture for the general grouping scheme indicated in Figure 42. Note that there are only a finite number of poles belonging to each eigenmode in this representation. The circular loop manifests an infinite number of poles associated with each eigenmode.

In the case of an infinite number of poles per eigenmode, the question arises as to whether all poles are necessary for PRness and, if not, how many poles must be included to have a PR function. In the case of mode 1, where the type I pole-pair forms a PR modified admittance by itself, inclusion of the type II pole of this mode destroyed this PR character in the low frequency region, although the maximum negative value is only $-.5\times10^{-8}$ mhos, compared to the positive peak value of 7.5×10^{-3} mhos. The systematic addition of type III poles reduced the maximum negative value, and pushed the frequency at which this maximum occurred closer to zero until, with the inclusion of four type III poles, the admittance was again PR. The inclusion of these poles is found to have little effect on the appearance of the admittance when compared to the type I pole-pair admittance, except for introducing some small high frequency variations due to the type III poles. The peak admittance value of the eigenmode grouping has been lowered by some .75 percent.

An interesting feature is observed when the eigenadmittance grouping is performed. As more type III poles are included, the difference between the modified and unmodified forms becomes smaller, and in the limit would appear to give the same admittance. In other words, the constant terms introduced into the modified form sum to zero for a given eigenmode.

A similar examination of mode 3 where the type I pole is not PR revealed the same behavior as that for mode 1. Increasing the number of

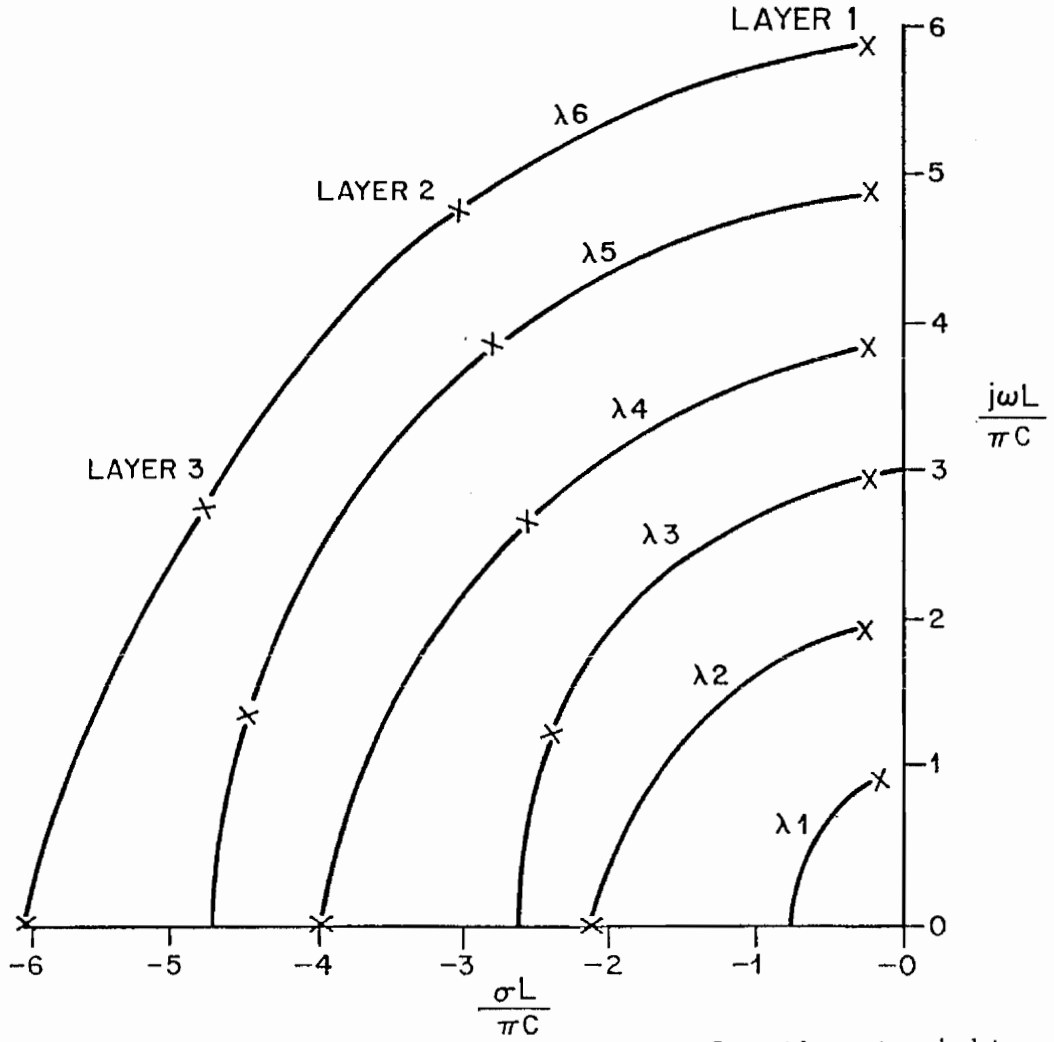

Figure 42: The postulated eigenmodes for the straight wire.

type III poles systematically reduces the negative portion of the admittance. However, inclusion of all seven type III poles available did not produce a PR result, although the maximum negative value was reduced to only $-.25\times10^{-8}$. For higher modes a similar result also holds. In general, to make an eigenadmittance PR requires the inclusion of many type III poles, making the circuit realization more complex, since the additional poles entail more circuit elements.

It is worthwhile to point out that if the problem at hand were merely to synthesize the total admittance of the wire or loop using SEM data, then the PR character of the admittance is assured. The mathematical reasoning leading to this conclusion is as follows. If the pole of the lowest frequency for the structure is PR or can be made PR, then when all the poles for the structure are grouped the low frequency non-PR character of the higher poles are negated by the large positive peaks of the lower poles. However, to include simple Norton generators in the synthesis, it is necessary to try to realize the admittance by some group of recognizable modules. Further, it is desirable that these modules be as simple as possible.

When the terminal eigenadmittances for the straight wire are considered, the results are found to be ambiguous. For eigenadmittance groupings using conjugate pole-pairs at the center of the wire, the results are PR, as indicated in Figures 43 and 44. However, when such groupings are attempted for a terminal taken at the quarter point of the wire, some non-PR results are discovered. These groupings are indicated in Figures 45 through 49. The postulated eigenmode groupings for eigenmodes 2, 3, 4, and 6 are non-PR, and in the case of modes 3 and 6 the negative part is not negligible. This result could have been foreseen by reference to the parameter test

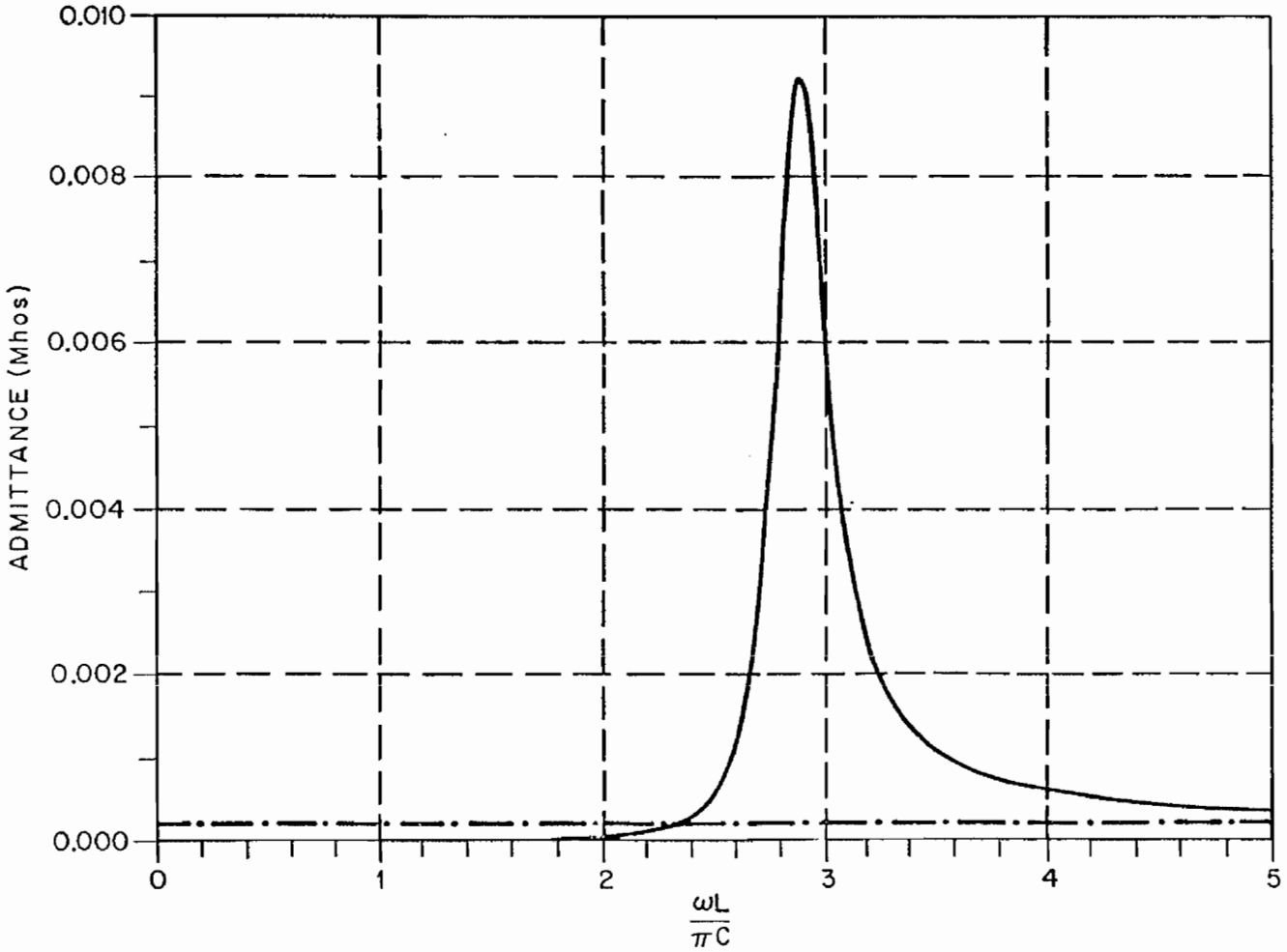

Figure 43: Real part of straight wire terminal eigen-admittances for mode 3 at z/L = .5. It is entirely positive.

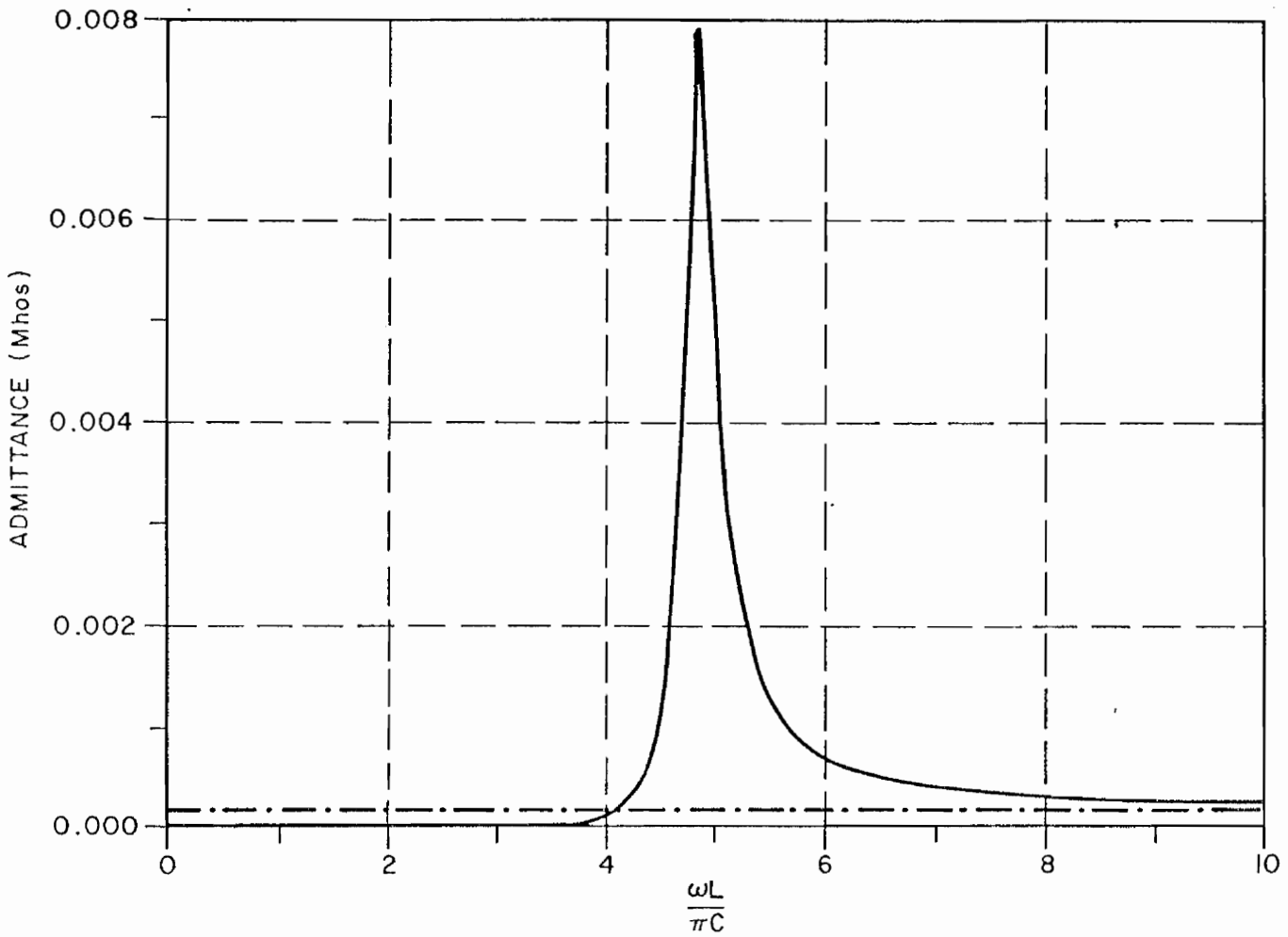

Figure 44: Real part of straight wire terminal eigen-admittance for mode 5 at z/L = .5. It is entirely positive.

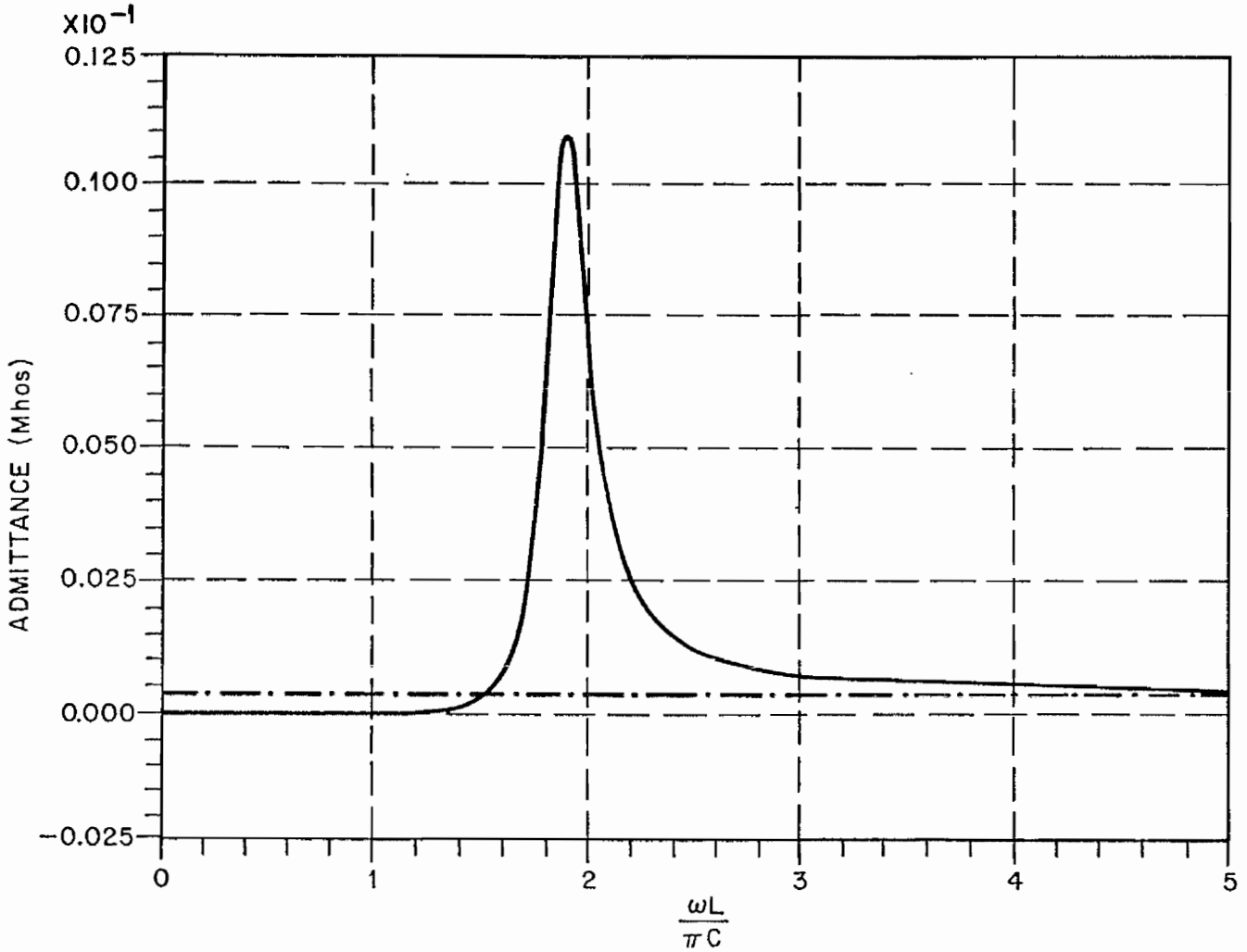

Figure 45: Real part of straight wire terminal eigen-admittance for mode 2 at z/L = .25. There is a slight negative area in the low frequency region.

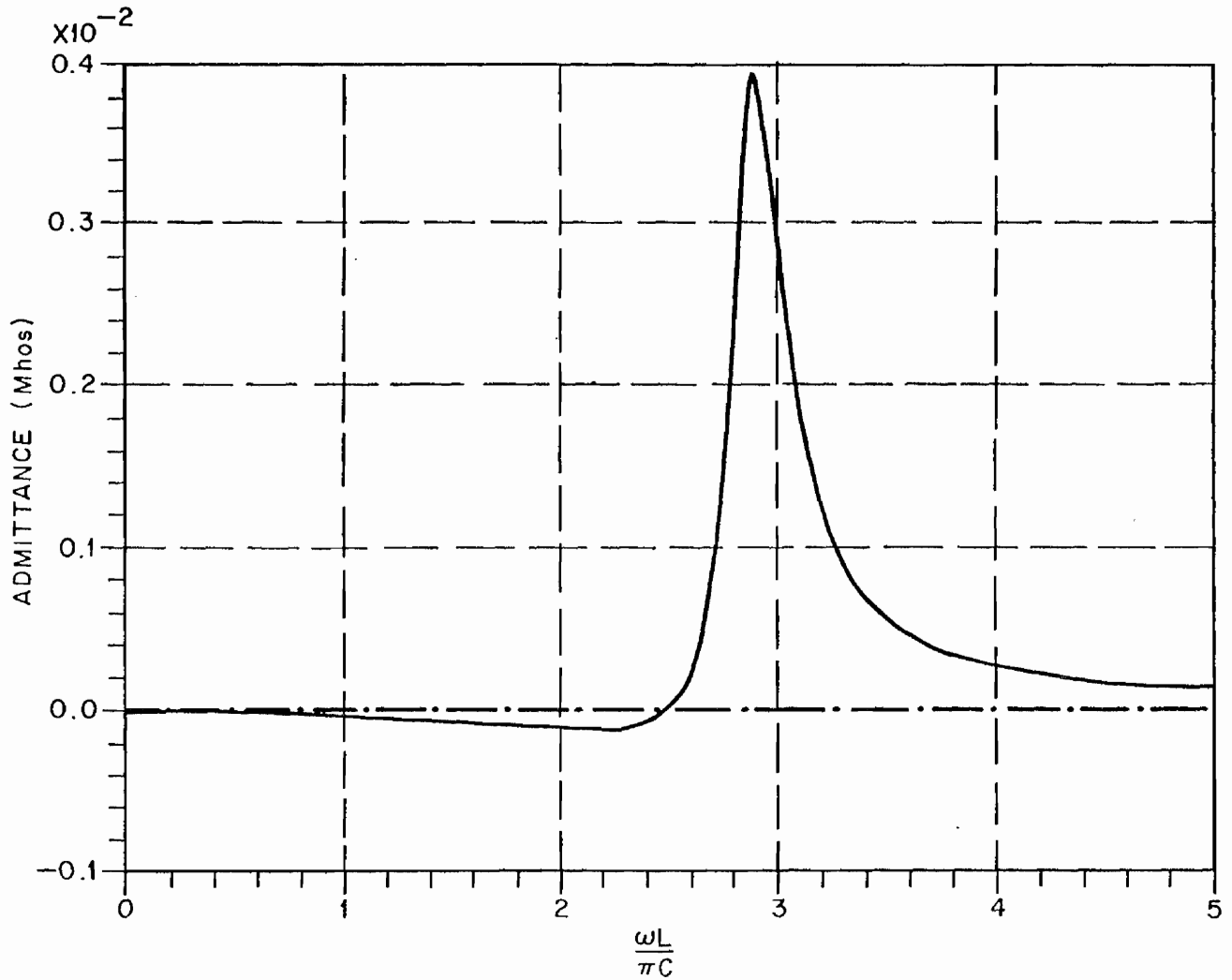

Figure 46: Real part of straight wire terminal eigen-admittance for mode 3 at z/L = .25.

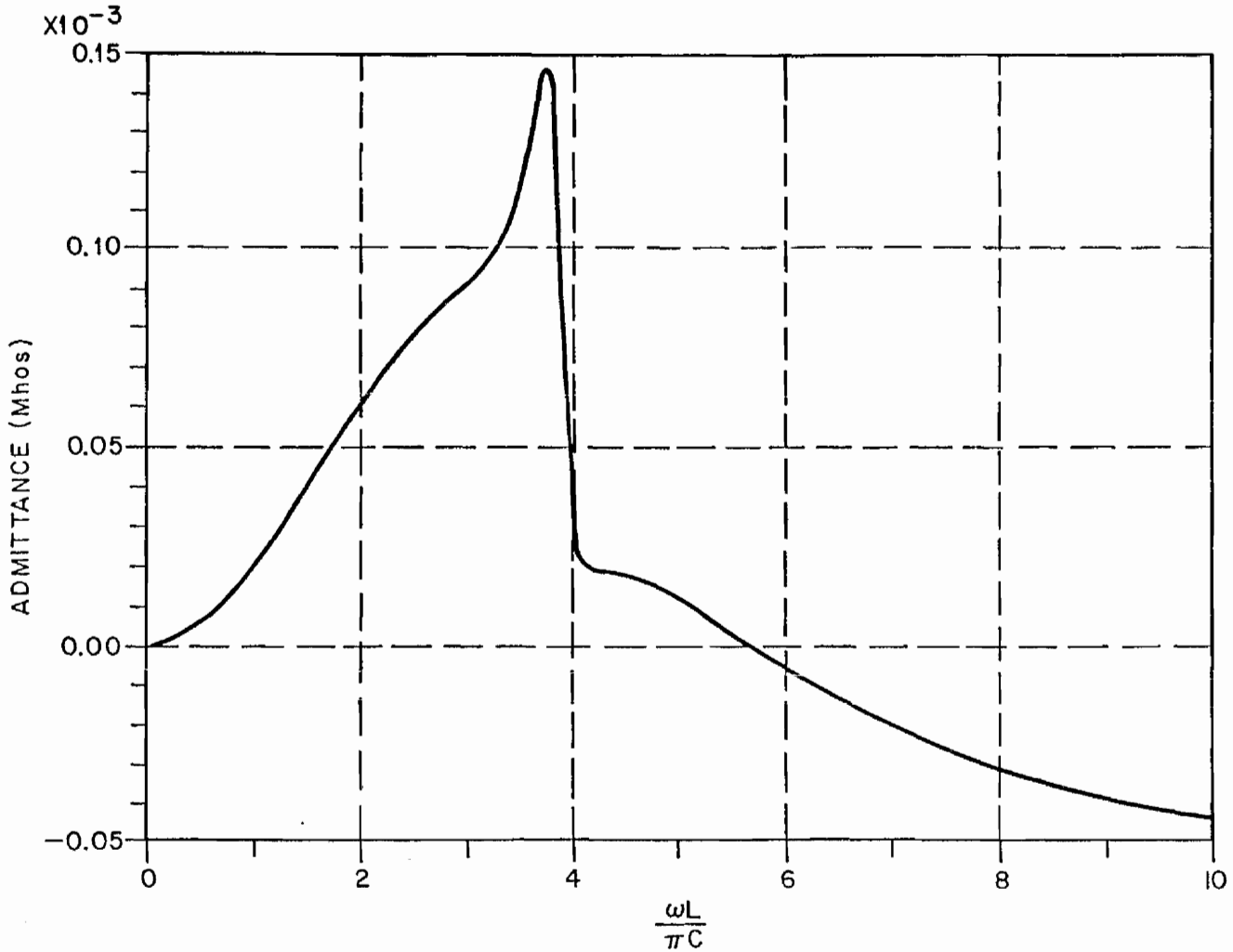

Figure 47: Real part of straight wire terminal eigen-admittance for mode 4 at z/L = .25.

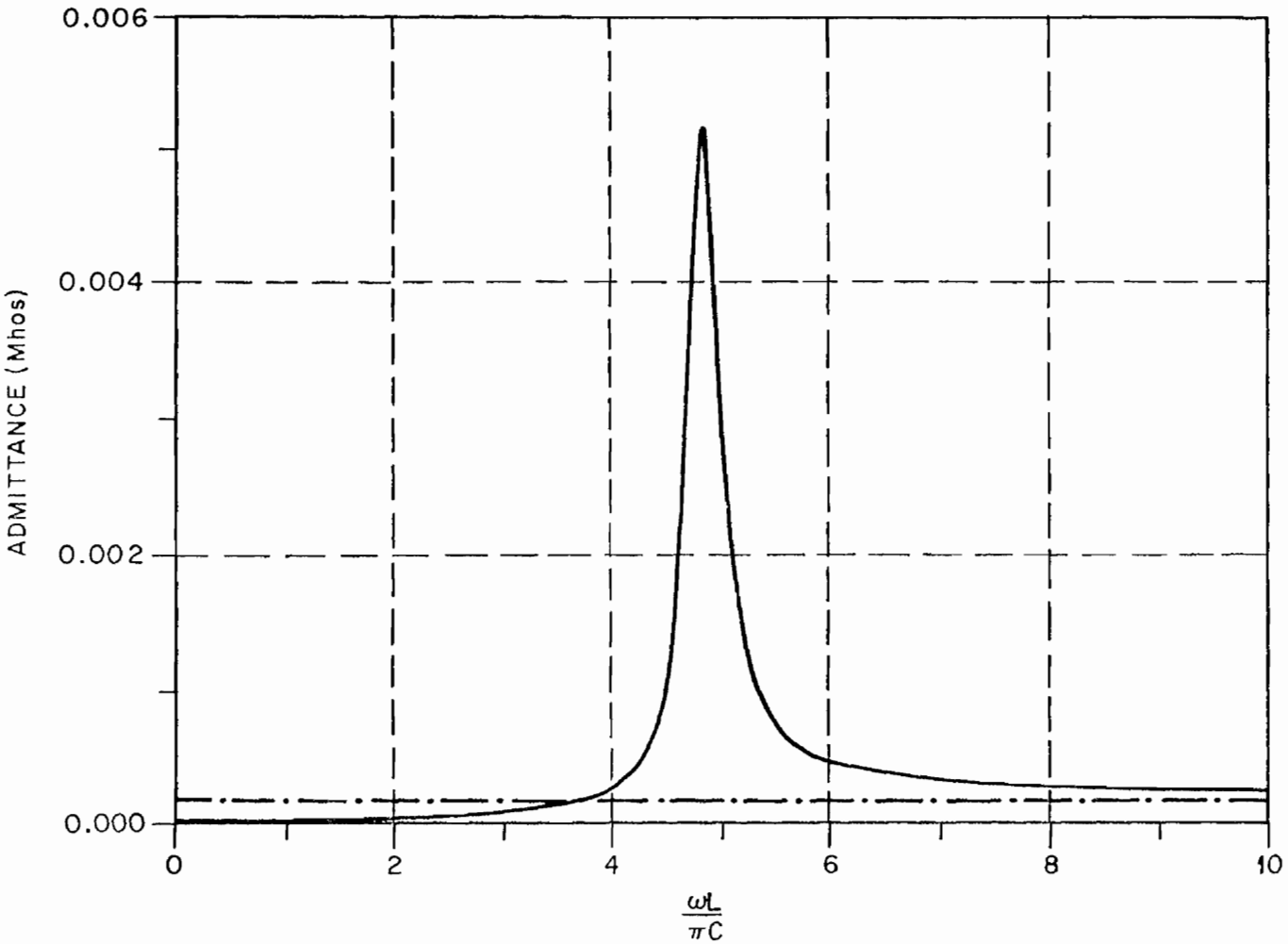

Figure 48: Real part of straight wire terminal eigen-admittance for mode 5 at z/L = .25. It is entirely positive.

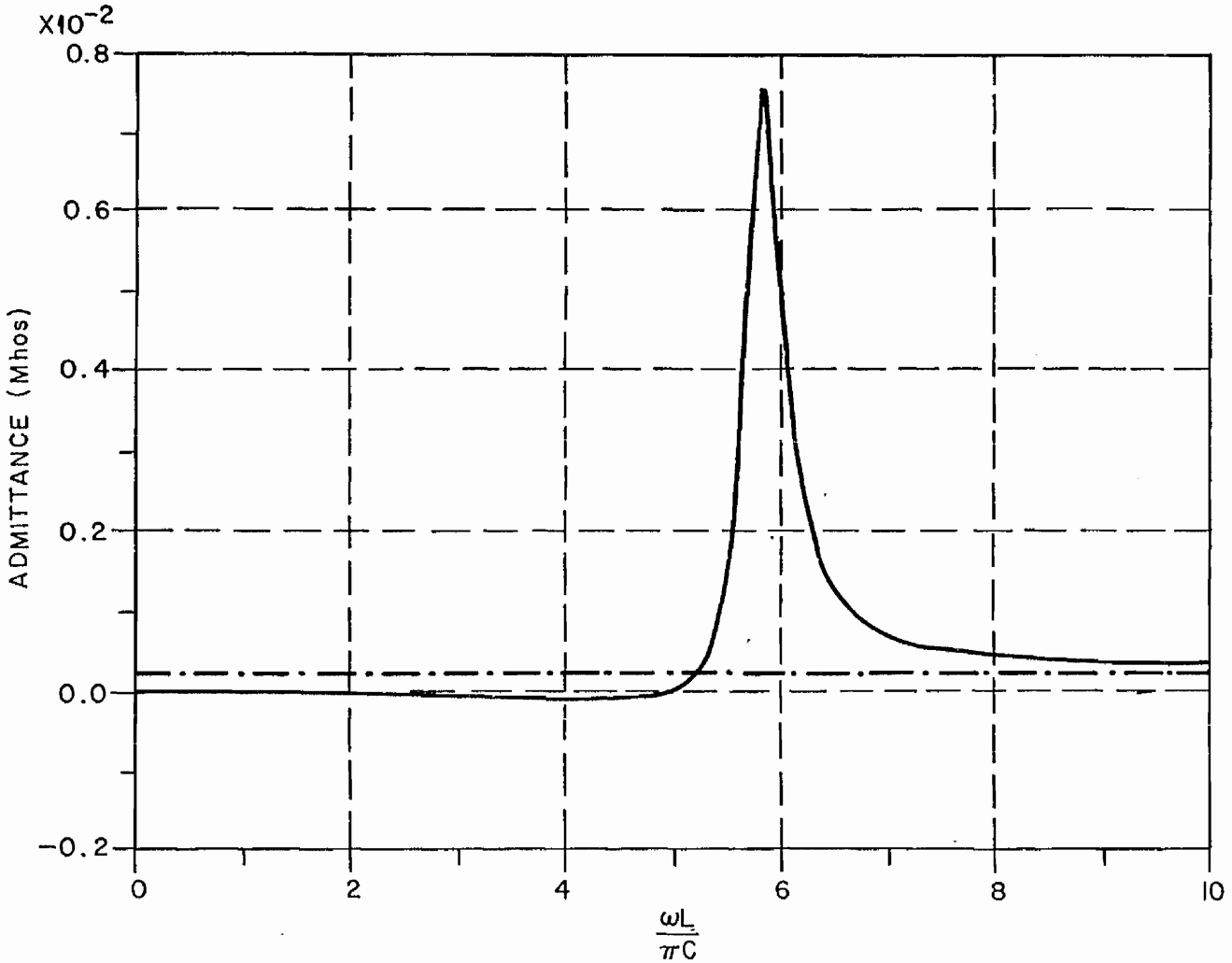

Figure 49: Real part of straight wire terminal eigen-admittance for mode 6 at z/L = .25.

results. Taking the case of mode 3, poles 3 in the first layer and 2 in the second layer, we see from the PR condition graphs that at the quarter point for these poles the PR conditions for the modified admittance form is violated for both poles. Since the real part of each pole adds algebraically to produce the total real part admittance, then the grouping of non-PR poles cannot produce a PR result. Similarly the unmodified admittance formed by grouping these two poles is non-PR.

While the discussion in the Appendix indicates that the terminal eigenadmittances are not demonstratively PR, it is interesting to speculate as to alternative reasons for the non-PR result. That numerical errors in pole/residue data is the source of departure from PRness is unlikely in light of the general error analysis discussed in the next section. Other possibilities include improper groupings of poles associated with the eigenvalues and missing components of the Mittag-Leffler expansion of the eigenvalues. Wilton's groupings are based on similarity of modal features and the topological kinship of the straight wire to the sphere. We are inclined to trust Wilton's conjectured groupings. Therefore it is difficult to draw more specific conclusions at the present time.

3.5 SEM Pole/Residue Error Effects on PR Considerations

The SEM data for the wire is numerically derived. This gives rise to the question as to how strongly numerical errors influence the PRness of the admittances derived from this data. This is especially important in light of the very small negative values encountered in the modified conjugate pole-pair admittances for first layer poles. We have elected to investigate this question in terms of the parameter tests given in Section 3.2. Errors in the real and imaginary parts of both the poles and the residues were introduced, and new parameter test curves were produced. In such a way

the sensitivity of these conditions to errors in the poles and residues can be observed. The study is centered on errors in the real part of the pole. The real part of a numerically derived pole is generally less trustworthy than the imaginary part.

Results for pole 1 of the wire are given in Figures 50 and 51. In these curves, the solid line is the original value, and the dashed lines indicate the changed values. Figure 50a shows the effect of a +5 percent change in the pole real part on the high frequency condition for pole 1. The change in this condition is very slight. Figures 50b through 50d indicate the effect of changing the other parameters by 5 percent. The largest change, of some 30 percent, occurs when the imaginary part of the pole is changed. Since this parameter is accurately known (within 2 percent) in the numerical data, this is not bothersome. Note that in none of these graphs is the basic character of the condition changed; that is, the shape remains the same and the condition remains positive.

An entirely different situation occurs when we modify the parameters by 5 percent for the low frequency test. These effects are illustrated in Figures 51a and 51b. In Figure 51a, a change of +5 percent in the real part of the pole results in an entirely positive condition. This change corresponds to forcing the real part of the pole slightly away from the $j\omega$ axis. The remaining figures indicate a similar occurrence when the imaginary part of the pole is forced towards the real axis, when the imaginary part of the residue is forced towards the real axis, and when the real part of the residue is forced away from the $j\omega$ axis.

The real part of this pole is modified to produce a PR function, both to study the effect on the admittance and for latter use in circuits.

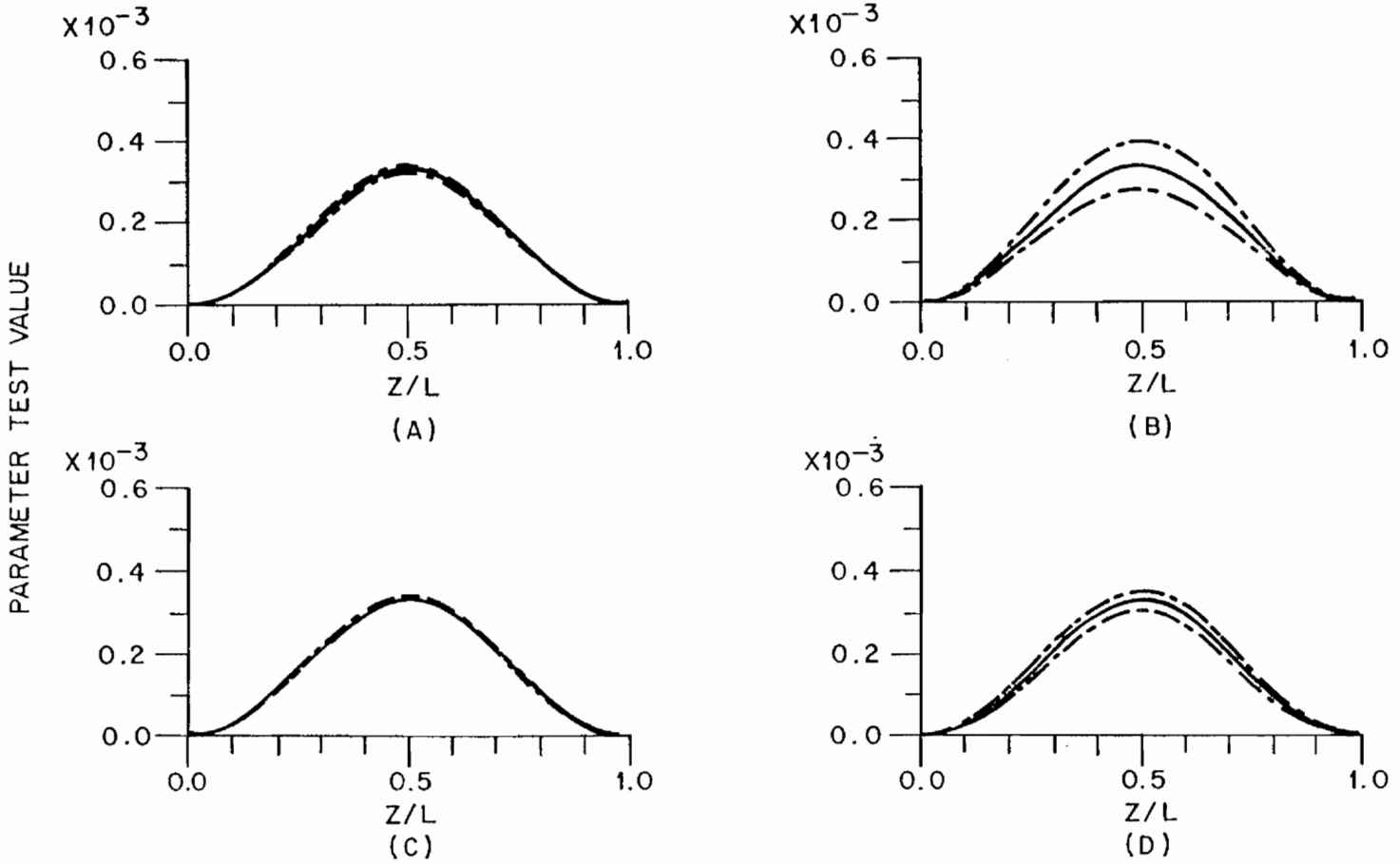

(A) ±5% CHANGE OF REAL PART OF POLE.
(B) ±5% CHANGE OF IMAGINARY PART OF POLE.
(C) ±5% CHANGE OF REAL PART OF RESIDUE
(D) ±5% CHANGE OF IMAGINARY PART OF RESIDUE.

Figure 50: Effect of ±5% change on parameter test IIB for pole-pair admittance of pole 1, first layer of the straight wire.

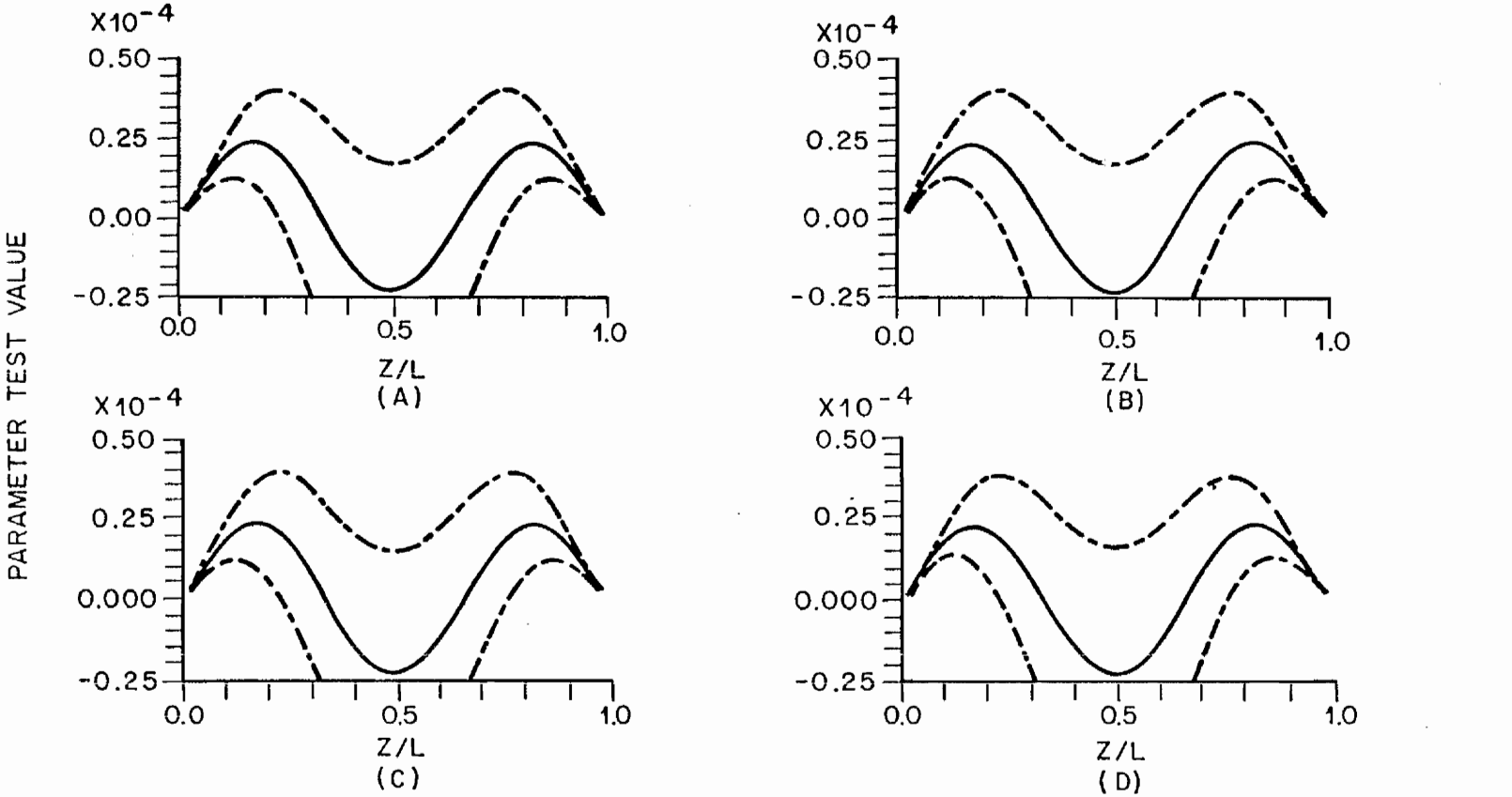

(A) ±5% CHANGE OF REAL PART OF POLE
(B) ±5% CHANGE OF IMAGINARY PART OF POLE
(C) ±5% CHANGE OF REAL PART OF RESIDUE
(D) ±5% CHANGE OF IMAGINARY PART OF RESIDUE

Figure 51: Effect of ±5% change on parameter test IIA for pole-pair admittance of pole 1, first layer of the straight wire.

Because an error of +5 percent for the real part of the pole is within the computational uncertainty of the data, a value of this pole with a real part changed by 3.5 percent is used, which allows the modified form of this admittance to be PR over the entire wire. When this is done, it is found that the peak value of the modified admittance formed from this pole decreases by 3 percent over the original value.

In light of these results for pole 1, the other poles were studied in the hope of producing PR results for the entire wire with adjustments in the pole value within the limit of numerical error. It was found however that all the other poles retained the essential characteristics of the non-PR conditions under as high an error as 10 percent. Figures 52 through 57 indicate these results for poles 2 and 3 for the first layer, and pole 2 of the second.

The conclusion to be reached is that the small negative low frequency admittance values found when forming modified conjugate pole-pair admittances are not attributable to any small numerical errors in either the poles or residues, but are inherent properties of these admittances. The important exception is pole 1 in the first layer. It was found that when large changes in the poles or residues were made in an attempt to make these pole-pair admittances PR, the peak value of the admittance, which we know to be accurate through comparison with integral equation admittance results, is changed substantially. Hence means other than parameter modification or approximation must be used to realize these admittances.

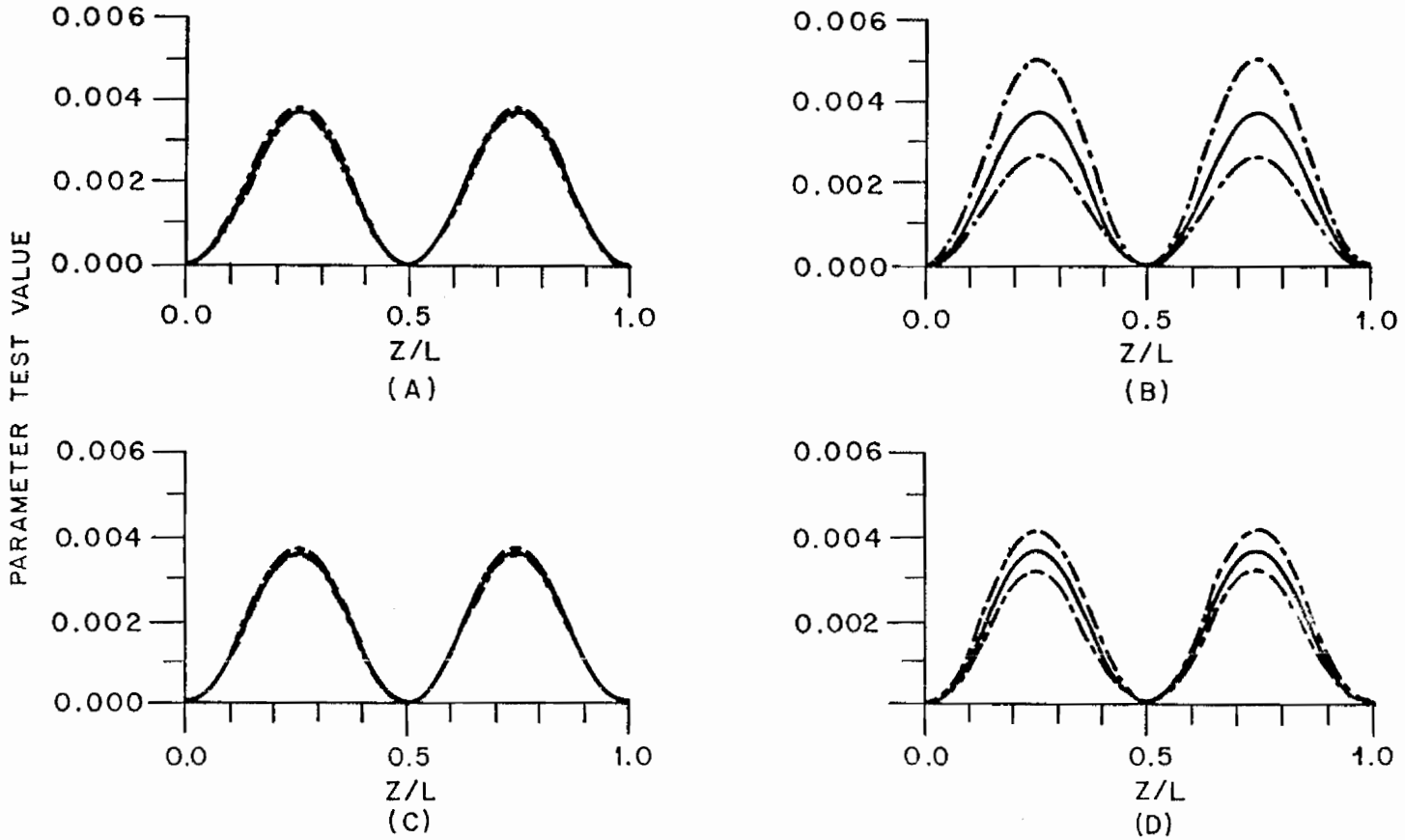

Figure 52: Effect of ±10% change on parameter test IIB for pole-pair admittance of pole 2, first layer of the straight wire.

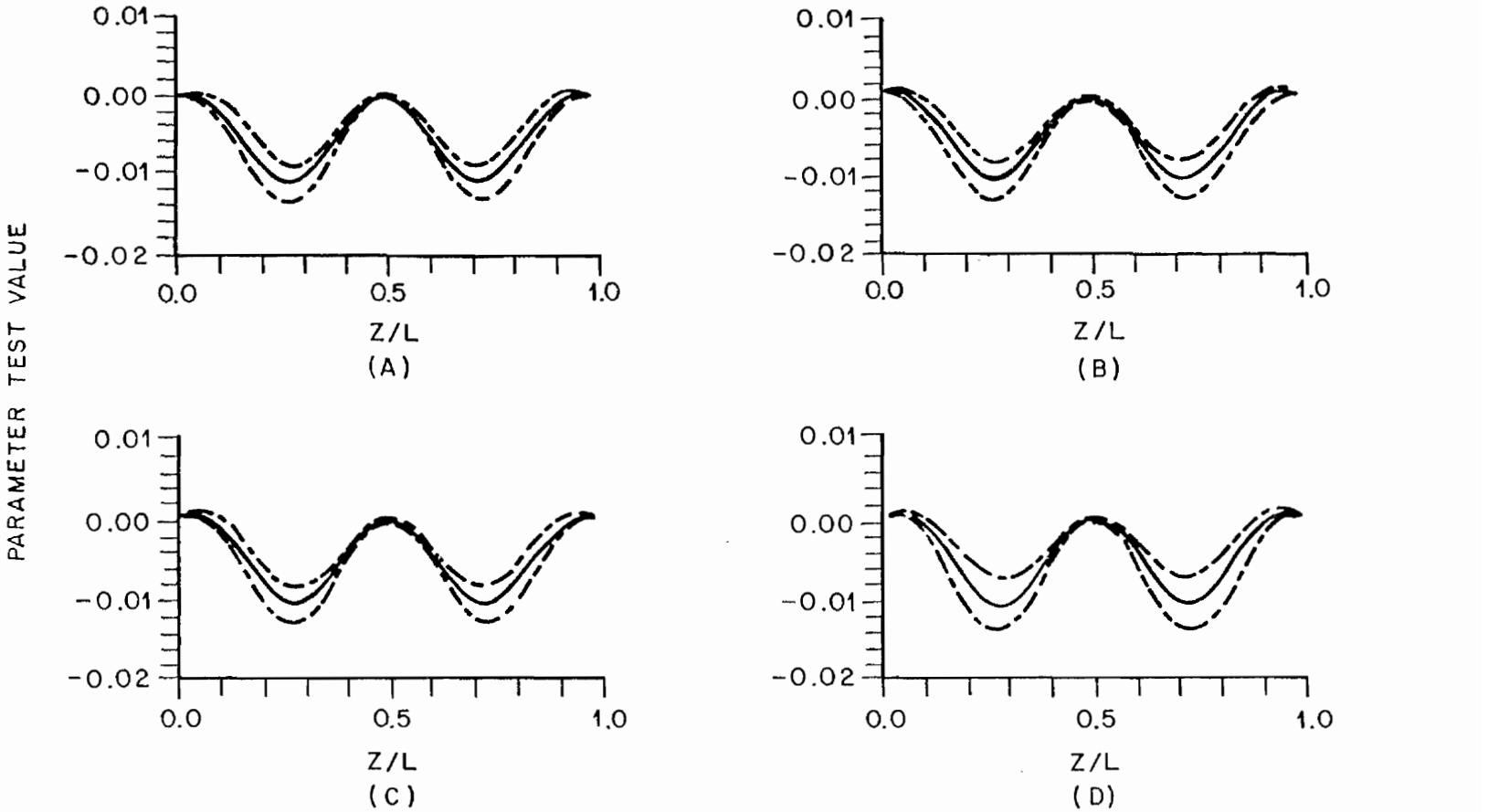

Figure 53: Effect of ±10% change on parameter test IIA for pole-pair admittance of pole 2, first layer of the straight wire.

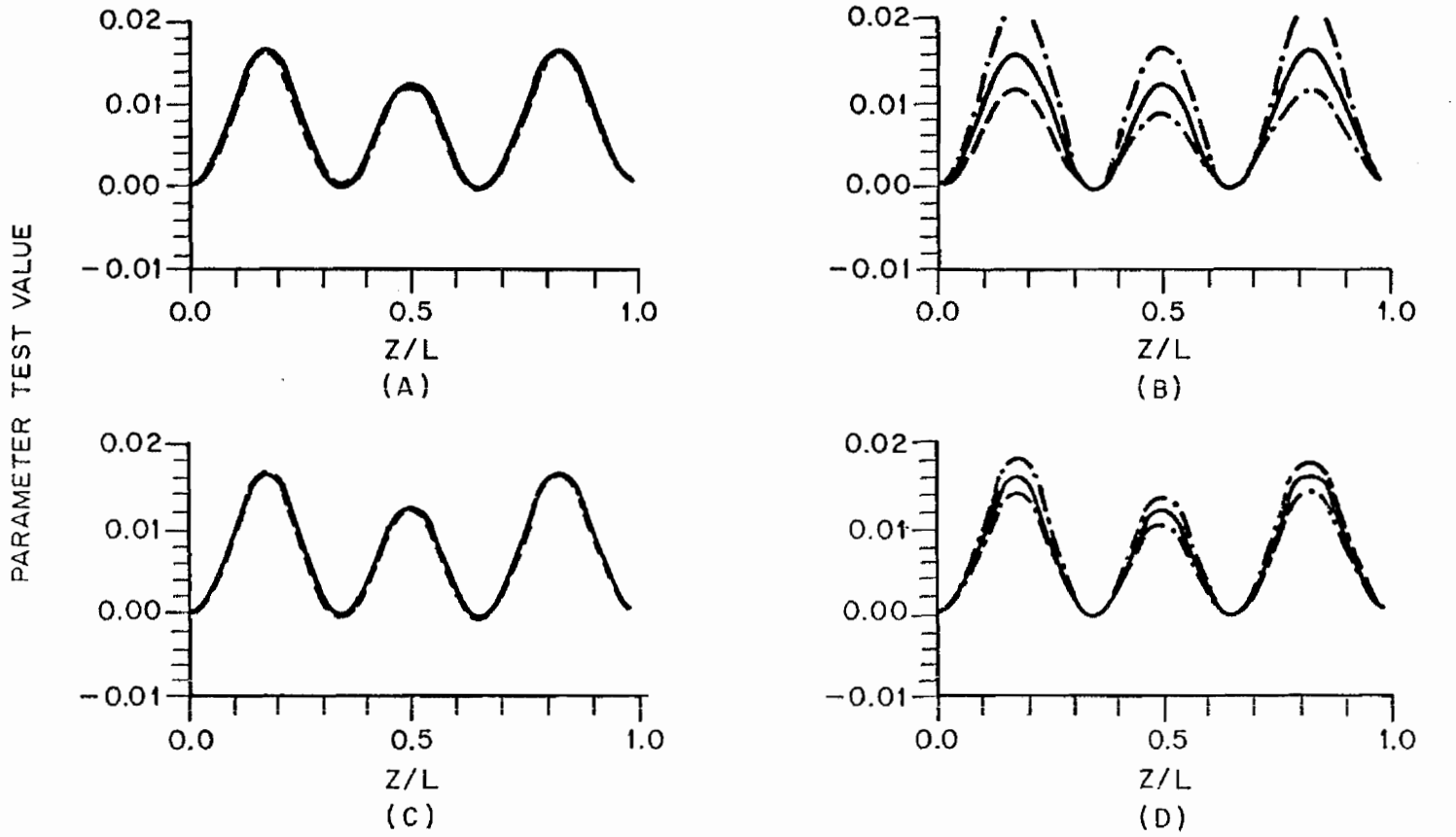

(A) ±10% CHANGE OF POLE REAL PART.
(B) ±10% CHANGE OF POLE IMAGINARY PART
(C) ±10% CHANGE OF RESIDUE REAL PART
(D) ±10% CHANGE OF RESIDUE IMAGINARY PART.

Figure 54: Effect of ±10% change on parameter test IIB for pole-pair admittance of pole 3, first layer of the straight wire.

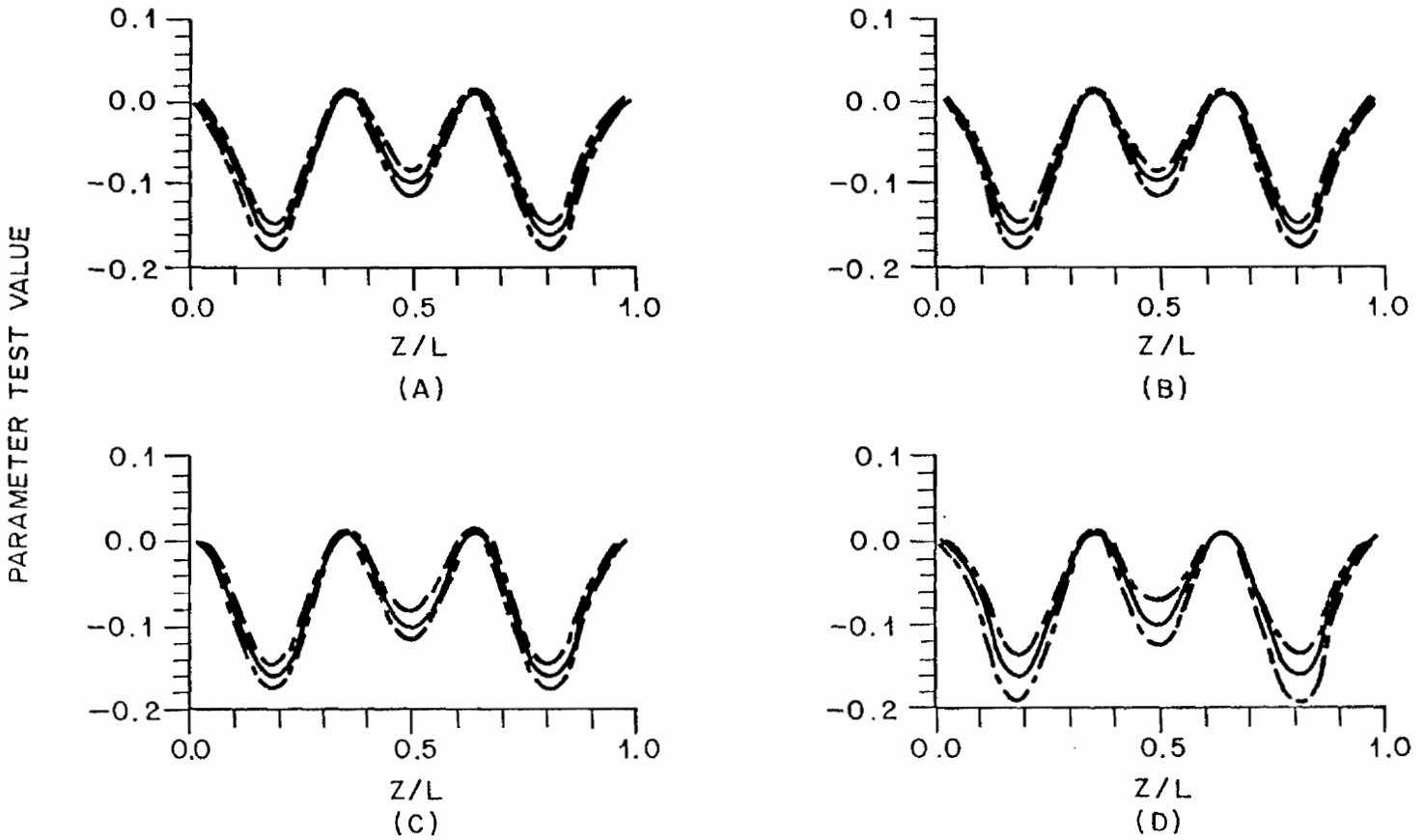

Figure 55: Effect of ±10% change of parameter test IIA for pole-pair admittance of pole 3, first layer of the straight wire.

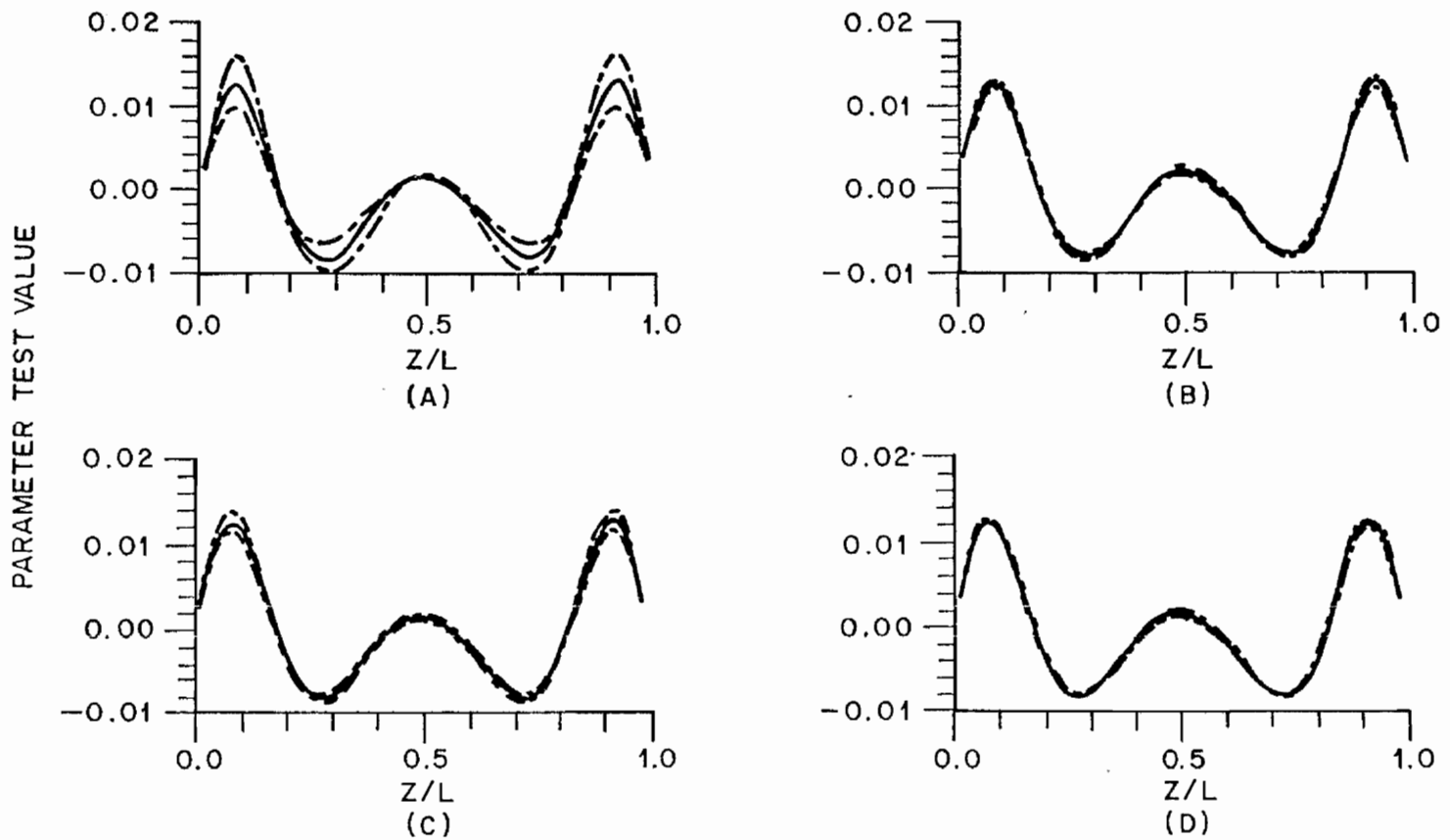

(A) ±10% CHANGE OF POLE REAL PART.
(B) ±10% CHANGE OF POLE IMAGINARY PART.
(C) ±10% CHANGE OF RESIDUE REAL PART.
(D) ±10% CHANGE OF RESIDUE IMAGINARY PART.

Figure 56: Effect of ±10% change on parameter test IIB for pole-pair admittance of pole 2, second layer of the straight wire.

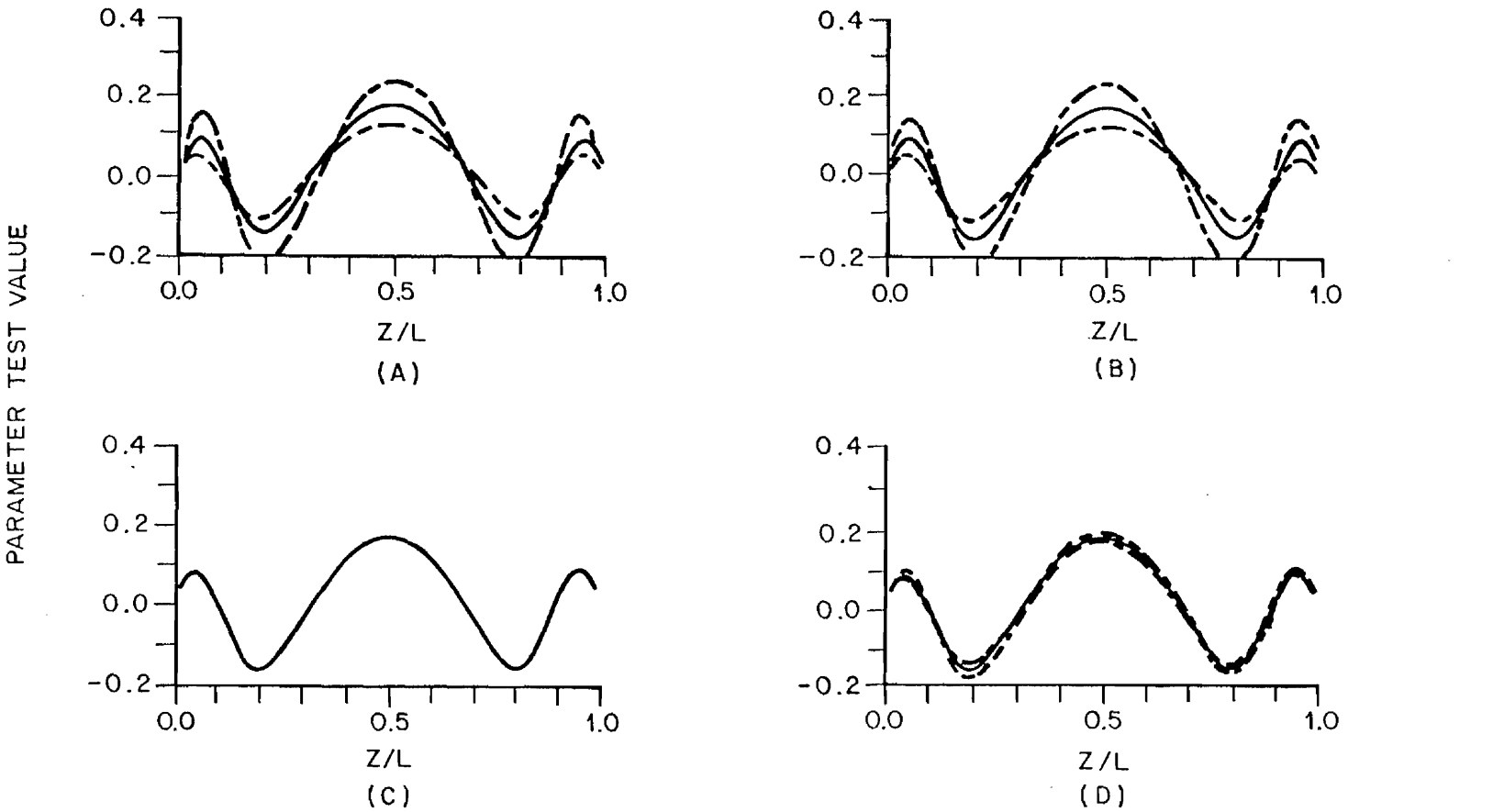

(A) ±10% CHANGE OF POLE REAL PART.
(B) ±10% CHANGE OF POLE IMAGINARY PART.
(C) ±10% CHANGE OF RESIDUE REAL PART.
(D) ±10% CHANGE OF RESIDUE IMAGINARY PART.

Figure 57: Effect of ±10% change on parameter test IIA for pole-pair admittance of pole 2, second layer of the straight wire.

CHAPTER IV

CIRCUIT SYNTHESIS

4.1 Introduction

This chapter addresses the construction of equivalent admittance circuits for three objects - the center-driven wire, the quarter-driven wire, and the circular loop. The circuits derived are physically realizable; that is, they are composed only of passive resistor, inductor, and capacitor elements. The circuits are composed of terminal eigenadmittance modules whenever possible. However, when terminal eigenadmittances are not PR, two other methods are used to create equivalent circuits. In the first, a method is devised by which an admittance having a negligible non-PR region can be made PR. In the second, poles are regrouped to produce a PR result. The response of these circuits to a transient voltage at the port are compared to the response of the original object to the same voltage. A study of the sensitivity of these circuits to element variations is also made.

4.2 Center-Driven Wire

Two equivalent circuits are constructed. The first is composed of terminal eigenadmittances, and the second employs first layer pole-pair admittances only. To construct this second circuit, a method is given by which the small non-PRness of these admittances can be neglected. The responses of both circuits are investigated.

4.2.1 Terminal Eigenadmittance Results

The PR results from Chapter III, which indicate that the summation of poles along the eigenmodes postulated in Figure 42 are PR and hence

physically realizable, are used as a basis to construct an equivalent circuit for the center-driven wire. The procedure followed is to construct the rational polynomial formed by the summing of those poles in an eigenmode and their conjugates, and then use standard circuit synthesis techniques to derive the equivalent circuits. The circuit synthesis is done by reducing the polynomial to a minimum conductance - minimum reactance form, and then applying the Bott-Duffin technique. Although a complete representation for the eigenmode grouping is available for only the first six eigenmodes, we chose to include mode seven, although the data base for this mode lacked one pole in the fourth layer, since it was PR without this pole. The poles and residues used are listed in Table 1. Figure 58 gives the result of this synthesis, and Table 2 lists the element values. The reactive components are normalized by $\frac{L}{\pi c}$. The real part of pole 1 is biased upward by 3.5 percent of the peak value, as indicated in Chapter III, to make it PR. Because only modes which possess current distributions which are even functions couple at the center of the antenna, eigenmodes one, three, five, and seven are realized. Table 2 also gives the actual circuit element values needed to realize the center-driven admittance of a 100-meter wire. This length was chosen because it gives element values which are in the picofarad, microhenry range. These values change proportionally to length, so that only a certain range of sizes for the wire may actually be realizable. This scaling of inductors and capacitors is frequency scaling, with the scaling factor equal to $\frac{L}{\pi c}$. Hence both capacitors and inductors increase with increasing length.

Table 1

Poles and Residues Used for Eigenmode Synthesis,

Center-Fed Cylindrical Antenna

Mode	Poles	Residues
1	$-.08427+j.9158$	$.1112\times10^{-2}+j.3121\times10^{-3}$
3	$-.1473+j2.870$	$.1319\times10^{-2}+j.3301\times10^{-3}$
	$-2.491+j1.328$	$.0988\times10^{-3}+j.2529\times10^{-3}$
5	$-.1877+j4.834$	$.1423\times10^{-2}+j.3521\times10^{-3}$
	$-2.894+j3.528$	$.1408\times10^{-3}+j.1850\times10^{-3}$
	$-4.517+j1.497$	$.3218\times10^{-4}+j.2378\times10^{-3}$
7	$-.2177+j6.792$	$.1496\times10^{-2}+j.3699\times10^{-3}$
	$-3.140+j5.600$	$.1647\times10^{-3}+j.1687\times10^{-3}$
	$-5.069+j3.890$	$.6818\times10^{-4}+j.1628\times10^{-3}$

Poles are normalized as per Tesche [9]

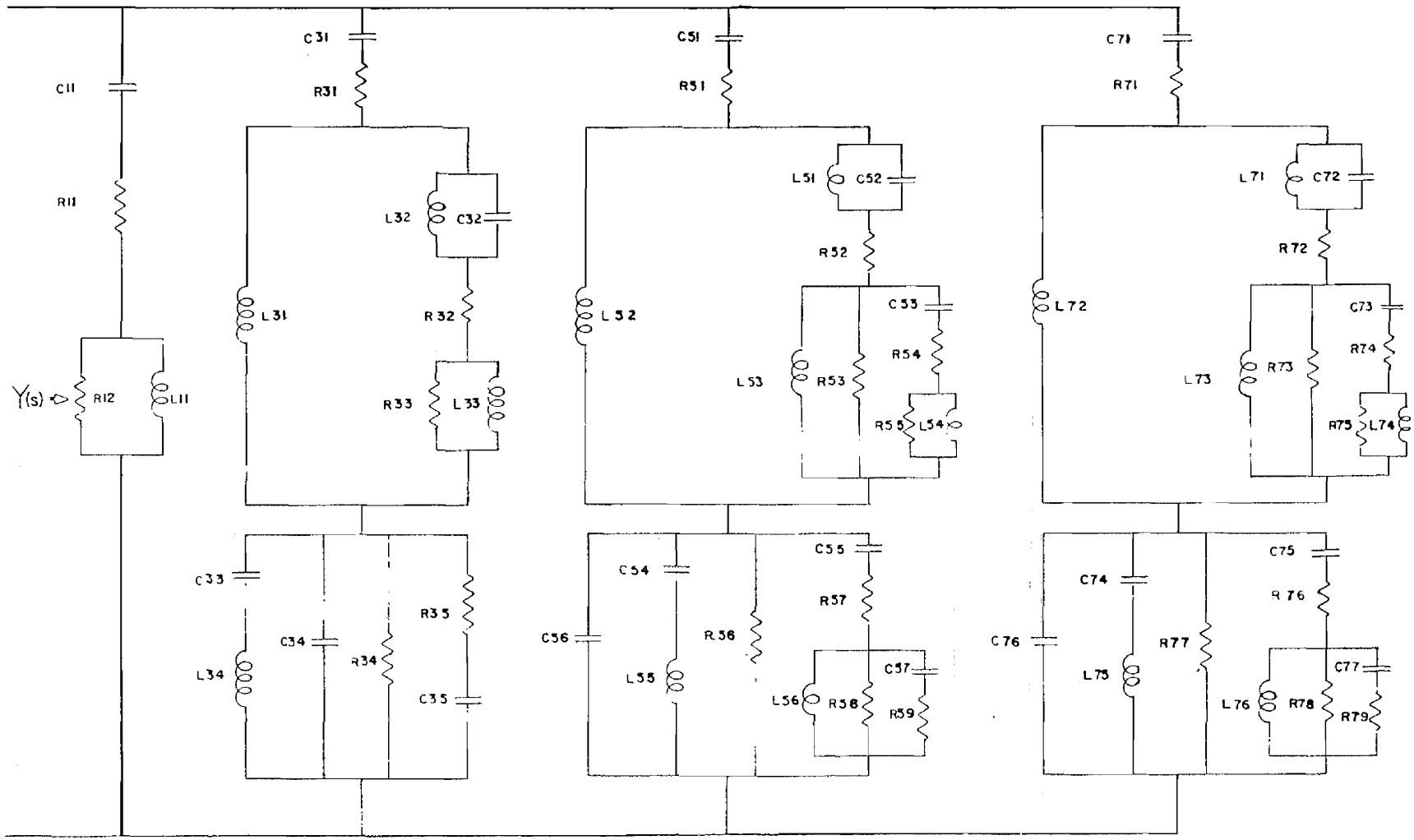

Figure 58: Equivalent circuit using terminal eigen-admittance modules for center-driven wire, modes 1,3,5,and 7.

Table 2

Element Values Normalized to $\frac{L}{\pi c}$ for Center-Driven Wire Admittance, Realized on a Terminal Eigenadmittance Basis

Mode	Element	Normalized Value	100 Meter Antenna (ohms, farads, henries)
1	R_{11}	.663	.663
	R_{12}	2200.6	2200.6
	C_{11}	2.72×10^{-3}	288.6×10^{-12}
	L_{11}	434.55	46.11×10^{-6}
2	R_{31}	29.76	29.76
	R_{32}	4280.	4280.
	R_{33}	571.4	571.4
	R_{34}	53.07	53.07
	R_{35}	397.4	397.4
	L_{31}	290.3	30.80×10^{-6}
	L_{32}	3817.	$405.\times10^{-6}$
	L_{33}	141.2	14.98×10^{-6}
	L_{34}	18.45	1.958×10^{-6}
	C_{31}	3.649×10^{-4}	38.72×10^{-12}
	C_{32}	8.126×10^{-5}	8.622×10^{-12}
	C_{33}	1.681×10^{-2}	1784×10^{-12}
	C_{34}	1.278×10^{-3}	135.6×10^{-12}
	C_{35}	6.218×10^{-4}	65.98×10^{-12}

Table 2 (continued)

Mode	Element	Normalized Value	100 Meter Antenna (ohms, farads, henries)
5	R_{51}	50.69	50.69
	R_{52}	5228	5228
	R_{53}	1003	1003
	R_{54}	2829	2829
	R_{55}	947.2	947.2
	R_{56}	137.9	137.9
	R_{57}	718.5	718.5
	R_{58}	761.1	761.1
	R_{59}	254.9	254.9
	C_{51}	1.539×10^{4}	16.33×10^{-12}
	C_{52}	3.926×10^{-5}	4.166×10^{-12}
	C_{53}	7.068×10^{-5}	7.499×10^{-12}
	C_{54}	3.362×10^{-4}	35.67×10^{-12}
	C_{55}	2.52×10^{-3}	267.4×10^{-12}
	C_{56}	2.608×10^{-4}	27.67×10^{-12}
	C_{57}	1.738×10^{-4}	18.44×10^{-12}
	L_{51}	242.4	25.72×10^{-6}
	L_{52}	1817.	192.8×10^{-6}
	L_{53}	188.	19.95×10^{-6}
	L_{54}	125.3	13.29×10^{-6}
	L_{55}	28.3	3.003×10^{-6}
	L_{56}	50.96	5.407×10^{-6}

Table 2 (continued)

Mode	Element	Normalized Value	100 Meter Antenna (ohms, farads, henries)
7	R_{71}	53.02	53.02
	R_{72}	5967	5967
	R_{73}	2500	2500
	R_{74}	1682	1682
	R_{75}	3611	3611
	R_{76}	106.5	106.5
	R_{77}	254.1	254.1
	R_{78}	377.7	377.7
	R_{79}	175.9	175.9
	C_{71}	8.368×10^{-5}	8.879×10^{-12}
	C_{72}	2.427×10^{-5}	2.575×10^{-12}
	C_{73}	2.285×10^{-5}	2.424×10^{-12}
	C_{74}	3.62×10^{-4}	38.41×10^{-12}
	C_{75}	2.161×10^{-3}	229.3×10^{-12}
	C_{76}	4.982×10^{-4}	52.86×10^{-12}
	C_{77}	1.129×10^{-3}	119.8×10^{-12}
	L_{71}	230.	24.40×10^{-16}
	L_{72}	1373	145.7×10^{-6}
	L_{73}	316.5	33.58×10^{-6}
	L_{74}	717.	76.08×10^{-6}
	L_{75}	15.42	1.636×10^{-6}
	L_{76}	14.52	1.541×10^{-6}

4.2.2 Pole-Pair Realization Using First Layer Poles

Although the previous section gives a practical circuit for the admittance of a center-driven wire, several factors limit its use. An eigenmode synthesis for modes higher than seven requires the SEM poles lying in the fifth and higher layers. Such poles are very hard to extract, and to date have not been extracted. This would result in a band limitation on the circuit if the higher modes are not represented. Also, as more modes are included in the representation more poles per mode are needed for realization, which leads to more circuit elements per mode.

For these reasons and because poles other than first layer appear to contribute negligibly to the total admittance, a circuit using only first layer pole-pair admittances is constructed. In light of the very small non-PR values associated with the first layer poles, it is reasonable to assume that some realization yields a circuit which includes some small, negligible negative elements.

The following observation in regard to the Bott-Duffin synthesis provided the necessary insight for approximate realization of the circuit. Suppose a negative conductance G_N, equal to the maximum negative value of a modified pole-pair admittance, is removed from the admittance. The resulting admittance is PR, since its real part has been raised by a level equal to the absolute value of G_N. If a Bott-Duffin synthesis is then performed on this PR admittance, the circuit module given in Figure 59 results.

Here Y_C and Y_L are functions obtained in the Bott-Duffin synthesis and are subsequently synthesized by the removal of a conjugate pole. The module is seen to consist of three branches: a shunt conductance, a capacitive branch, and an inductive branch. Since the overall admittance of this

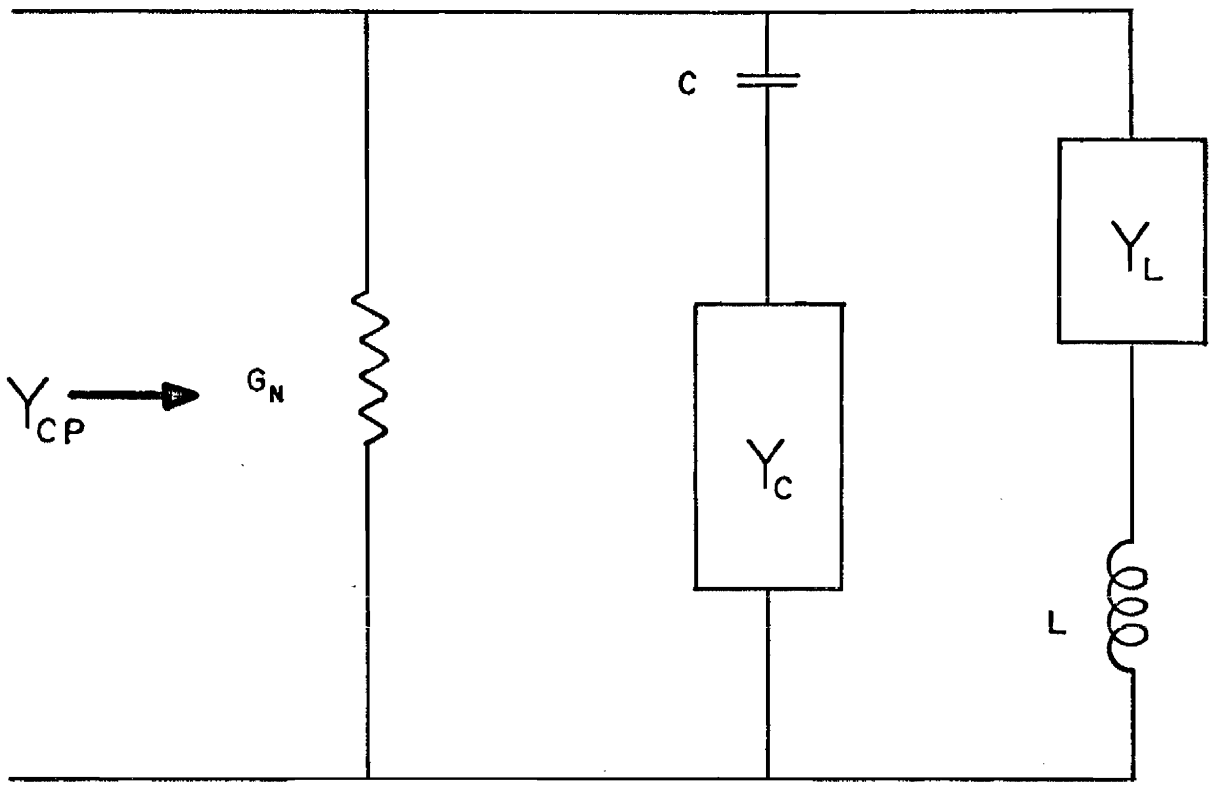

Figure 59: Modified Bott-Duffin synthesis module. The negative resistor branch and the inductor branch are negligible.

module at $\omega = 0$ is zero, then the admittance real part of Y_L, G_L, must equal G_N. Furthermore, the conductance of the inductance branch is limited to a maximum of G_L, since the elements in the branch are in series with G_L. Now since

$$|G_N| << |Y_{ni}^{cp}| \tag{5.1}$$

for the first layer poles, then

$$|G_L| << |Y_{ni}^{cp}| \tag{5.2}$$

as well.

This demonstrates that only the capacitive branch need be included in the synthesis and the other branches are negligible. This realization has the correct behavior at zero frequency, and has the proper pole at the proper peak value. The peak value does not differ from the original because, at the pole, the inductive branch contributes admittance G_N, while the resistor contributes $-G_N$. Only the final value of the admittance would differ from the original pole-pair admittance, and this is negligible.

This scheme is used to synthesize an equivalent circuit using only first layer poles for the center-driven wire. The resulting circuit is given in Figure 60, and a table of circuit element values given in Table 3.

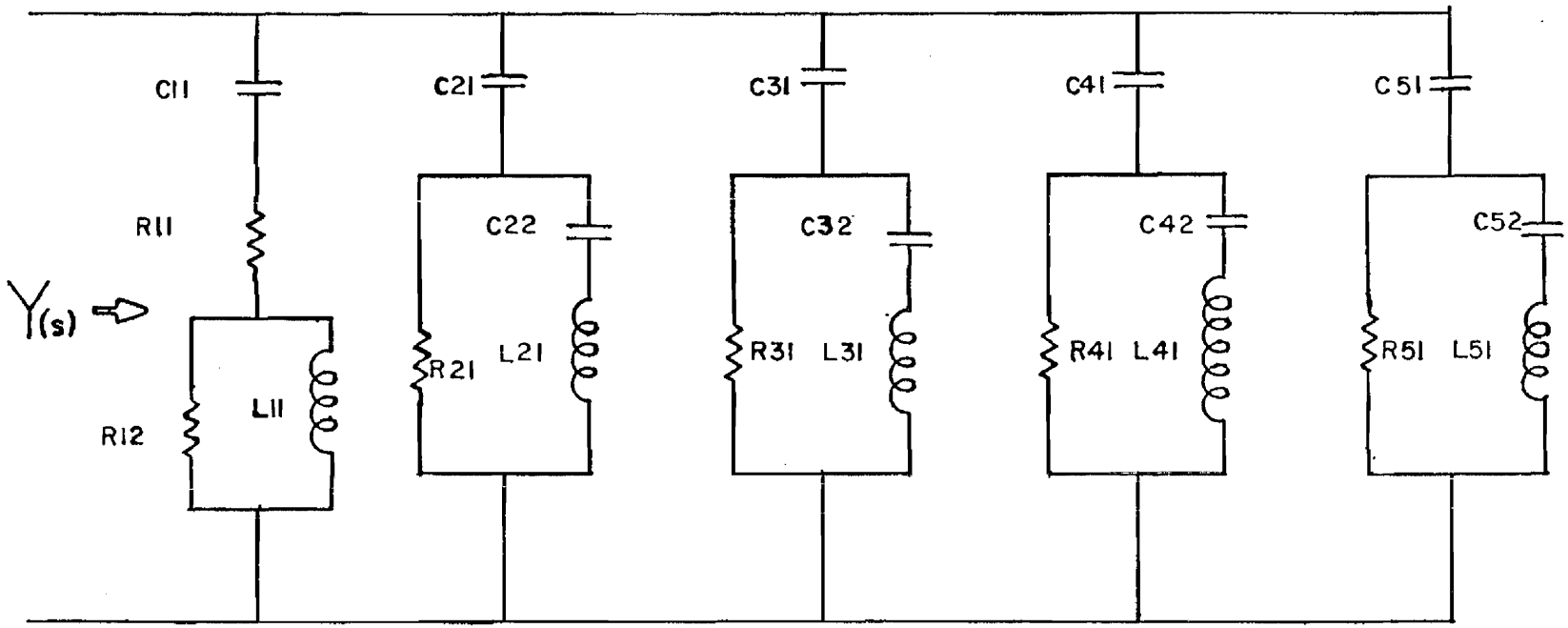

Figure 60: Equivalent circuit using nine first layer pole-pair admittances of the center-driven wire.

Table 3

Element Values for Center-Driven Wire Equivalent Circuit

Realized by First Layer Pole-Pair Admittances

Pole	Element	Normalized Value	100 Meter Antenna (ohms, farads, henries)
1	R_{11}	.663	.663
	R_{12}	2200.6	2200.6
	C_{11}	2.72×10^{-3}	288.6×10^{-12}
	L_{11}	434.55	46.11×10^{-6}
3	R_{21}	4958.7	4958.7
	C_{21}	4.728×10^{-4}	50.17×10^{-12}
	C_{22}	1.063×10^{-3}	112.8×10^{-12}
	L_{21}	368.22	39.07×10^{-6}
5	R_{31}	6513.5	6513.5
	C_{31}	2.253×10^{-4}	23.9×10^{-12}
	C_{32}	2.787×10^{-4}	29.57×10^{-12}
	L_{31}	341.4	36.22×10^{-6}
7	R_{41}	7542.3	7542.3
	C_{41}	1.418×10^{-4}	15.05×10^{-12}
	C_{42}	1.249×10^{-4}	13.25×10^{-12}
	L_{41}	324.6	34.44×10^{-6}

Table 3 (continued)

Pole	Element	Normalized Value	100 Meter Antenna (ohms, farads, henries)
9	R_{51}	8374.8	8374.8
	C_{51}	1.011×10^{-4}	10.73×10^{-12}
	C_{52}	7.124×10^{-5}	7.559×10^{-12}
	L_{51}	311.91	33.09×10^{-6}

4.2.3 Circuit Performance

The transient current response at the port of the circuits is analyzed by means of a SCEPTRE circuit analysis program implemented on an IBM 370 computer. The circuit is excited at the port by a Gaussian pulse of the form

$$V(t) = e^{-(AN(t-TMAX))^2}, \qquad (5.3)$$

where $AN = 3.25\times10^{7}$ and $TMAX = 60.802\times10^{-9}$ seconds. These results are then compared to results from the thin wire time domain (TWTD) program for a similar wire. Figure 61 illustrates these results for the eigenadmittance circuit, and Figure 62 illustrates the results for the first layer circuit synthesis.

The response for the two circuits is almost identical. The eigenadmittance circuit shows more oscillatory behavior but this is due to the truncation of the modes at mode seven. For late times the response is very close to the TWTD response. Note that both circuits miss the early time,

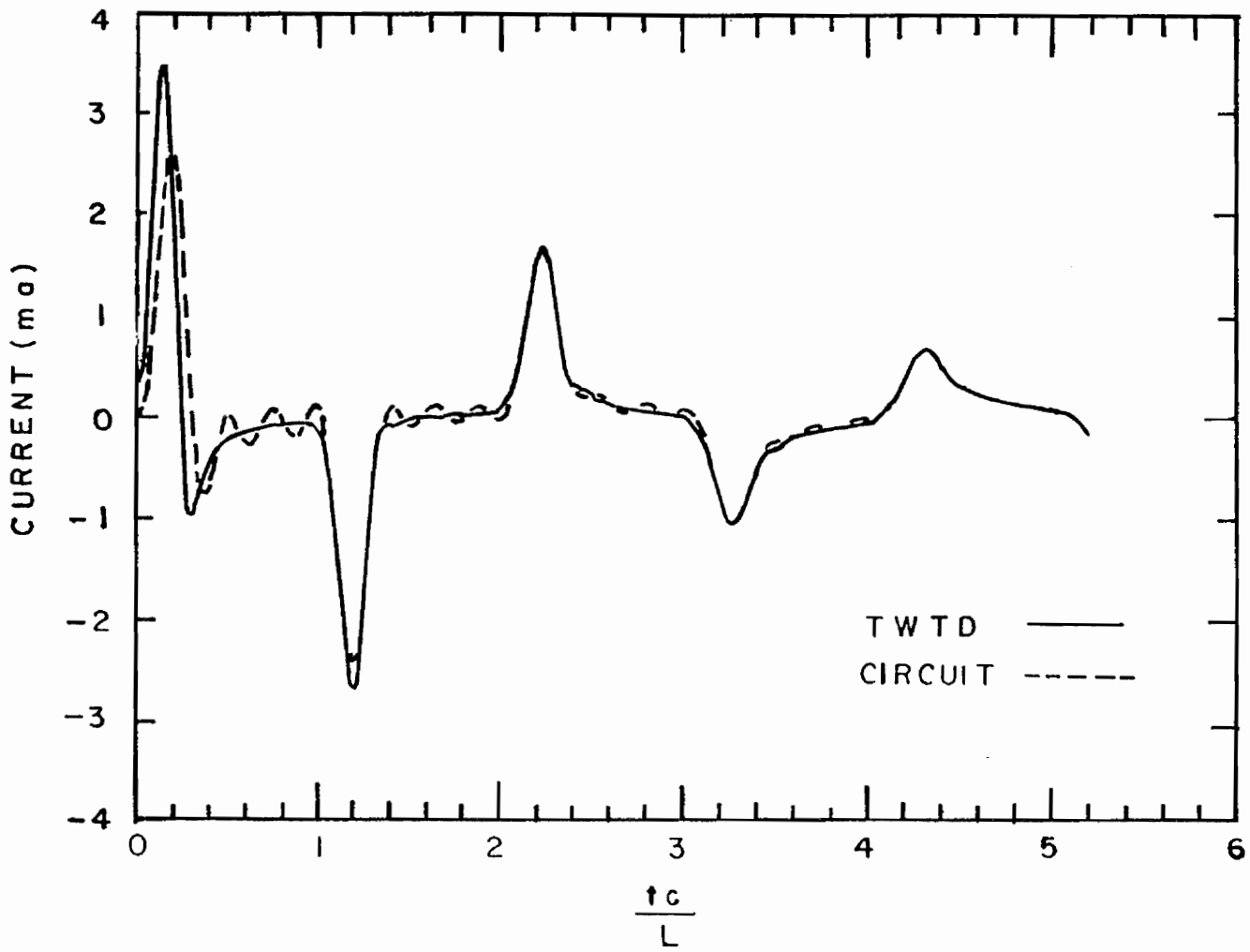

Figure 61: Comparison of the response of the eigenadmittance circuit to TWTD.

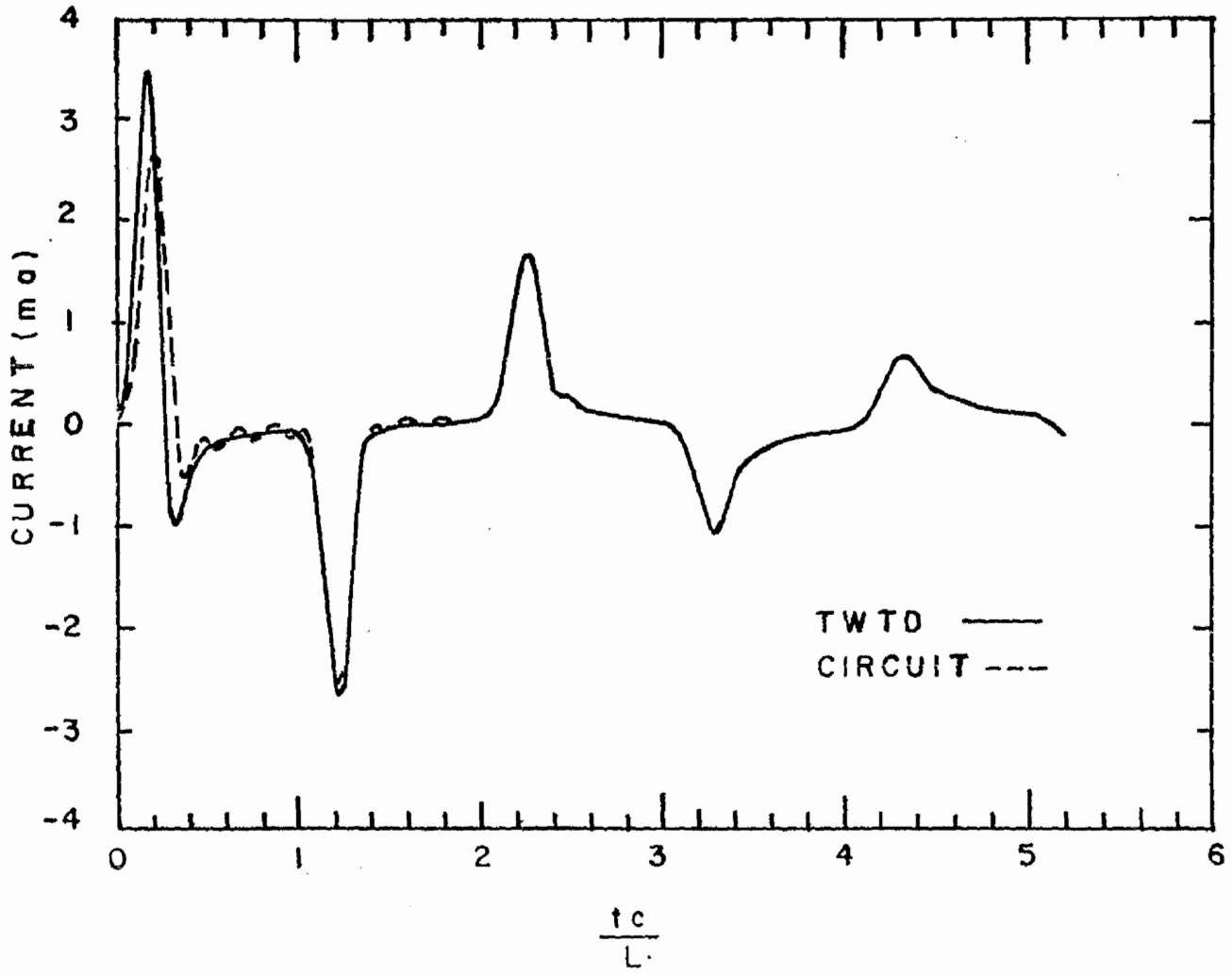

Figure 62: Comparison of the response of the first layer pole-pair circuit to TWTD.

or forced, response. This indicates that the representation for the wire is not complete. A study was made to attempt to discover what was missing to cause this early time response error. If we observe that the wire is a capacitive object, then it can be theorized that the SEM representation of the admittance should include a shunt capacitor across the port. Such a capacitor would correspond to a pole at infinity. It can be demonstrated that the response of such a capacitor would be such that it would give the correct forced response and not affect the late time. The current response of a capacitor is given by

$$i(t) = C \frac{dv}{dt} \quad . \tag{5.5}$$

If the forcing function is a Gaussian pulse then the current contributed by the shunt capacitor is given by

$$i(t) = C\, e^{-(AN(t-TMAX))^2}\, 2(AN(t - TMAX)) \quad . \tag{5.6}$$

Such a shunt capacitor can be viewed as a lumping of the static capacitances associated with an infinite number of poles neglected in the synthesis. This conjecture is supported by work done by Franceschetti [14] on the quasi-static capacitance of spheroidal antennas.

4.3 Quarter-Driven Wire

In the last chapter we showed that some of the terminal eigenadmittances for this structure are non-PR. Thus an alternate means of realizing the equivalent circuit is employed here. In order to perform the synthesis at this

feed point, we resorted to an *ad hoc* grouping of poles so as to achieve PR "pole group" admittances. The groups used are as follows:

Group 1

pole 1, first layer

Group 2

pole 2, first layer

pole 1, second layer

Group 3

pole 3, first layer

pole 2, second layer

pole 1, third layer

Group 4

pole 5, first layer

Group 5

pole 6, first layer

pole 7, second layer

pole 1, fourth layer

Group 6

pole 7, first layer

pole 8, second layer

pole 4, third layer

Group 7

pole 9, first layer

Group 8

pole 10, first layer

pole 9, second layer

pole 8, third layer

Poles 4 and 8 of the first layer were not included, because of their negligible pole-pair admittances. Table 4 lists the values of the poles and residues used.

Table 4

Poles and Residues Used for 1/4-Fed Synthesis of Cylindrical Antenna

'ad hoc' Group	Poles	Residues
1	$-.08427+j.9158$	$.6192\times10^{-3}+j.1619\times10^{-3}$
2	$-.1199+j1.890$	$.1268\times10^{-2}+j.3537\times10^{-3}$
	$-2.149+j0.0$	$-.1707\times10^{-3}+j.0$
3	$-.1473+j2.870$	$.5496\times10^{-3}+j.2259\times10^{-3}$
	$-2.491+j1.328$	$.1159\times10^{-3}-j.1483\times10^{-3}$
	$-4.098+j0.0$	$-.2497\times10^{-3}+j0.0$
4	$-.1877+j4.834$	$.9177\times10^{-3}+j.1117\times10^{-3}$
5	$-.2038+j5.814$	$.1500\times10^{-2}+j.4254\times10^{-3}$
	$-3.225+j6.620$	$.9804\times10^{-3}-j.2504\times10^{-3}$
	$-6.006-j.884\times10^{-2}$	* *
6	$-.2177+j6.792$	$.5494\times10^{-3}+j.3144\times10^{-3}$
	$-3.297+j7.632$	$.5421\times10^{-3}+j.1116\times10^{-2}$
	$-5.069+j3.890$	$.6790\times10^{-3}+j.8824\times10^{-3}$
7	$-.2426+j8.736$	$.1074\times10^{-2}+j.7253\times10^{-4}$
8	$-.1783+j9.766$	$.1641\times10^{-2}+j.5373\times10^{-3}$
	$-3.363+j8.636$	$-.1079\times10^{-2}+j.6414\times10^{-3}$
	$-5.638+j8.235$	$.2912\times10^{-2}+j.8177\times10^{-3}$

Poles are normalized as per Tesche [9]

*Residue value unavailable

Figure 63 gives the circuit synthesized from the above groupings using the Bott-Duffin procedure. Table 5 gives the element values. The circuit was analyzed with the SCEPTRE program, using the same Gaussian pulse as in the previous example, and a comparison with results computed by TWTD was made. Figure 64 illustrates this comparison. The circuit response exhibited (when compared to TWTD) oscillations of relatively high magnitude. These oscillations cause the signal to be degraded in late time. However, the general shape was replicated. The early time response shows the same departure from TWTD as did the center-driven wire. There are two possible sources of the oscillations. One is an incorrect element value in one of the modules. The other more likely possibility is an error in the SEM poles, particularly in the higher frequency, deeply embedded ones.

4.4 Admittance Synthesis for Circular Loop

As stated in Chapter III, there are an infinite number of poles in an eigenmode of the circular loop. Therefore, a terminal eigenadmittance module has an infinite number of elements and is unrealizable in a practical sense. By truncating the set of eigenmode poles, a truncated terminal eigenadmittance module can be constructed. Two problems remain, however. First, the truncation may not result in a PR admittance, in which case the modified Bott-Duffin procedure of Section 4.2.2 must be used. Namely, the admittance is made PR by removing a negative conductance, and then neglecting this conductance branch and the inductance branch in the subsequent Bott-Duffin synthesis. Second, even if the truncated admittance is PR, the complexity of the Bott-Duffin circuit grows quickly with pole count. The number of elements required for a Bott-Duffin synthesis grows by $7\times2^{N}-6$, where N is the number of pole-pairs. Thus an admittance composed of 4 pole-pairs requires 106 elements.

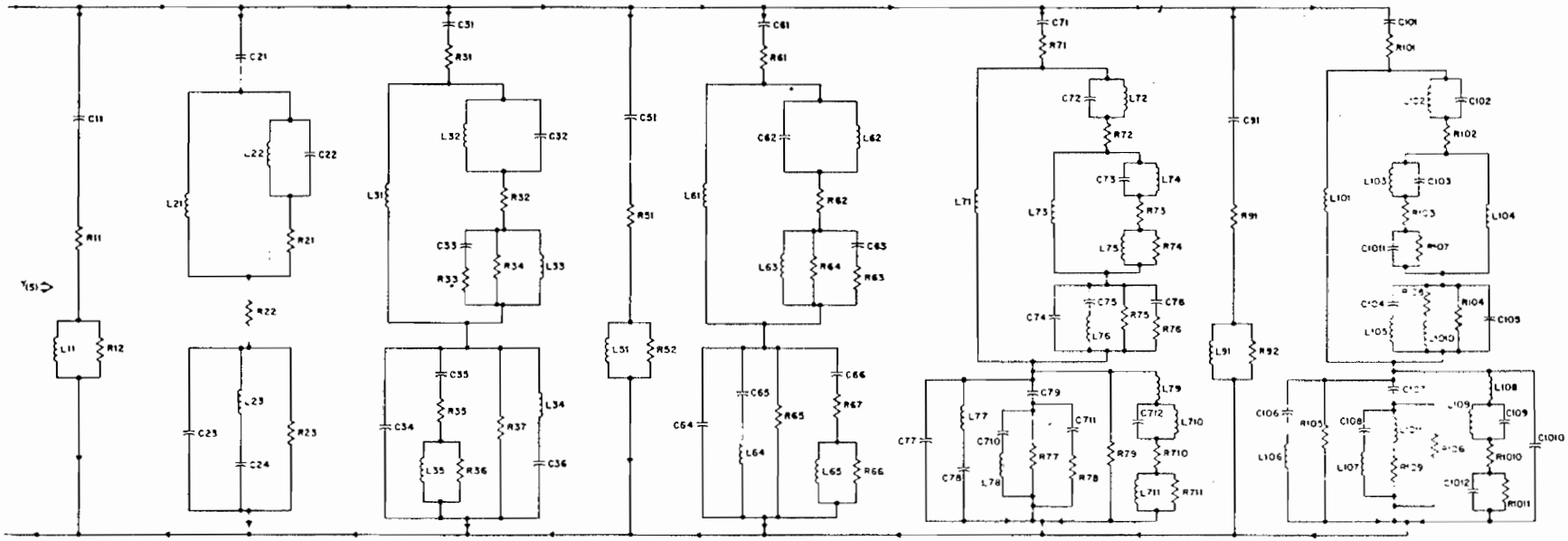

FIGURE 63. EQUIVALENT CIRCUIT FOR QUARTER-DRIVEN ANTENNA

Figure 63: Equivalent circuit for quarter-driven antenna.

Table 5

Element Values for Pole Groupings of Quarter-Driven Antenna

Pole Group	Element	Normalized Value	100 Meter Antenna (ohms, farads, henries)
1	R_{11}	7.427	7.427
	R_{12}	4311.9	4311.9
	C_{11}	1.51×10^{-3}	160.2×10^{-12}
	L_{11}	782.3	83×10^{-6}
2	R_{21}	2234.4	2234.4
	R_{22}	3.405	3.405
	R_{23}	.752	.752
	C_{21}	8.003×10^{-4}	84.91×10^{-12}
	C_{22}	2.288×10^{-4}	24.28×10^{-12}
	C_{23}	1.787×10^{-1}	18.96×10^{-9}
	C_{24}	1.026×10^{1}	108.9×10^{-9}
	L_{21}	300.5	31.88×10^{-6}
	L_{22}	17256.	1.831×10^{-3}
	L_{23}	.3846	40.81×10^{-9}
3	R_{31}	36.13	36.13
	R_{32}	5806.	5806.
	R_{33}	4677	4677
	R_{34}	1597	1597
	R_{35}	1042	1042
	R_{36}	355.6	355.6
	R_{37}	286.5	286.5

Table 5 (continued)

Pole Group	Element	Normalized Value	100 Meter Antenna (ohms, farads, henries)
3	C_{31}	1.843×10^{-4}	19.56×10^{-12}
	C_{32}	6.606×10^{-5}	7.009×10^{-12}
	C_{33}	3.24×10^{-5}	3.438×10^{-12}
	C_{34}	3.174×10^{-4}	33.68×10^{-12}
	C_{35}	1.634×10^{-4}	17.34×10^{-12}
	C_{36}	2.007×10^{-3}	213.0×10^{-12}
	L_{31}	527.9	56.02×10^{-6}
	L_{32}	3339	354.2×10^{-6}
	L_{33}	271.8	28.84×10^{-6}
	L_{34}	107.9	11.66×10^{-6}
	L_{35}	53.9	5.719×10^{-6}
4	Does not couple		
5	R_{51}	1.418	1.418
	R_{52}	32510.	32510.
	C_{51}	7.893×10^{-6}	837.5×10^{-12}
	L_{51}	541.3	57.43×10^{-6}
6	R_{61}	65.91	65.91
	R_{62}	17640.	17640.
	R_{63}	38400.	38400.
	R_{64}	32450.	32450.
	R_{65}	258.3	258.3
	R_{66}	118.7	118.7
	R_{67}	140.4	140.4

Table 5 (continued)

Pole Group	Element	Normalized Value	100 Meter Antenna (ohms, farads, henries)
6	C_{61}	1.182×10^{-4}	12.54×10^{-12}
	C_{62}	1.258×10^{-5}	1.335×10^{-12}
	C_{63}	1.790×10^{-6}	1899×10^{-12}
	C_{64}	4.909×10^{-5}	5.209×10^{-12}
	C_{65}	7.124×10^{-4}	75.58×10^{-12}
	C_{66}	2.471×10^{-4}	26.22×10^{-12}
	L_{61}	223.7	23.74×10^{-6}
	L_{62}	3246.	344.4×10^{-6}
	L_{63}	1126.	119.5×10^{-6}
	L_{64}	57.33	6.083×10^{-6}
	L_{65}	8.156	$.8654\times10^{-6}$
7	R_{71}	108.3	108.3
	R_{72}	2615.	2615.
	R_{73}	708.	708.
	R_{74}	65.4	65.4
	R_{75}	31.12	31.12
	R_{76}	336.9	336.9
	R_{77}	2661.	2661.
	R_{78}	28810.	28810.
	R_{79}	720.5	720.5
	R_{710}	60540	60540
	R_{711}	5592.	5592.

Table 5 (continued)

Pole Group	Element	Normalized Value	100 Meter Antenna (ohms, farads, henries)
7	C_{71}	9.245×10^{-5}	9.809×10^{-12}
	C_{72}	1.065×10^{-4}	11.3×10^{-12}
	C_{73}	2.084×10^{-4}	22.11×10^{-12}
	C_{74}	3.532×10^{-3}	374.8×10^{-12}
	C_{75}	1.642×10^{-2}	1743×10^{-12}
	C_{76}	3.355×10^{-4}	35.6×10^{-12}
	C_{77}	8.445×10^{-5}	8.961×10^{-12}
	C_{78}	1.277×10^{-4}	13.55×10^{-12}
	C_{79}	4.131×10^{-5}	4.383×10^{-12}
	C_{710}	1.921×10^{-4}	20.38×10^{-12}
	C_{711}	3.924×10^{-6}	$.4163\times10^{-12}$
	C_{712}	2.437×10^{-6}	$.2586\times10^{-12}$
	L_{71}	159.1	16.88×10^{-6}
	L_{72}	240.6	25.52×10^{-6}
	L_{73}	77.82	8.257×10^{-6}
	L_{74}	361.9	38.39×10^{-6}
	L_{75}	7.392	$.7843\times10^{-6}$
	L_{76}	4.592	$.4872\times10^{-6}$
	L_{77}	200.6	21.28×10^{-6}
	L_{78}	392.6	41.66×10^{-6}
	L_{79}	6654.	706.0×10^{-6}
	L_{710}	30940.	3.283×10^{-3}
	L_{711}	632.0	67.06×10^{-6}
8	Does not couple		

Table 5 (continued)

Pole Group	Element	Normalized Value	100 Meter Antenna (ohms, farads, henries)
9	R_{91}	64.38	64.38
	R_{92}	102300.	102300.
	C_{91}	2.819×10^{-5}	2.991×10^{-12}
	L_{91}	464.2	49.26×10^{-6}
10	R_{101}	5.875	5.875
	R_{102}	3920.	3920.
	R_{103}	4209.	4209.
	R_{104}	1610.0	1610.
	R_{105}	694.0	694.
	R_{106}	646.3	646.3
	R_{107}	84.55	84.55
	R_{108}	80150.	80150.
	R_{109}	32170.	32170
	R_{1010}	1690.	1690.
	R_{1011}	33.94	33.94
	C_{101}	6.284×10^{-5}	6.668×10^{-12}
	C_{102}	2.144×10^{-5}	2.275×10^{-12}
	C_{103}	5.458×10^{-1}	5.791×10^{-12}
	C_{104}	4.066×10^{-5}	4.314×10^{-12}
	C_{105}	2.147×10^{-5}	2.278×10^{-12}
	C_{106}	2.418×10^{-4}	25.66×10^{-12}
	C_{107}	5.348×10^{-5}	5.674×10^{-12}
	C_{108}	1.013×10^{-4}	10.75×10^{-12}
	C_{109}	1.359×10^{-4}	14.42×10^{-12}
	C_{1010}	4.989×10^{-5}	5.294×10^{-12}
	C_{1011}	7.346×10^{-4}	77.94×10^{-12}
	C_{1012}	1.830×10^{-4}	19.42×10^{-12}

Table 5 (continued)

Pole Group	Element	Normalized Value	100 Meter Antenna (ohms, farads, henries)
10	L_{101}	135.7	14.40×10^{-6}
	L_{102}	658.	69.82×10^{-6}
	L_{103}	275.5	29.23×10^{-6}
	L_{104}	145.5	15.44×10^{-6}
	L_{105}	369.8	39.24×10^{-6}
	L_{106}	58.33	6.189×10^{-6}
	L_{107}	148.4	15.75×10^{-6}
	L_{108}	58.4	6.196×10^{-6}
	L_{109}	110.7	11.74×10^{-6}
	L_{1010}	497.8	52.82×10^{-6}
	L_{1011}	1998.	212.0×10^{-6}

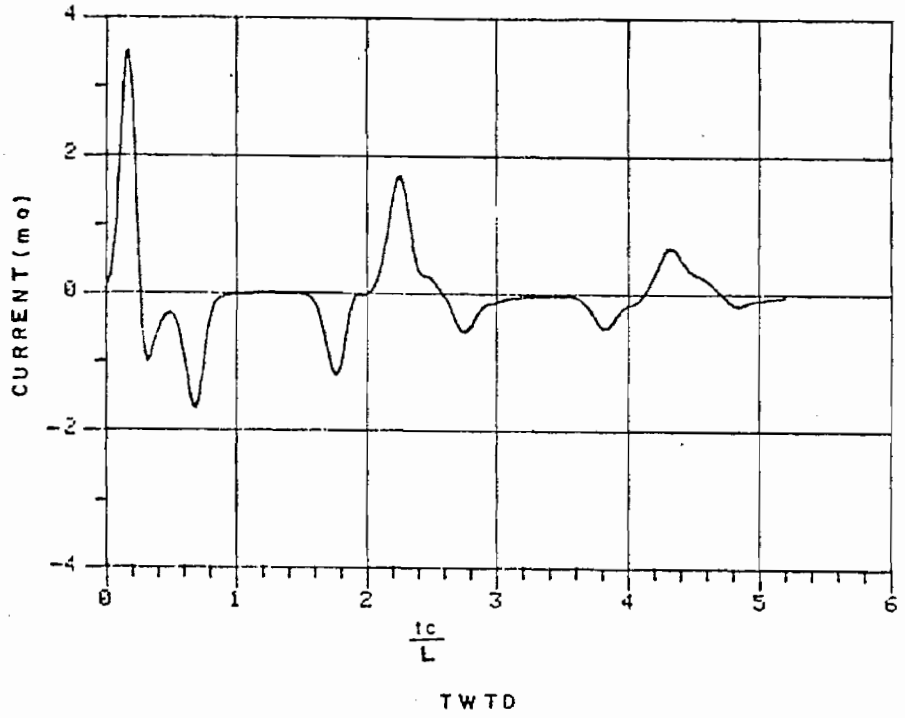

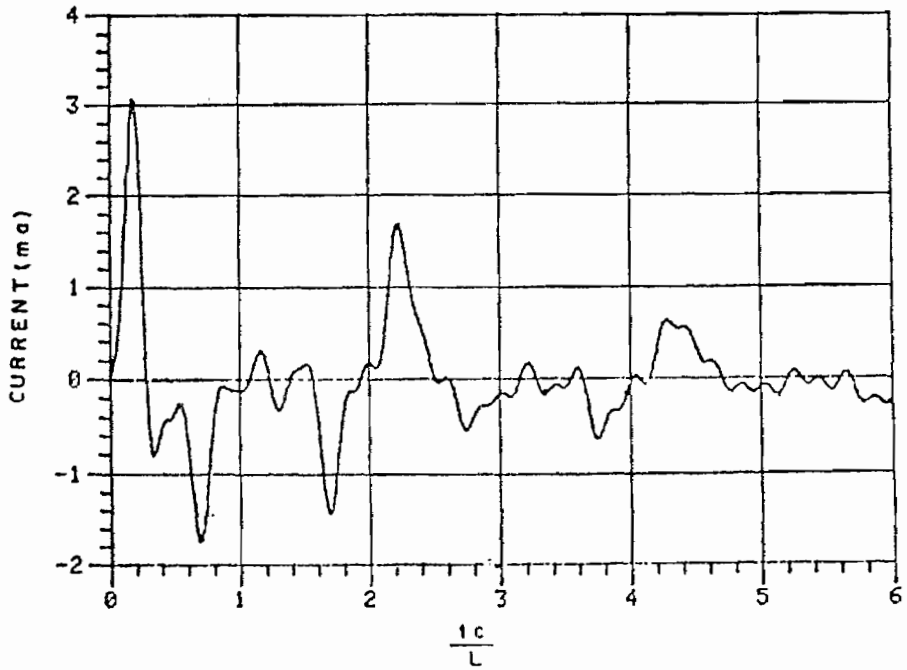

Figure 64: Comparison of the response of the quarter-driven wire circuit to TWTD.

For these reasons, two circuits for the circular loop are constructed, representing two degrees of complexity. In the first, only the type I poles of each eigenmode are used. In the second, all poles necessary for a PR result are used, except when the data is insufficient for a PR result, in which case the type I and type III poles are used.

4.4.1 Type I Poles

Given that the type I poles are the major contributors to the total admittance of the loop, and that the non-PR excursions of these pole-pair admittances are quite small, a modified Bott-Duffin synthesis of the type used for realizing the first layer poles on the straight wire is implemented. Because the loop is a closed object, it has a pole located at $s = 0$. This pole represents the magnetostatic inductance of the loop which was realized straightforwardly as a lumped inductor. Only the type I poles for the first 10 modes were used in the equivalent circuit. These are sufficient to realize the response to the bandwidth of excitation used. The resulting circuit is shown in Figure 65. Table 6 lists the element values, both normalized and for a 100 meter radius antenna.

Again the circuit was analyzed by SCEPTRE and compared to TWTD results. Figure 66 displays this comparison. The agreement in early time is excellent, but the peak values of the circuit are approximately 15 percent higher than the TWTD response. In the late time the circuit response is offset from the TWTD response by about 0.2 ma, and the circuit response shows oscillations.

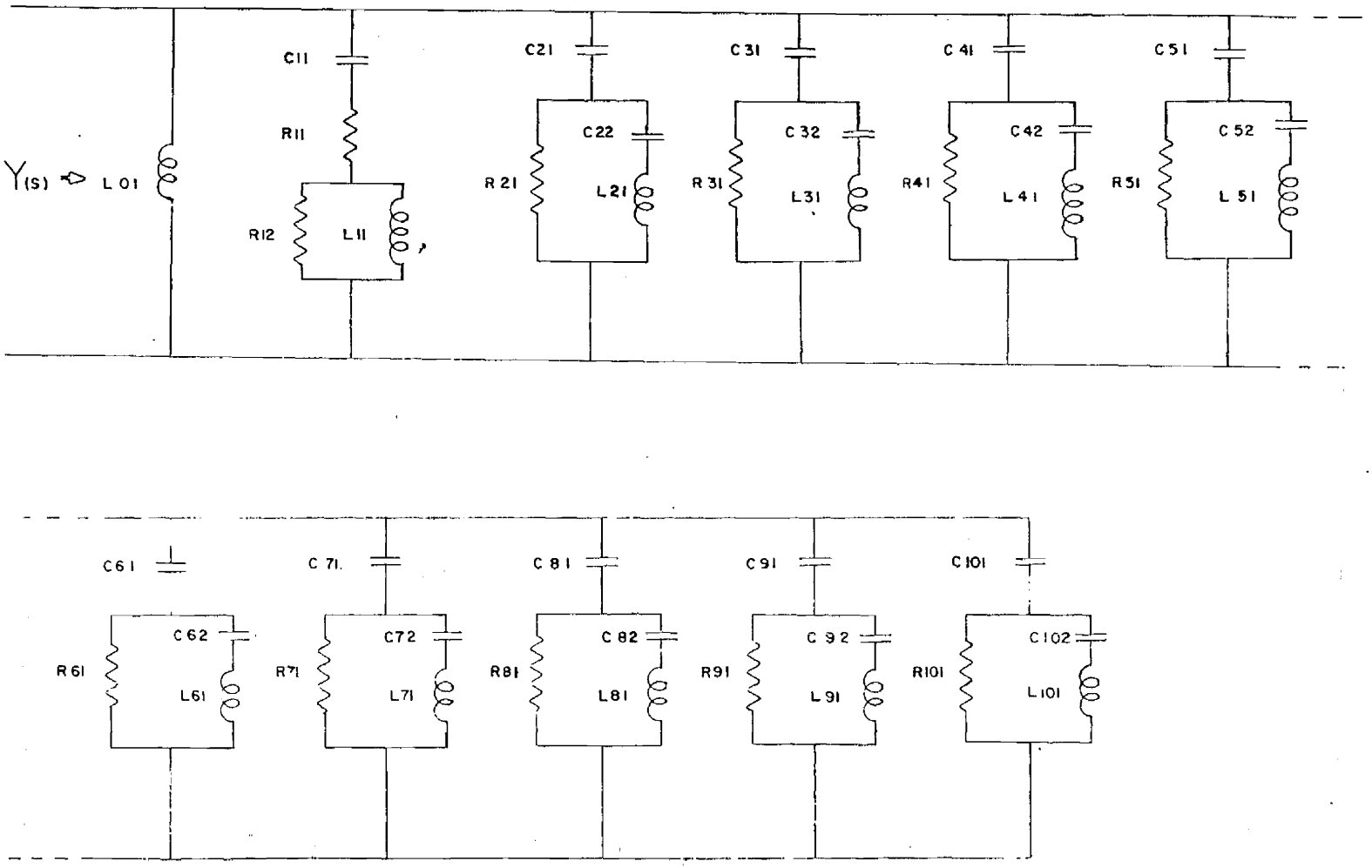

Figure 65: Equivalent circuit for the circular loop using type I pole-pair admittances. The pole at zero is represented by the shunt inductor.

Table 6

Element Values for Circular Loop Equivalent Circuit Using Type I Poles

Mode	Element	Normalized Value	100 Meter Antenna (ohms, farads, henries)
0	L_{01}	2165.	721.5×10^{-6}
1	R_{11}	47.35	47.35
	R_{12}	10.16×10^{3}	10.16×10^{3}
	C_{11}	9.918×10^{-4}	330.6×10^{-12}
	L_{11}	925.5	308.5×10^{-6}
2	R_{21}	16.63×10^{3}	16.63×10^{3}
	C_{21}	2.802×10^{-4}	93.4×10^{-12}
	C_{22}	1.335×10^{-2}	$4450.\times10^{-12}$
	L_{21}	862.5	287.5×10^{-6}
3	R_{31}	20.71×10^{3}	20.71×10^{3}
	C_{31}	1.529×10^{-5}	50.98×10^{-12}
	C_{32}	8.616×10^{-4}	287.1×10^{-12}
	L_{31}	818.1	272.7×10^{-6}
4	R_{41}	24.21×10^{3}	24.21×10^{3}
	C_{41}	1.007×10^{-4}	33.58×10^{-12}
	C_{42}	3.189×10^{-4}	106.3×10^{-12}
	L_{41}	785.7	261.9×10^{-6}

Table 6 (continued)

Mode	Element	Normalized Value	100 Meter Antenna (ohms, farads, henries)
5	R_{51}	26.98×10^{3}	26.98×10^{3}
	C_{51}	7.332×10^{-5}	24.44×10^{-12}
	C_{52}	1.660×10^{-4}	55.32×10^{-12}
	L_{51}	760.2	253.4×10^{-6}
6	R_{61}	29.24×10^{3}	29.24×10^{3}
	C_{61}	5.682×10^{1}	18.94×10^{-12}
	C_{62}	1.016×10^{-4}	33.86×10^{-12}
	L_{61}	738.9	246.3×10^{-6}
7	R_{71}	31.11×10^{3}	31.11×10^{3}
	C_{71}	4.596×10^{-5}	15.32×10^{-12}
	C_{72}	6.858×10^{-5}	22.86×10^{-12}
	L_{71}	720.9	240.3×10^{-6}
8	R_{81}	32.68×10^{3}	32.68×10^{3}
	C_{81}	3.831×10^{-5}	12.77×10^{-12}
	C_{82}	4.938×10^{-5}	16.46×10^{-12}
	L_{81}	705.3	235.1×10^{-6}

Table 6 (continued)

Mode	Element	Normalized Value	100 Meter Antenna (ohms, farads, henries)
9	R_{91}	34.02×10^{3}	34.02×10^{3}
	C_{91}	3.27×10^{-5}	10.9×10^{-12}
	C_{92}	3.729×10^{-5}	12.43×10^{-12}
	L_{91}	691.2	230.4×10^{-6}
10	R_{101}	35.17×10^{3}	35.17×10^{3}
	C_{101}	2.838×10^{-5}	9.46×10^{-12}
	C_{102}	2.916×10^{-5}	9.72×10^{-12}
	L_{101}	678.6	226.2×10^{-6}

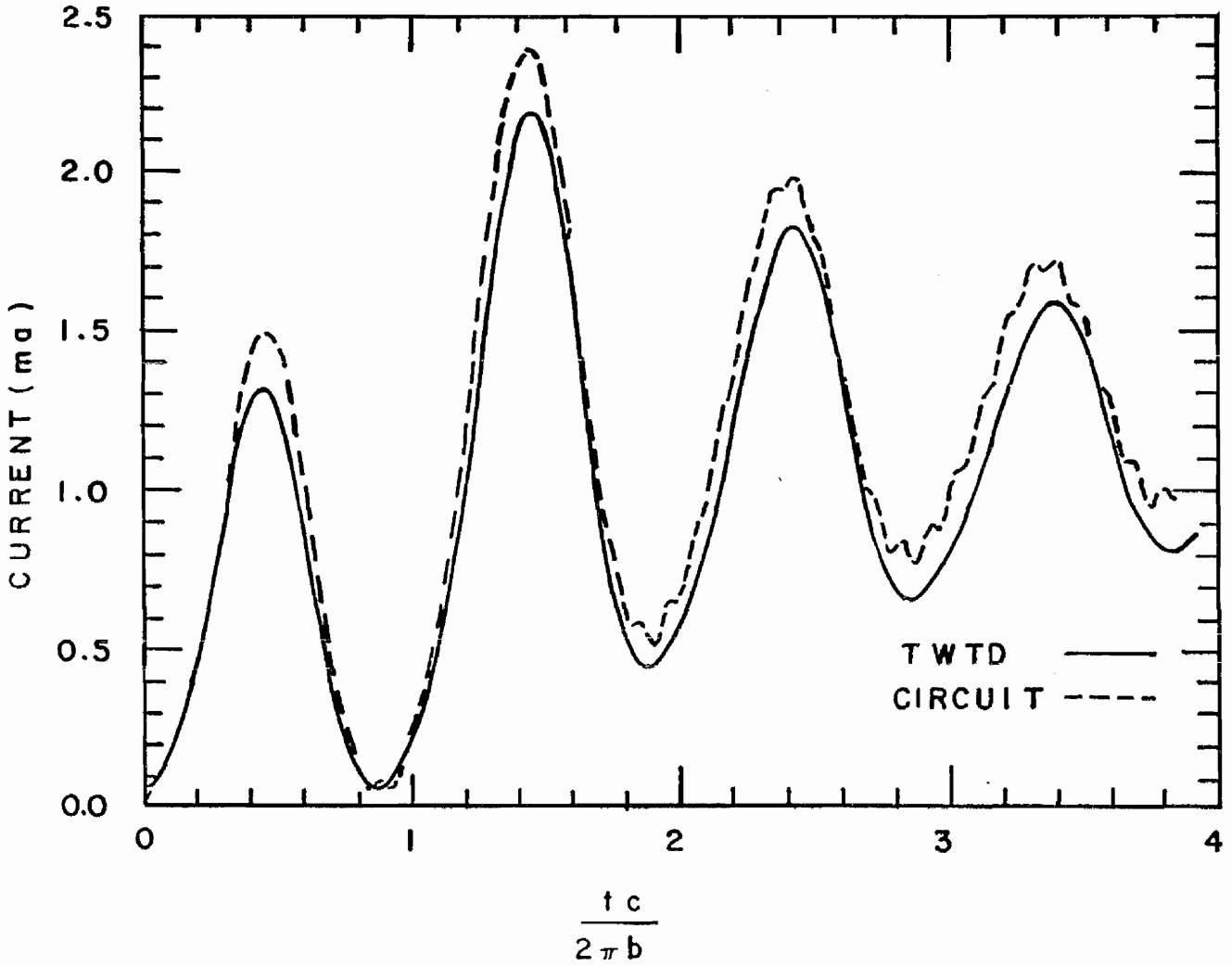

Figure 66: Comparison of the response of the type I pole-pair circuit to TWTD.

4.4.2 Type I and Type III Poles

The departure of the transient current response of the circuit from that of the TWTD model in late time displayed in Figure 65 for the type I pole-pair synthesis is attributable to the omission of type III poles in the frequency range of interest. Therefore a circuit is constructed which includes all type III poles for each eigenmode, up to the cutoff frequency given by mode 10. For mode 0, the type II pole is grouped with the type III poles, since this results in a PR function. For modes 1 and 2 and type I plus type III pole groupings, the admittances are PR; for higher modes, they are not. For these higher modes the modified Bott-Duffin procedure is used to make the groupings PR. The circuit derived is given in Figure 67, with element values given in Table 7.

An analysis of this circuit on SCEPTRE and comparison to TWTD showed an improved response, particularly in the late time, as indicated in Figure 68.

4.5 Sensitivity of Circuits

Although the circuits derived for the straight wire and the loop are in principle realizable, practicality of the realization still may be limited by sensitivity considerations. In order to assess the sensitivity, the two circuits previously described for the center-driven wire are subjected to pseudorandom changes in element value over a range of +10% to -10%. The random number generator is given in Reference [19]. In the range of -10 to +10 it has a mean of zero and a standard deviation of 5.8. No attempt was made to do a complete Monte Carlo or worst-case analysis on circuit performance. Several circuits with errors were made. The resulting circuits

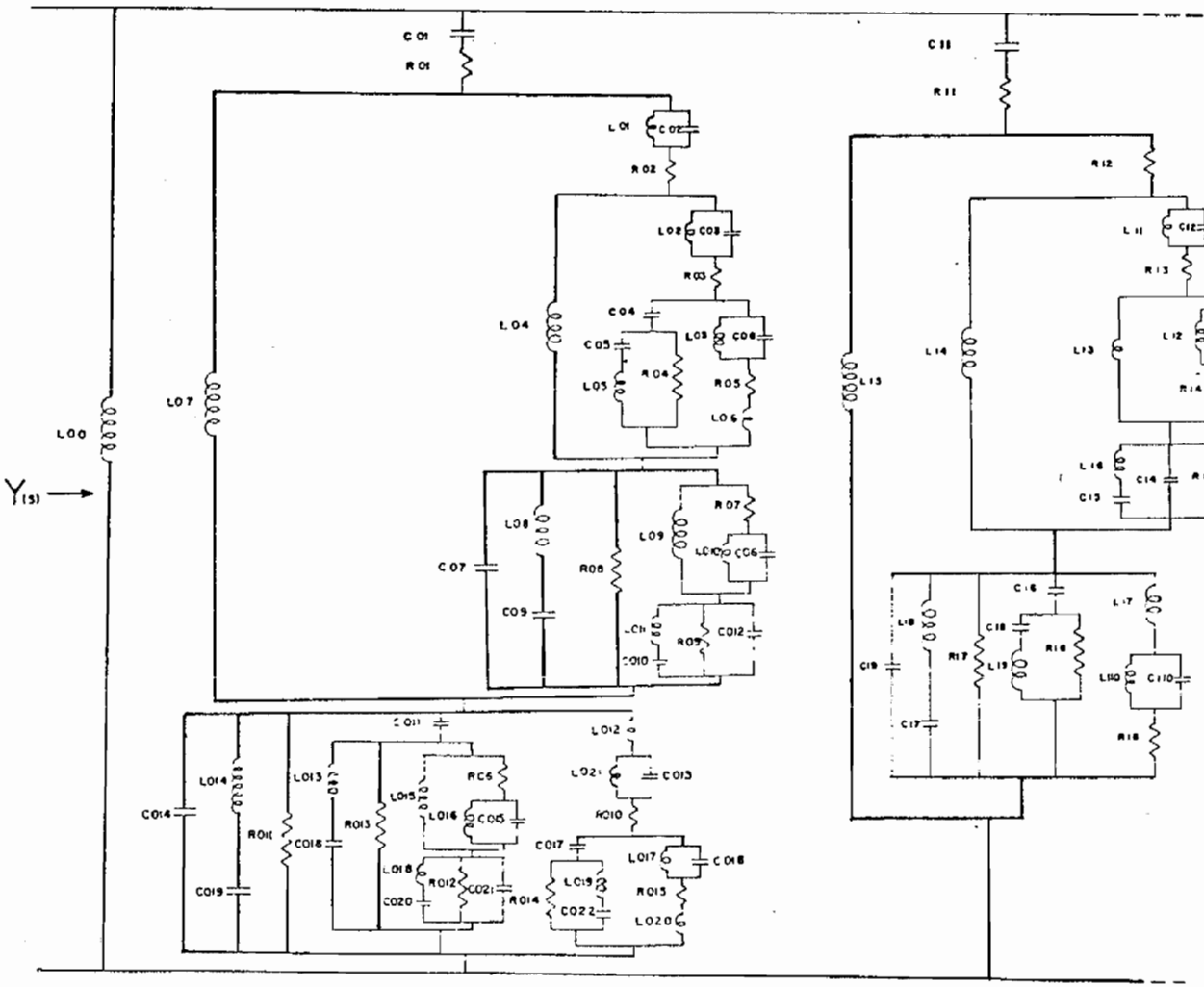

Figure 67a: Equivalent circuit for the circular loop using type I and type III poles, modes 0 and 1.

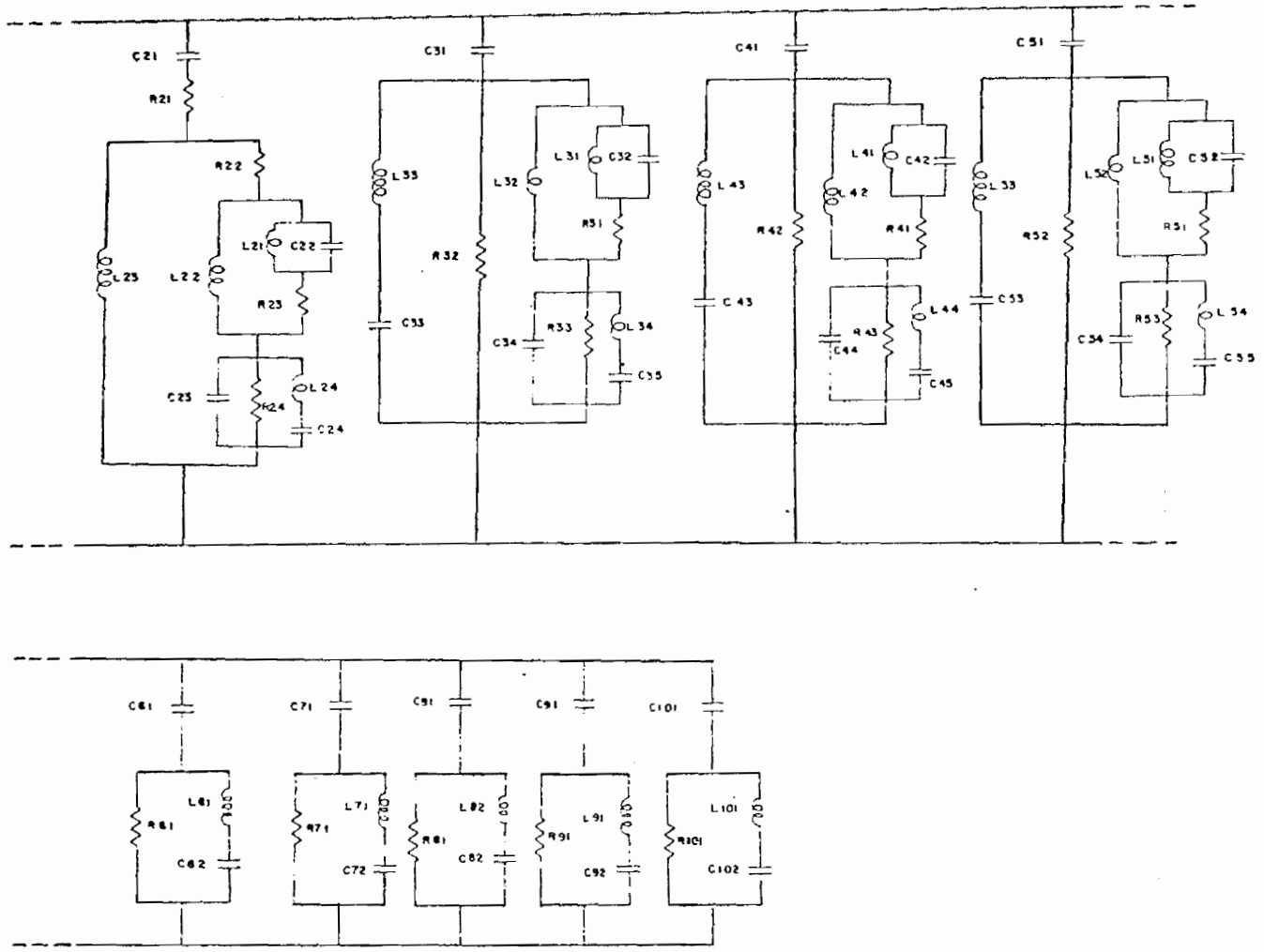

Figure 67b: Equivalent circuit for the circular loop using type I and type III poles, modes 2-10.

Table 7

Element Values for Equivalent Circuit for the Circular Loop Using Type I and III Poles

Mode	Element	Normalized Value	100 Meter Antenna (ohms, farads, henries)
0	R_{01}	12.6×10^{3}	12.6×10^{3}
	R_{02}	22.34×10^{3}	22.34×10^{3}
	R_{03}	1.123×10^{3}	1.123×10^{3}
	R_{04}	120.7	120.7
	R_{05}	819.2	819.2
	R_{06}	408.4×10^{3}	408.4×10^{3}
	R_{07}	1143	1143.
	R_{08}	122.9	122.9
	R_{09}	168.4	168.4
	R_{010}	401.3×10^{3}	401.3×10^{3}
	R_{011}	2208	2208
	R_{012}	60.2×10^{3}	60.2×10^{3}
	R_{013}	43.92×10^{3}	43.92×10^{3}
	R_{014}	43.15×10^{3}	43.15×10^{3}
	R_{015}	292.8×10^{3}	292.8×10^{3}
	C_{01}	5.334×10^{-5}	17.78×10^{-12}
	C_{02}	1.233×10^{-5}	4.111×10^{-12}
	C_{03}	8.289×10^{-6}	2.763×10^{-12}
	C_{04}	2.473×10^{-5}	8.242×10^{-12}
	C_{05}	2.896×10^{-3}	965.3×10^{-12}
	C_{06}	1.089×10^{-5}	3.631×10^{-12}
	C_{07}	1.699×10^{-2}	5663×10^{-12}
	C_{08}	1.520×10^{-5}	5.065×10^{-12}
	C_{09}	6.999×10^{-2}	23330×10^{-12}
	C_{010}	2.076×10^{-3}	691.9×10^{-12}
	C_{011}	4.752×10^{-5}	15.84×10^{-12}

Table 7 (continued)

Mode	Element	Normalized Value	100 Meter Antenna (ohms, farads, henries)
0	C_{012}	1.772×10^{-5}	5.907×10^{-12}
	C_{013}	2.319×10^{-8}	$.00773\times10^{-12}$
	C_{014}	6.486×10^{-5}	21.62×10^{-12}
	C_{015}	3.048×10^{-8}	$.01016\times10^{-12}$
	C_{016}	1.958×10^{-4}	65.27×10^{-12}
	C_{017}	6.915×10^{-8}	$.02305\times10^{-12}$
	C_{018}	4.260×10^{-8}	$.0142\times10^{-12}$
	C_{019}	1.552×10^{-4}	51.73×10^{-12}
	C_{020}	5.808×10^{-6}	1.936×10^{-12}
	C_{021}	4.959×10^{-8}	$.01653\times10^{-12}$
	C_{022}	8.103×10^{-6}	2.701×10^{-12}
	L_{00}	2165	721.5×10^{-6}
	L_{01}	7653	2551×10^{-6}
	L_{02}	9657	3219×10^{-6}
	L_{03}	286.4	95.46×10^{-6}
	L_{04}	2344	781.3×10^{-6}
	L_{05}	1.503	$.5009\times10^{-6}$
	L_{06}	2.445	$.815\times10^{-6}$
	L_{07}	3198	1066×10^{-6}
	L_{08}	1.144	$.3812\times10^{-6}$
	L_{09}	3.411	1.132×10^{-6}
	L_{010}	399.6	133.2×10^{-6}
	L_{011}	2.1	$.7\times10^{-6}$
	L_{012}	8.376×10^{5}	.1792
	L_{013}	408.6	136.2×10^{-6}
	L_{014}	608.1	202.7×10^{-6}
	L_{015}	1219.	406.4×10^{-6}
	L_{016}	1.428×10^{5}	47598×10^{-6}

Table 7 (continued)

Mode	Element	Normalized Value	100 Meter Antenna (ohms, farads, henries)
0	L_{017}	1.026×10^{5}	.03412
	L_{018}	749.4	249.8×10^{-6}
	L_{019}	537.0	$179.\times10^{-6}$
	L_{020}	873.9	291.3×10^{-6}
	L_{021}	3.45×10^{6}	1.15
1	R_{11}	49.36	49.36
	R_{12}	1182	1182
	R_{13}	27.07×10^{3}	27.07×10^{3}
	R_{14}	2294	2294
	R_{15}	8.314	8.314
	R_{16}	111.6×10^{3}	111.6×10^{3}
	R_{17}	9460	9460
	R_{18}	30801×10^{3}	30801×10^{3}
	C_{11}	9.891×10^{-4}	329.7×10^{-12}
	C_{12}	6.309×10^{-6}	2.103×10^{-12}
	C_{13}	1.958×10^{-5}	6.528×10^{-12}
	C_{14}	8.027×10^{-2}	$26757.\times10^{-12}$
	C_{15}	1.258	$.4193\times10^{-6}$
	C_{16}	5.979×10^{-6}	1.993×10^{-12}
	C_{17}	6.636×10^{-6}	2.212×10^{-12}
	C_{18}	9.369×10^{-5}	31.23×10^{-12}
	C_{19}	8.433×10^{-6}	2.811×10^{-12}
	C_{110}	1.459×10^{-9}	$.4862\times10^{-15}$

Table 7 (continued)

Mode	Element	Normalized Value	100 Meter Antenna (ohms, farads, henries)
1	L_{11}	1700	566.5×10^{-6}
	L_{12}	2.399×10^{4}	7997×10^{-6}
	L_{13}	1531	510.3×10^{-6}
	L_{14}	2159	719.7×10^{-6}
	L_{15}	930.3	310.1×10^{-6}
	L_{16}	.3735	$.1245\times10^{-6}$
	L_{17}	20.56×10^{6}	6.852
	L_{18}	1616	538.6×10^{-6}
	L_{19}	5016	1672×10^{-6}
	L_{110}	322.2×10^{6}	107.4
2	R_{21}	1.521	1.521
	R_{22}	5199.	5199.
	R_{23}	29.63×10^{3}	29.63×10^{3}
	R_{24}	12.69×10^{3}	12.69×10^{3}
	C_{21}	2.734×10^{-4}	91.14×10^{-12}
	C_{22}	6.549×10^{-6}	2.183×10^{-12}
	C_{23}	6.627×10^{-6}	2.209×10^{-12}
	C_{24}	7.314×10^{-6}	2.438×10^{-12}
	L_{21}	2750	916.5×10^{-6}
	L_{22}	2492	830.6×10^{-6}
	L_{23}	868.5	289.5×10^{-6}
	L_{24}	2462	820.8×10^{-6}

Table 7 (continued)

Mode	Element	Normalized Value	100 Meter Antenna (ohms, farads, henries)
3	R_{31}	62.01×10^{3}	62.01×10^{3}
	R_{32}	181.9×10^{3}	181.9×10^{3}
	R_{33}	27.98×10^{3}	27.98×10^{3}
	C_{31}	1.469×10^{-4}	48.95×10^{-12}
	C_{32}	2.535×10^{-6}	$.8451\times10^{-12}$
	C_{33}	1.090×10^{-3}	363.4×10^{-12}
	C_{34}	2.242×10^{-6}	$.7474\times10^{-12}$
	C_{35}	2.448×10^{-6}	$.8159\times10^{-12}$
	L_{31}	4248	1416×10^{-6}
	L_{32}	3891	$1297.\times10^{-6}$
	L_{33}	823.5	274.5×10^{-6}
	L_{34}	4398.	1466×10^{-6}
4	R_{41}	71.58×10^{3}	71.58×10^{3}
	R_{42}	212.4×10^{3}	212.4×10^{3}
	R_{43}	34.31×10^{3}	34.31×10^{3}
	C_{41}	9.588×10^{-5}	31.96×10^{-12}
	C_{42}	2.046×10^{-6}	$.6821\times10^{-12}$
	C_{43}	3.735×10^{-4}	124.5×10^{-12}
	C_{44}	1.607×10^{-6}	$.5355\times10^{-12}$
	C_{45}	1.644×10^{-6}	$.548\times10^{-12}$
	L_{41}	4038	1346×10^{-6}
	L_{42}	3945	1315×10^{-6}
	L_{43}	789.9	263.3×10^{-6}
	L_{44}	5025	1675×10^{-6}

Table 7 (continued)

Mode	Element	Normalized Value	100 Meter Antenna (ohms, farads, henries)
5	R_{51}	79.92×10^{3}	79.92×10^{3}
	R_{52}	215.6×10^{3}	215.6×10^{3}
	R_{53}	40.3×10^{3}	40.3×10^{3}
	C_{51}	6.942×10^{-5}	23.14×10^{-12}
	C_{52}	1.732×10^{-6}	$.5773\times10^{-12}$
	C_{53}	1.883×10^{-4}	62.78×10^{-12}
	C_{54}	1.229×10^{-6}	$.4095\times10^{-12}$
	C_{55}	1.151×10^{-6}	$.3837\times10^{-12}$
	L_{51}	3804	1268×10^{-6}
	L_{52}	3957	1319×10^{-6}
	L_{53}	763.2	254.4×10^{-6}
	L_{54}	5580	1860×10^{-6}
6	R_{61}	29.24×10^{3}	29.24×10^{3}
	C_{61}	5.682×10^{-5}	18.94×10^{-12}
	C_{62}	1.016×10^{-4}	33.86×10^{-12}
	L_{61}	738.9	246.3×10^{-6}
7	R_{71}	31.11×10^{3}	31.11×10^{3}
	C_{71}	4.596×10^{-5}	15.32×10^{-12}
	C_{72}	6.858×10^{-5}	22.86×10^{-12}
	L_{71}	720.9	240.3×10^{-6}

Table 7 (continued)

Mode	Element	Normalized Value	100 Meter Antenna (ohms, farads, henries)
8	R_{81}	32.68×10^{3}	32.68×10^{3}
	C_{81}	3.831×10^{-5}	12.77×10^{-12}
	C_{82}	4.938×10^{-5}	16.46×10^{-12}
	L_{81}	705.3	235.1×10^{-6}
9	R_{91}	34.02×10^{3}	34.02×10^{3}
	C_{91}	3.27×10^{-5}	10.9×10^{-12}
	C_{92}	3.729×10^{-5}	12.43×10^{-12}
	L_{91}	691.2	230.4×10^{-6}
10	R_{101}	35.17×10^{3}	35.17×10^{3}
	C_{101}	2.838×10^{-5}	9.46×10^{-12}
	C_{102}	2.916×10^{-5}	9.72×10^{-12}
	L_{101}	678.6	226.2×10^{-6}

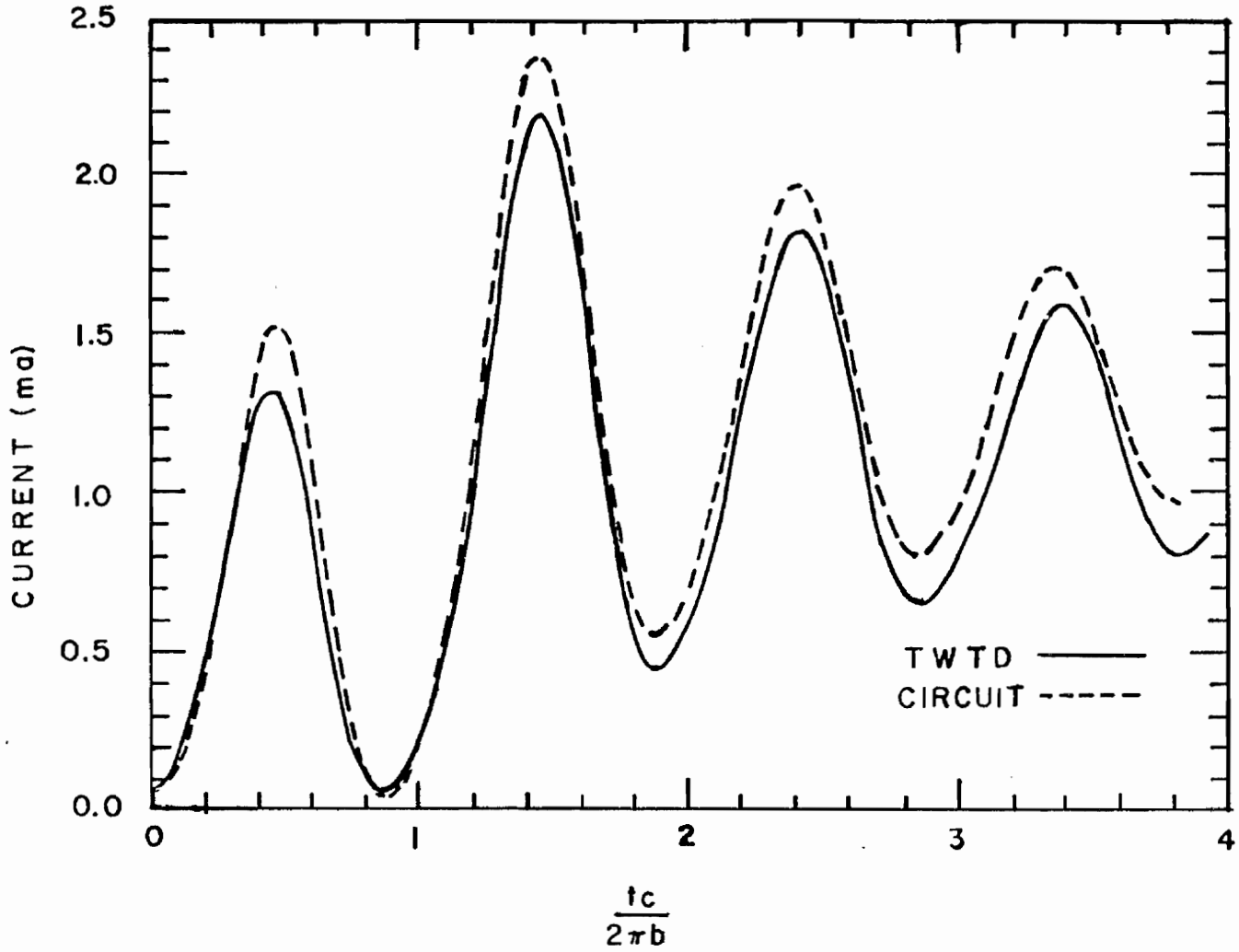

Figure 68: Comparison of the response of the type I and type III pole circuit to TWTD.

were then run on SCEPTRE. A typical result, compared to the uncorrupted run, is given in Figure 69 for the first layer pole-pair synthesis. The responses are identical in the early time, where only the object's force response is important. In late time, the pole shifting caused by the element variations results in a distorted response. The sensitivity of the eigenadmittance circuit was also examined this way, with a similar result. This is not surprising, since it is well known that a Bott-Duffin synthesis is very sensitive to element errors [15].

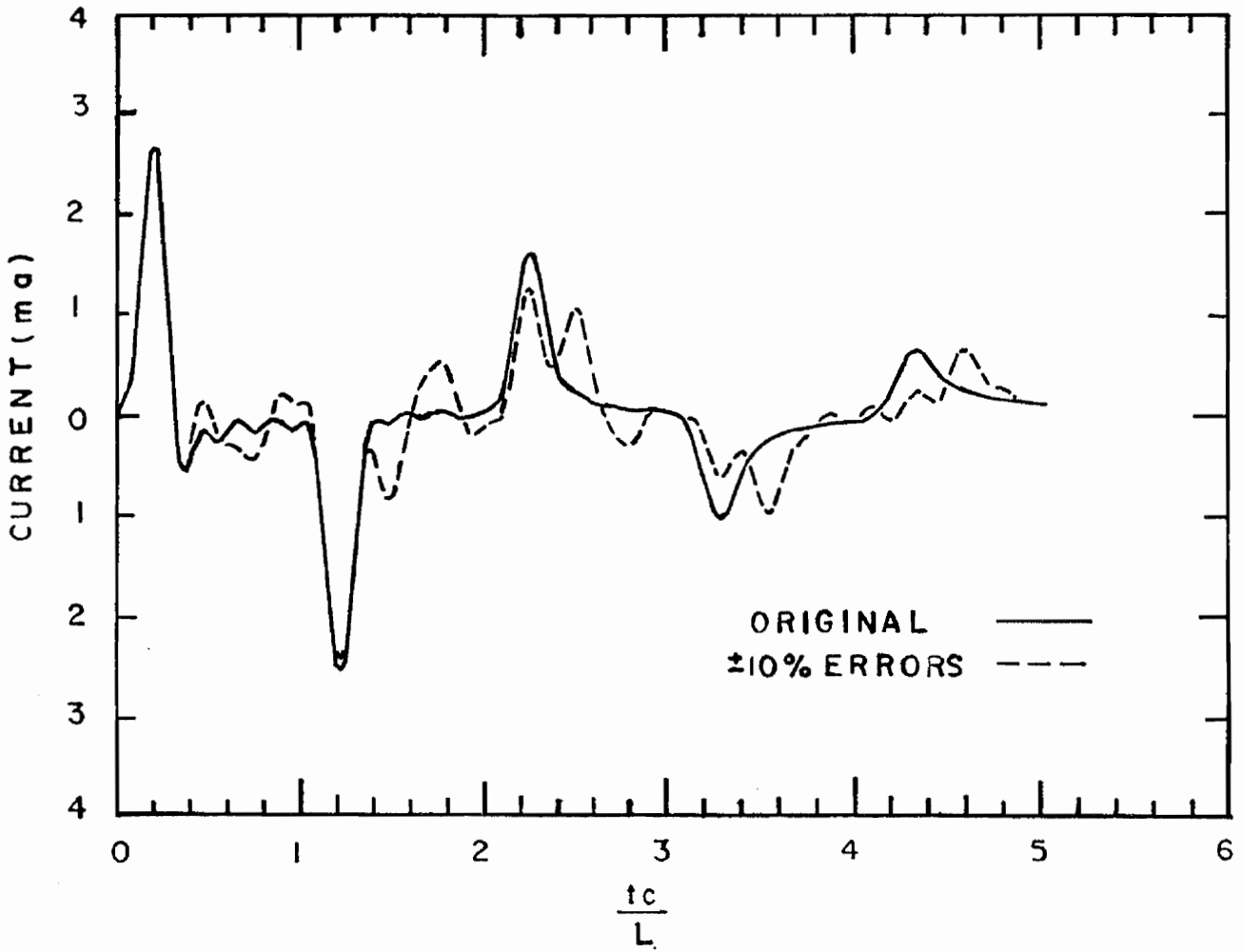

Figure 69: Effect of element errors on circuit performance.

CHAPTER V

CONCLUSIONS

We have demonstrated the feasibility of synthesizing passive-component equivalent circuits which simulate a single-port immittance of a passive antenna/scatterer. Circuits developed here replicate well the terminal response of straight-wire and wire-loop structures except in the early time. It is conjectured that circuits which account for the static capacitance of the structure completely, can bring this early time behavior into agreement, as well.

From the point of view of developing simple systematic equivalent circuits, one would desire that pole-pair contributions to immittance would prove to be positive real functions. Disappointingly, this study reveals an abundance of counterexamples to this desirable result. We have observed, however, that the dominant poles in the resonant structure of the object - those nearest the $j\omega$ axis - have admittances which manifest a near PR behavior. Through negligible adjustments to these admittances, PR behavior was achieved.

Terminal eigenadmittances for the circular loop and center-driven wire are shown to be PR within the limits of numerical accuracy. However, certain terminal eigenadmittances for the quarter-driven wire are non-PR. Although it is known that the inverse eigenvalues are PR, the PRness of all terminal eigenadmittances remains to be demonstrated. Since the eigenset grouping of poles is only conjectured, it is not possible to reach a definite conclusion at this time in regard to terminal eigenadmittance PRness.

The spherical antenna is suggested as an object for study of admittance synthesis properties in the future. That eigensets are well-defined and that each eigenset embraces a finite collection of poles provide the potential for complete and conclusive studies.

The present work has addressed only the admittance element of Norton equivalent modules. The companion source terms need to be studied in light of the present work. In particular, when sources are combined even on a pole-pair basis, the composite source exhibits a frequency dependent transfer function from the excitation waveform. This frequency dependence introduces circuit complexities which are likely to preclude physical realization. Approximate methods for circumventing this frequency dependence are warranted.

APPENDIX

The proof of the positive realness of the integral operators for the antenna scattering problem is given here. This proof is due to Wilton [13] and reproduced here.

Consider a conducting scatterer S with unit surface normal $\hat{n}$ illuminated by an incident field $(\bar{E}^i, \bar{H}^i)$. A surface current $\bar{J}$ is induced on S which produces a scattered field $(\bar{E}^S, \bar{H}^S)$ satisfying the boundary condition

$$\hat{n} \times (\bar{E}^i + \bar{E}^S) = \bar{0} \tag{A.1}$$

on S. By the equivalence theorem, the scatterer may be removed and replaced by the surface current $\bar{J}$ radiating in free space. This current, radiating in the absence of the sources of the incident field, produces the scattered field $(\bar{E}^S, \bar{H}^S)$ exterior to S.

In the absence of other sources, the total energy radiated by the current distribution $\bar{J}$ is always positive semidefinite:

$$E(t) = \int_{-\infty}^{t} W(t)\, dt \geq 0 , \tag{A.2}$$

where E is the energy and W(t) is the total power radiated by $\bar{J}$ at time t and is computed as follows:

$$\begin{aligned} W(t) &= - \int_S \bar{e}^s \cdot \bar{j}\, dS \\ &= \int_S \bar{e}^i \cdot \bar{j}\, dS , \end{aligned} \tag{A.3}$$

where the lower case quantities are time-domain counterparts of the corresponding upper case transform-domain quantities. The current $\bar{j}$ and incident field $\bar{e}^i$ are related through an integral equation, which fact will be exploited subsequently.

We next suppose the incident electric field and induced current are given by

$$\bar{j}(\bar{r},t) = \bar{J}_0(\bar{r})e^{s_0 t} + \bar{J}_0^*(\bar{r})e^{s_0^* t} = 2\ \mathrm{Re}\left\{\bar{J}_0 e^{s_0 t}\right\}, \qquad \text{(A.4a)}$$

$$\bar{e}^i(\bar{r},t) = \bar{E}_0(\bar{r})e^{s_0 t} + \bar{E}_0^*(\bar{r})e^{s_0^* t} = 2\ \mathrm{Re}\left\{\bar{E}_0 e^{s_0 t}\right\}, \qquad \text{(A.4b)}$$

where $s_0 = \sigma_0 + j\omega_0$, $\sigma_0 > 0$, and where $\bar{E}_0$ is an arbitrary complex vector function of position, and $\bar{J}_0$ is the resulting complex current response. The excitation is assumed to start at $t = -\infty$, where there is no initial energy in the system. Since $e^{\sigma_0 t} = 0$ for $t = -\infty$, both $\bar{e}^i$ and $\bar{j}$ are zero and there is no transient term. That is, the 'forced' response above is the total response.

The power W(t) radiated is now

$$W(t) = \int_S \left\{ \bar{J}_0 \cdot \bar{E}_0 e^{2s_0 t} + \bar{J}_0^* \cdot \bar{E}_0^* e^{2s_0^* t} + (\bar{E}_0 \cdot \bar{J}_0^* + \bar{E}_0^* \cdot \bar{J}_0) e^{2\sigma_0 t} \right\} dS$$

$$= 2\ \mathrm{Re} \int_S \left\{ \bar{E}_0 \bar{J}_0 e^{2s_0 t} + \bar{E}_0 \cdot \bar{J}_0^* e^{2\sigma_0 t} \right\} dS$$

and hence the total energy radiated is

$$E(t) = \mathrm{Re} \int_S \left\{ \frac{\bar{E}_0 \cdot \bar{J}_0}{s_0} \, e^{2s_0 t} + \frac{\bar{E}_0 \cdot \bar{J}_0}{\sigma_0} \, e^{2\sigma_0 t} \right\} dS \, . \qquad (A.5)$$

If we write the first integral in polar form,

$$\int_S \frac{\bar{E}_0 \cdot \bar{J}_0}{s_0} \, dS = \left| \int_S \frac{\bar{E}_0 \cdot \bar{J}_0}{s_0} \, dS \right| e^{j\phi} \, ,$$

then E(t) can be written as

$$E(t) = e^{2\sigma_0 t} \left[\left| \int_S \frac{\bar{E}_0 \cdot \bar{J}_0}{s_0} \, dS \right| \cos (2\omega_0 t + \phi) + \mathrm{Re} \, \frac{\int_S \bar{E}_0 \cdot \bar{J}_0^* \, dS}{\sigma_0} \right] \geq 0 \, . \qquad (A.6)$$

We must consider the case $\omega_0 = 0$ and $\omega_0 \neq 0$ separately.

Case I, $\omega_0 = 0$

In this case, (A.5) can be written as

$$E(t) = \frac{e^{2\sigma_0 t}}{\sigma_0} \int_S \left\{ \mathrm{Re}(\bar{E}_0 \cdot \bar{J}_0) + \mathrm{Re}(\bar{E}_0 \cdot \bar{J}_0^*) \right\} dS$$

$$= \frac{e^{2\sigma_0 t}}{\sigma_0} \int_S \mathrm{Re} \left\{ \bar{E}_0 \cdot (\bar{J}_0 + \bar{J}_0^*) \right\} dS$$

$$= \frac{2e^{2\sigma_0 t}}{\sigma_0} \int_S \mathrm{Re} \left\{ \bar{E}_0 \cdot \mathrm{Re} \, \bar{J}_0 \right\} dS$$

$$= \frac{2e^{2\sigma_0 t}}{\sigma_0} \int_S \mathrm{Re} \, \bar{E}_0 \cdot \mathrm{Re} \, \bar{J}_0 \, dS \, ,$$

from which we conclude that

$$\int_S \text{Re}\ \bar{E}_0 \cdot \text{Re}\ \bar{J}_0\ dS \geq 0 . \tag{A.7}$$

But since $\bar{E}_0$ is arbitrary, we could replace it by $j\bar{E}_0$ and the corresponding current response would be $j\bar{J}_0$ by the linearity of the system. Hence, from (A.7), it must also be true that

$$\int_S \text{Re}(j\bar{E}_0) \cdot \text{Re}(j\bar{J}_0)\ dS = \int_S \text{Im}\ \bar{E}_0 \cdot \text{Im}\ \bar{J}_0\ dS \geq 0 . \tag{A.8}$$

Equations (A.7) and (A.8) together imply that

$$\text{Re} \int_S \bar{E}_0 \cdot \bar{J}_0^*\ dS = \int_S (\text{Re}\ \bar{E}_0 \cdot \text{Re}\ \bar{J}_0 + \text{Im}\ \bar{E}_0 \cdot \text{Im}\ \bar{J}_0)\ dS \geq 0 . \tag{A.9}$$

Case II, $\omega_0 \neq 0$

From (A.6), we note that since the maximum negative value for the cosine is -1, we must have

$$\text{Re} \int_S \frac{\bar{E}_0 \cdot \bar{J}_0^*}{\sigma_0}\ dS \geq \left| \int_S \frac{\bar{E}_0 \cdot \bar{J}_0}{s_0}\ dS \right| \geq 0 . \tag{A.10}$$

Thus for both cases we have

$$\text{Re} \int_S \bar{E}_0 \cdot \bar{J}_0^*\ dS \geq 0 , \qquad \sigma_0 > 0 , \tag{A.11}$$

which is a necessary condition on all solutions of scattering problems involving passive scatterers.

Using (A.11) we next derive a condition similar to the positive real condition on driving-point immittances in circuit theory. The condition

applies to the dyadic kernel of the operator relating $\bar{J}$ to $\bar{E}^i$ through the electric field integral equation

$$\hat{n} \times \bar{E}^i(\bar{r},s) = \hat{n} \times \int_S \bar{\bar{Z}}(\bar{r},\bar{r}';s) \cdot \bar{J}(\bar{r}';s)\, dS' \,. \tag{A.12}$$

Since $\bar{E}^i$ and $\bar{J}$ are transform quantities, (A.11) applies for a point $\sigma = \mathrm{Re}\, s$ in the right half plane:

$$\begin{aligned}
&\mathrm{Re} \int_S \int_S \bar{J}^*(\bar{r}) \cdot \bar{\bar{Z}}(\bar{r},\bar{r}') \cdot \bar{J}(\bar{r}')\, dS'\, dS \\
&= \tfrac{1}{2} \int_S \int_S \left\{ \bar{J}^*(\bar{r}) \cdot \bar{\bar{Z}}(\bar{r},\bar{r}') \cdot \bar{J}(\bar{r}') + \left[\bar{J}^*(\bar{r}) \cdot \bar{\bar{Z}}(\bar{r},\bar{r}') \cdot \bar{J}(\bar{r}') \right]^\dagger \right\} dS'\, dS \\
&= \tfrac{1}{2} \int_S \int_S \left\{ \bar{J}^*(\bar{r}) \cdot \bar{\bar{Z}}(\bar{r},\bar{r}') \cdot \bar{J}(\bar{r}') + \bar{J}^*(\bar{r}') \cdot \bar{\bar{Z}}^\dagger(\bar{r},\bar{r}') \cdot \bar{J}(\bar{r}) \right\} dS'\, dS \\
&= \tfrac{1}{2} \int_S \int_S \left\{ \bar{J}^*(\bar{r}) \cdot \bar{\bar{Z}}(\bar{r},\bar{r}') \cdot \bar{J}(\bar{r}') + \bar{J}^*(\bar{r}) \cdot \bar{\bar{Z}}^*(\bar{r},\bar{r}') \cdot \bar{J}(\bar{r}') \right\} dS'\, dS \\
&= \tfrac{1}{2} \int_S \int_S \left\{ \bar{J}^*(\bar{r}) \cdot \left[\bar{\bar{Z}}(\bar{r},\bar{r}') + \bar{\bar{Z}}^*(\bar{r},\bar{r}') \right] \cdot \bar{J}(\bar{r}') \right\} dS'\, dS \\
&= \int_S \int_S \bar{J}^*(\bar{r}) \cdot \mathrm{Re}\, \bar{\bar{Z}}(\bar{r},\bar{r}') \cdot \bar{J}(\bar{r}')\, dS'\, dS \geq 0 \,,
\end{aligned} \tag{A.13}$$

where the dagger denotes the transpose conjugate and where we have used the reciprocity condition that

$$\bar{\bar{Z}}^\dagger(\bar{r},\bar{r}') = \bar{\bar{Z}}^*(\bar{r},\bar{r}') = \bar{\bar{Z}}^*(\bar{r}',\bar{r}) \,.$$

Thus, $\mathrm{Re}\, \bar{\bar{Z}}$ must be positive semidefinite for $\sigma > 0$; i.e.,

$$\mathrm{Re}\, \bar{\bar{Z}} \geq 0 \,, \qquad \sigma > 0 \,, \tag{A.14}$$

where (A.14) is a shorthand notation for (A.13), except for operators which are merely complex constants.

We note that condition (A.14) is analogous to one of the so-called positive real conditions for immittances of m-port networks. For such networks, the positive real condition is shown to be both a necessary and sufficient condition for the realizability of a passive network. The sufficiency of the condition is established by actually deriving algorithms for synthesizing such networks. We are not yet at this stage in electromagnetics, but we are now in a position to list several independent conditions, analogous to those of an m-port immittance matrix, which the impedance operator for a passive scatterer must necessarily satisfy:

(1) $\bar{\bar{Z}}(\bar{r},\bar{r}';s)$ is analytic in $\mathrm{Re}(s) > 0$;

(2) $\bar{\bar{Z}}(\bar{r},\bar{r}';s)$ is real for real positive s;

(3) $\mathrm{Re}\ \bar{\bar{Z}}(\bar{r},\bar{r}';s) \geq 0$ for $\mathrm{Re}\ s > 0$.

Though the sufficiency condition has not been demonstrated, we nevertheless term operators with kernels satisfying these conditions as positive real. As in network theory, it is possible to find alternative conditions for (1)-(3), which are simpler to test. We also note that to arrive at these conditions, we must write the integral equation in the form of (A.12). We point this out because it is common to view the right-hand side of (A.12) as the scattered field, in which case the left-hand side, in view of the boundary conditions, would have a negative sign. In this form, the resulting impedance operator could be termed 'negative real'.

Next, we note that $\bar{\bar{Z}}(\bar{r},\bar{r}';s)$ can be written in terms of its eigenspectrum as

$$\bar{\bar{Z}}(\bar{r},\bar{r}';s) = \sum_n \lambda_n(s)\bar{J}_n(\bar{r};s)\bar{J}_n(\bar{r}';s) \ , \tag{A.15}$$

where λ_n is an eigenvalue and $\bar{J}_n$ is the corresponding eigenvector satisfying the eigenvalue equation

$$\int_S \bar{\bar{Z}}(\bar{r},\bar{r}';s) \cdot \bar{J}_n(\bar{r}';s) \ dS' = \lambda_n(s)\bar{J}_n(\bar{r};s) \tag{A.16}$$

and where $\bar{J}_n$ is orthogonal to all other eigenvectors

$$\int_S \bar{J}_m(\bar{r};s) \cdot \bar{J}_n(\bar{r};s) \ dS = \delta_{mn} \ . \tag{A.17}$$

Note that $\bar{\bar{Z}}$ is an operator-valued analytic function of s and we assume that λ_n and $\bar{J}_n$ are likewise analytic. The absence of the complex conjugate in the second eigenvector in (A.17) is at first disconcerting, but it should be remembered that the operator $\bar{\bar{Z}}$ is not self-adjoint, but is complex symmetric; i.e., $\bar{\bar{Z}}^\dagger(\bar{r}',\bar{r}) = \bar{\bar{Z}}^*(\bar{r},\bar{r}')$. Briefly, the eigenvectors $\bar{J}_n$ should be biorthogonal to the eigenvectors of the adjoint operator, $\bar{\bar{Z}}^\dagger(\bar{r}',\bar{r})$, which, in view of the complex symmetry of $\bar{\bar{Z}}$, are just $\bar{J}_n^*$. The resulting biorthogonality condition is (A.17).

We note that (A.13) must be true for all possible current distributions $\bar{J}$ and hence must be true for $\bar{J}(\bar{r};s) = \bar{J}_m(\bar{r};s)$. Substituting this condition and (A.15) into (A.13) results in

$$\text{Re} \int_S \int_S \bar{J}_m^*(\bar{r}) \cdot \sum_n \lambda_n(s) \bar{J}_n(\bar{r}) \bar{J}_n(\bar{r}') \cdot \bar{J}_m(r^{-1}) \, dS' \, dS$$

$$= \text{Re} \left\{ \lambda_m(s) \int_S \bar{J}_m^*(\bar{r}) \cdot \bar{J}_m(\bar{r}) \, dS \right\}$$

$$= \text{Re} \left\{ \lambda_m(s) \int_S |\bar{J}_m(\bar{r})|^2 \, dS \right\} \geq 0 \, ,$$

from which we conclude that $\lambda_n(s)$ is positive real

$$\text{Re } \lambda_n(s) \geq 0 \, , \qquad \sigma > 0 \, . \tag{A.18}$$

It can be shown that for scalar quantities, (A.18), together with the requirement $\lambda_n(s)$ is real when s is real, is equivalent to the following conditions:

(a) $\lambda_n(s)$ has no poles or zeros in the right half plane;

(b) poles of $\lambda_n(s)$ on the imaginary axis must be simple and the residues evaluated at these poles must be real and positive;

(c) $\text{Re } \lambda_n(j\omega) \geq 0 \, , \qquad 0 \leq \omega \leq \infty \, .$

The latter condition is particularly important because it requires only the examination of λ_n on the $j\omega$ axis rather than in the whole of the right half plane. As an example of the application of these conditions, we note that for a wire loop there exists only a ϕ-directed current, which is found by requiring the ϕ-component of electric field to vanish on the loop. Thus the kernel is scalar-valued and has been found by T. T. Wu to be

$$Z(\phi,\phi') = \sum_{n=-\infty}^{\infty} j\eta_0\pi\alpha_n \, e^{-jn(\phi-\phi')}$$

$$= j\eta_0\pi\alpha_0 + \sum_{n=1}^{\infty} j\eta_0\pi\alpha_n \left[e^{-jn(\phi-\phi')} + e^{jn(\phi-\phi')}\right], \qquad (A.19)$$

where the rearrangement to the trigonometric form is made to more closely compare with (A.15). Thus, $j\alpha_n(s)$ must be positive real. But $j\alpha_n(s)$ is positive real if and only if $\frac{1}{j\alpha_n(s)}$ is positive real and it has been verified by direct computation that $\frac{1}{j\alpha_n(s)}$ has no poles either in the right half plane or on the $j\omega$ axis, thus satisfying conditions (a) and (b). Condition (c) implies that we must have

$$\text{Re}\,\frac{1}{j\alpha_n(j\omega)} = \text{Im}\,\frac{1}{\alpha_n(j\omega)} \geq 0 , \qquad 0 \leq \omega \leq \infty ,$$

which appears to be true [18].

Finally, we consider the $j\omega$ axis poles of the inverse operator, whose kernel is the resolvent kernel

$$\bar{\bar{Z}}^{-1}(\bar{r},\bar{r}',s) = \sum_n \frac{\bar{J}_n(\bar{r},s)\bar{J}_n(\bar{r}',s)}{\lambda_n(s)} . \qquad (A.20)$$

We know that poles on the $j\omega$ axis must be simple and that the vector components of the current $\bar{J}_n$, which are cavity mode currents, are cophasal and hence, because of the normalization (A.17), are real. Furthermore, at a pole, one of the eigenvalues, say λ_m, has a simple zero and can be approximated by the first term in its Taylor series for a pole at s_0 by

$$\lambda_m(s) = \alpha_1(s - s_0)$$

or in polar form by

$$\lambda_m(s) = \alpha_1 \varepsilon\, e^{j\phi} ,$$

where $(s - s_0) = \varepsilon\, e^{j\phi}$. Since the pole term will dominate, then on the semicircle of radius ε in the right plane, we have the condition

$$\text{Re} \int_S \int_S \bar{J}^* \cdot \bar{\bar{Z}} \cdot \bar{J}\, dS'\, dS$$

$$\cong \text{Re} \int_S \int_S \frac{\bar{J}^*(\bar{r},s) \cdot \bar{J}_n(\bar{r},s)\, \bar{J}_n(\bar{r}',s_0) \cdot \bar{J}(\bar{r}',s_0)}{\alpha_1 \varepsilon\, e^{j\phi}}\, dS'\, dS$$

$$= \left| \int_S \bar{J}_n(\bar{r},s) \cdot \bar{J}(\bar{r},s)\, dS \right|^2 \text{Re} \frac{1}{\alpha_1 \varepsilon\, e^{j\phi}}$$

$$= \frac{\left| \int_S \bar{J}_n(\bar{r},s) \cdot \bar{J}(\bar{r},s)\, dS \right|^2}{|\alpha_1| \varepsilon} \cos(\phi + \theta) \geq 0 , \qquad \text{(A.21)}$$

where $\alpha_1 = |\alpha_1| e^{j\theta}$. The condition (A.21) must hold for $-\frac{\pi}{2} \leq \phi \leq \frac{\pi}{2}$, i.e., for s in the right half plane, which is possible only if $\theta = 0$. This implies that

$$\alpha_1 = \left. \frac{d\lambda_m}{ds} \right|_{s=s_0} \qquad \text{(A.22)}$$

is real and positive. It can easily be checked that this condition is contained in condition (c) above.

Note that for antenna problems, we can take $\bar{E}_0$ to be a unit voltage source (i.e., a δ function) at some pair of terminals on s and conclude that the input admittance is positive real. The above proof establishes the PRness of the inverse eigenvalues, but does not address the question of the PRness of terminal eigenadmittances. The PRness of the terminal eigenadmittances may be explored based on the PRness of the eigenadmittances $\frac{1}{\lambda_n(s)}$ established above and on (2.13), which is written here in terms of the natural current modes and gap geometry as*

$$\tilde{Y}_n(s) = \left\{ \frac{1}{\lambda_n(s)} \quad \frac{<\tilde{\bar{J}}_n(\bar{r},s) \; ; \; \hat{a}_g>^2 S_g}{\Delta^2 <\tilde{\bar{J}}_n(\bar{r},s) \; ; \; \tilde{\bar{J}}_n(\bar{r},s)>} \right\} . \tag{A.23}$$

It is convenient to define $\gamma_n(s) = \frac{1}{\lambda_n(s)}$ and

$$\tilde{F}_n(s) = \frac{<\tilde{\bar{J}}_n(\bar{r},s) \; ; \; \hat{a}_g>^2 S_g}{\Delta^2 <\tilde{\bar{J}}_n(\bar{r},s) \; ; \; \tilde{\bar{J}}_n(\bar{r},s)>} , \tag{A.24}$$

such that

$$\tilde{Y}_n(s) = (\gamma_n^r F_n^r - \gamma_n^i F_n^i) + j(\gamma_n^r F_n^i + \gamma_n^i F_n^r) ,$$

where the superscripts denote respective real and imaginary parts. It follows that PRness of $\tilde{Y}_n(s)$ hinges on the adherence to

$$\gamma_n^r F_n^r \geq \gamma_n^i F_n^i , \qquad \mathrm{Re}\{s\} \geq 0 . \tag{A.25}$$

*The foregoing material due to Wilton used his notation of explicit expression of integration. From here forward, we revert to the symmetric product notation used throughout the body of this work.

Because of the complexity of (A.24), it is difficult to draw general conclusions regarding the satisfaction of (A.25). Clearly, one might test (A.25) on a numerical basis, but to do so would be computationally costly since an eigenvalue problem would need to be solved. For the case that the eigenmodes $\tilde{\tilde{J}}_n$ are pure real for $s = j\omega$, it follows directly from (A.24) and (A.25) that the terminal eigenadmittances $\tilde{Y}_n(s)$ are PR. This is the case for both the loop and sphere geometries, but the real modes for these structures devolve from symmetry degeneracies. On the other hand, the first few natural modes on the straight wire exhibit small real parts for s near the $j\omega$ axis, and (A.25) is likely to be satisfied.

With the respective high-Q and low-Q extremes of the straight wire and the sphere likely yielding PR terminal eigenadmittances, one might be tempted to draw broad conclusions. However, some common topological feature, such as convexity, might bear on the results for these two special cases, thereby qualifying any general conclusions which one might draw.

REFERENCES

1. Baum, C. E., "On the Singularity Expansion Method for the Solution of Electromagnetic Interaction Problems," EMP Interaction Note 88, Air Force Weapons Laboratory, Kirtland AFB, NM, December 11, 1971.

2. Baum, C. E., "The Singularity Expansion Method," Ch. 3 of Transient Electromagnetic Fields, L. B. Felsen, ed., Springer-Verlag, Heidelberg, 1976.

3. Marin, L., "Natural Mode Representation of Transient Scattered Fields," IEEE Trans. Ant. Prop., Vol. AP-21, pp. 809-818, November, 1973.

4. Baum, C. E., "On the Eigenmode Expansion Method for Electromagnetic Scattering and Antenna Problems, Part I: Some Basic Relations for Eigenmode Expansions and Their Relation to the Singularity Expansion," EMP Interaction Note 229, Air Force Weapons Laboratory, Kirtland AFB, NM, January, 1975.

5. Baum, C. E., "Single Port Equivalent Circuits for Antennas and Scatterers," EMP Interaction Note 295, Air Force Weapons Laboratory, Kirtland AFB, NM, March 29, 1976.

6. Baum, C. E., "Emerging Technology for Transient Broad-Band Analysis and Synthesis of Antennas and Scatterers," Proc. IEEE, Vol. 64, No. 11, pp. 1598-1616, November, 1976, and also Interaction Note 300, November, 1976.

7. Guillemin, E. A., Synthesis of Passive Networks, pp. 330-332, John Wiley and Sons, 1957.

8. Pearson, L. W., Wilton, D., Hsu, F., and Mittra, R., "Conditions of Validity for the Class 1 and Class 2 SEM Coupling Coefficients," International Union of Radio Science Meeting, Boulder, CO, November 6-9, 1978.

9. Tesche, F. M., "Application of the Singularity Expansion Method to the Analysis of Impedance Loaded Linear Antennas," EMP Sensor and Simulation Note 177, Air Force Weapons Laboratory, Kirtland AFB, NM, May, 1973.

10. Wu, T. T., "Theory of the Thin Circular Loop Antenna," J. Math. Phys., Vol. 3, pp. 1301-1304, November-December, 1962.

11. Umashankar, K. R., "The Calculation of Electromagnetic Transient Current on Thin Perfectly Conducting Bodies Using SEM," Dissertation, University of Mississippi, August, 1974.

12. Blackburn, F., "Analysis and Synthesis of an Impedance-Loaded Loop Antenna Using the Singularity Expansion Method," Sensor and Simulation Note 214, May, 1976.

13. Wilton, D., private communication, February 1, 1978.

14. Bucci, O. M., and Franceschetti, G., "Input Admittance and Transient Response of Spheroidal Antennas in Dispersive Media," IEEE Trans. Ant. Prop., Vol. AP-22, No. 4, July, 1974.

15. Van Valkenburg, M. E., Introduction to Modern Network Synthesis, pp. 180-182, John Wiley and Sons, 1960.

16. Schaubert, D. H., "Application of Prony's Method to Time-Domain Reflectometer Data and Equivalent Circuit Synthesis," IEEE Trans. Ant. Prop., Vol. AP-27, No. 2, pp. 180-184, March, 1979.

17. Hess, R. F., "EMP Coupling Analysis Using the Frequency (Transfer Function) Method with the SCEPTRE Computer Program," IEEE Trans. Electromag. Compat., pp. 181-185, August, 1975.

18. Collin, R. E., and Zucker, F. J., eds., Antenna Theory, Part I, p. 465, Fig. 11.2(b), McGraw-Hill, 1969.

19. Hewlett-Packard HP-25 Applications Programs 00025-90011 Rev. C 8/75, 1975.